



Applications of TiO₂ with energy in visible light region

Supat Buddee

**A Thesis Submitted in Fulfillment of the Requirements for the Degree of
Doctor of Philosophy in Chemistry
Prince of Songkla University
2015
Copyright of Prince of Songkla University**

Thesis Title Applications of TiO₂ with energy in visible light region
Author Mr. Supat Buddee
Major Program Chemistry

Major Advisor :

.....
 (Assoc. Prof. Dr. Sumpun Wongnawa)

Examining Committee :

.....Chairperson
 (Assoc. Prof. Dr. Nurak Grisadanurak)

.....Committee
 (Assoc. Prof. Dr. Sumpun Wongnawa)

..... Committee
 (Assoc. Prof. Dr. Sumetha Suwanboon)

..... Committee
 (Asst. Prof. Dr. Pongsaton Amornpitoksuk)

..... Committee
 (Dr. Uraiwan Sirimahachai)

The Graduate School, Prince of Songkla University, has approved this thesis as fulfillment of the requirements for the Degree of Doctor of Philosophy in Chemistry

.....
 (Assoc. Prof. Dr. Teerapon Srichana)
 Dean of Graduate School

This is to certify that the work here submitted is the result of the candidate's own investigations. Due acknowledgement has been made of any assistance received.

..... Signature
(Assoc. Prof. Dr. Sumpun Wongnawa)
Major Advisor

..... Signature
(Mr. Supat Buddee)
Candidate

I hereby certify that this work has not been accepted in substance for any degree, and is not being currently submitted in candidature for any degree.

..... Signature

(Mr. Supat Buddee)

Candidate

ชื่อวิทยานิพนธ์	การประยุกต์ใช้ไทเทเนียมไดออกไซด์ด้วยพลังงานในช่วงแสงวิสิเบิล
ผู้เขียน	นายสุพัฒน์ บุตรดี
สาขาวิชา	เคมี
ปีการศึกษา	2557

บทคัดย่อ

งานวิจัยนี้มีวัตถุประสงค์เพื่อศึกษาการใช้ขี้ผึ้งเป็นตัวเคลือบในการปรับปรุงประสิทธิภาพของไทเทเนียมไดออกไซด์อสังฐาน (Cur-AMO) และเพิ่มความสามารถของไทเทเนียมไดออกไซด์แบบผลึก (Cur-TiO₂) ทั้งอนาเทส (Cur-TiO₂-an), รูไทล์ (Cur-TiO₂-ru) และ Degussa P25 (Cur-TiO₂-P25) ในการเป็นโฟโตคะตะลิสต์ โดยเคลือบด้วยวิธีอิมเพรกเนชันแบบเปียก ศึกษาคุณสมบัติทางกายภาพและทางเคมีของสารที่เตรียมได้โดยใช้เทคนิค XRD, FT-IR, SEM, TEM, BET, DRS, และ UV-vis พบว่าขี้ผึ้งที่เคลือบในช่วงความเข้มข้นที่ศึกษาตั้งแต่ 0.5-7 wt% สำหรับ Cur-TiO₂ และ 1-10 wt% สำหรับ Cur-AMO ไม่มีผลต่อการเปลี่ยนแปลงเฟสของ TiO₂ พลังงานของแถบช่องว่างลดลงจากค่าปกติเหลือประมาณ 2.8-2.9 eV และ 1.6-2.1 eV สำหรับ Cur-TiO₂ และ Cur-AMO ตามลำดับ ทดสอบความสามารถในการเป็นโฟโตคะตะลิสต์ของสารตัวอย่างโดยใช้การสลายสีย้อมสามชนิด ได้แก่ คริสตัลไวโอเลต (CV), เมทิลีนบลู (MB) และออเรนจ์ทู (O II) ภายใต้การฉายแสงยูวีและแสงวิสิเบิล พบว่าภายใต้การฉายแสงยูวี Cur-TiO₂ มีความสามารถในการสลายสีย้อมใกล้เคียงกับ TiO₂ ที่ไม่ได้เคลือบด้วยขี้ผึ้ง และภายใต้การฉายแสงวิสิเบิล ทั้ง Cur-TiO₂ และ Cur-AMO มีความสามารถในการสลายสีย้อมได้ดีกว่าสารตัวอย่างที่ไม่เคลือบขี้ผึ้ง ยกเว้น Cur-TiO₂-ru ที่ไม่แสดงความเป็นโฟโตคะตะลิสต์ ความเข้มข้นของการเคลือบขี้ผึ้งที่ 5 wt% และ 7.5 wt% แสดงประสิทธิภาพการเป็นโฟโตคะตะลิสต์ที่ดีที่สุดสำหรับ Cur-TiO₂ และ Cur-AMO ตามลำดับ กลไกการสลายสีย้อมด้วยการใช้โมเลกุลของขี้ผึ้งเคลือบบนผิวของ TiO₂ ใช้หลักการเป็นเซนซิไทเซอร์ เมื่อแสงมีพลังงานน้อย TiO₂ จะไม่ถูกกระตุ้น แต่โมเลกุลของขี้ผึ้งจะได้รับการกระตุ้น และเกิดการถ่ายเทอิเล็กตรอนไปยังแถบตัวนำของ TiO₂ เพื่อสลายสีย้อม งานวิจัยนี้สามารถเพิ่มประสิทธิภาพการเป็นโฟโตคะตะลิสต์ของไทเทเนียมไดออกไซด์แบบผลึกและเปลี่ยนไทเทเนียมไดออกไซด์ อสังฐานให้สามารถเป็นโฟโตคะตะลิสต์ได้ด้วยการเคลือบโมเลกุลของขี้ผึ้งลงไปโดยอาศัยวิธีที่ง่ายและมีราคาถูก จึงเป็นอีกทางเลือกหนึ่งที่สามารถใช้ในการบำบัดน้ำเสียจากอุตสาหกรรมได้

Thesis Title	Applications of TiO ₂ with energy in visible light region
Author	Mr. Supat Buddee
Major Program	Chemistry
Academic Year	2014

Abstract

In this work, curcumin coating was applied for photocatalytic improvement of amorphous TiO₂ (Cur-AMO) and crystalline TiO₂ (Cur-TiO₂), the latter composed of anatase (Cur-TiO₂-an), rutile (Cur-TiO₂-ru), and Degussa P25 (Cur-TiO₂-P25), by using an incipient wetness impregnation processes. The resulting products were characterized by X-ray diffraction, Fourier-transformed infrared spectroscopy, scanning electron microscopy, transmission electron microscopy, specific surface area by the Brunauer Emmett and Teller method, diffused reflectance spectroscopy and UV-vis absorption spectroscopy. Experimental results revealed that the coating agent had no effect on the phase of products in all study range, from 0.5 to 7 wt% and 1 to 10 wt% of nominal curcumin concentrations for Cur-TiO₂ and Cur-AMO, respectively. The band gap energies shifted from normal value to 2.8-2.9 eV and 1.6-2.1 eV for Cur-TiO₂ and Cur-AMO, respectively. The photocatalytic efficiencies of all products were evaluated from the degradation of three selected model dyes, crystal violet (CV), methylene blue (MB), and orange II (OII), under UV or visible light irradiation. Under UV irradiation, Cur-TiO₂ showed photodegradation efficiency comparable to uncoated one, however, under visible light both the coated samples, Cur-TiO₂ and Cur-AMO, exhibited higher photodegradation efficiency than the uncoated TiO₂ for all three dyes, except Cur-TiO₂-ru prepared by this method was inactive. Under visible light activation, curcumin acted as the sensitizer with the excited electron injected into the conduction band of TiO₂ leading to the photocatalytic processes. This work successfully improved the photocatalytic property of crystalline TiO₂ with low visible light response to highly photoactive and turned inert amorphous TiO₂ to become photocatalytically active by means of dye-sensitized pathway. Considering the simplicity in preparation and low cost due to exclusion of calcination process, this should be an attractive choice to wastewater treatment.

Contents

Subject	Page
Abstract (Thai)	v
Abstract (English)	vi
Acknowledgments	vii
The relevancy of the research work to Thailand	viii
Contents	ix
List of Figures	xii
Lists of Tables	xiii
Lists of Schemes	xiv
Abbreviation and Symbols	xv
List of papers and Proceedings	xvi
Reprint 1	
Reprint 2	
Chapter 1: Introduction	1
Introduction	1
Objectives	4
Chapter 2: Principles and literature reviews	5
Principles	5
Literature reviews	27
Chapter 3: Result and Discussion	37
Syntheses and characterizations of TiO ₂ powders	37
Photocatalytic study	68
Chapter 4: Concluding remarks	83
References	84
Appendix	98
Vitae	101

List of Figures

Figure	Page
1. Crystal structures of TiO ₂ (a) anatase, (b) brookite, and (c) rutile	6
2. Various steps in the sol-gel process to control the final morphology of the product	11
3. Structure of curcuminoids in turmeric	14
4. Main methods applied to the removal of synthetic dyes from wastewaters	24
5. Mechanism of electron-hole pair formation in a TiO ₂ particle in the presence of pollutant in water	26
6. The photograph of synthesized TiO ₂ powder	37
7. The photograph of uncoated commercial TiO ₂ powders (a) anatase (Carlo Erba), (b) rutile (R706, TOA), and Degussa P25	38
8. The photographs of coated TiO ₂ powders; (a) 5Cur-TiO ₂ -an, (b) 5Cur-TiO ₂ -ru, (c) 5Cur-P25, and (d) 7.5Cur-AMO	40
9. X-ray diffraction patterns of Cur-TiO ₂ -P25 for (a) uncoated P25-TiO ₂ , (b) 0.5Cur-TiO ₂ -P25, (c) 3Cur-TiO ₂ -P25, (d) 5Cur-TiO ₂ -P25, (e) 7Cur-TiO ₂ -P25, and (f) curcumin	41
10. X-ray diffraction patterns of Cur-TiO ₂ -an and Cur-TiO ₂ -ru for (a) uncoated anatase TiO ₂ , (b) 5Cur-TiO ₂ -an, (c) uncoated rutile TiO ₂ , and (d) 5 Cur-TiO ₂ -ru	41
11. X-ray diffraction patterns of Cur-AMO for (a) uncoated amorphous TiO ₂ , (b) 1Cur-AMO, (c) 2.5Cur-AMO, (d) 5Cur-AMO, (e) 7.5Cur-AMO, (f) 10Cur-AMO, and (g) curcumin	42
12. DRS spectra of curcumin coated anatase TiO ₂	43
13. DRS spectra of curcumin coated rutile TiO ₂	44
14. DRS spectra of curcumin coated P25-TiO ₂	44
15. DRS spectra of curcumin coated amorphous TiO ₂	44
16. IUPAC classification of adsorption isotherms	48

List of Figures (Continued)

Figure	Page
17. The N ₂ adsorption isotherms of samples for (a) uncoated P25-TiO ₂ , (b) 5Cur-TiO ₂ -P25, and (c) curcumin powder	50
18. SEM images (10,000x) of samples for (a) uncoated anatase TiO ₂ , (b) 0.5Cur-TiO ₂ -an, (c) 3Cur-TiO ₂ -an, (d) 5Cur-TiO ₂ -an, (e) 7Cur-TiO ₂ -an and (f) curcumin powder	52
19. SEM images (10,000x) of samples for (a) uncoated P25-TiO ₂ , (b) 0.5Cur-TiO ₂ -P25, (c) 3Cur-TiO ₂ -P25, (d) 5Cur-TiO ₂ -P25, (e) 7Cur-TiO ₂ -P25, and (f) curcumin powder	53
20. SEM images of samples at various magnification for (a) uncoated amorphous TiO ₂ (15,000x), (b) uncoated amorphous TiO ₂ (50,000x), (c) 1Cur-AMO (15,000x), (d) 1Cur-AMO (50,000x), (e) 10Cur-AMO (15,000x), (f) 10Cur-AMO (50,000x), and (g) curcumin powder (50,000x)	54
21. TEM images of samples for (a) uncoated anatase TiO ₂ , (b) 5Cur-TiO ₂ -an, (c) uncoated rutile TiO ₂ , (d) 5Cur-TiO ₂ -ru, (e) uncoated P25-TiO ₂ , (f) 5Cur-TiO ₂ -P25, (g) uncoated amorphous TiO ₂ , (h) 10Cur-AMO, and (i) curcumin powder	56
22. FT-IR spectra for (a) uncoated P25 TiO ₂ , (b) 0.5Cur-TiO ₂ -P25, (c) 3Cur-TiO ₂ -P25, (d) 5Cur-TiO ₂ -P25, (e) 7Cur-TiO ₂ -P25, and (f) curcumin powder	59
23. FT-IR spectra of neat curcumin, neat P25, and mixture of curcumin + P25- TiO ₂	59
24. Elemental mapping of (a) amorphous TiO ₂ and (b) 7.5Cur-AMO	62
25. The thermograms of (a) amorphous TiO ₂ and (b) 7.5Cur-AMO	63
26. The pH _{pzc} graphs of samples (a) uncoated P25-TiO ₂ , (b) 0.5Cur-TiO ₂ -P25, (c) 3Cur-TiO ₂ -P25, (d) 5Cur-TiO ₂ -P25, and (e) 7Cur-TiO ₂ -P25	67
27. Adsorption efficiencies of TiO ₂ samples for (a) Cur-TiO ₂ -an, (b) Cur-TiO ₂ -ru, and (c) Cur-TiO ₂ -P25 with three selected dyes (1h)	69

List of Figures (Continued)

Figure	Page
28. Adsorption efficiencies of curcumin coated amorphous TiO ₂ samples with two selected dyes (1h)	70
29. Degradation efficiencies of three selected dyes under UV irradiation (5h) by uncoated and coated P25-TiO ₂ samples	72
30. Degradation efficiencies under visible light irradiation (9 h) by uncoated and coated P25-TiO ₂ samples for dyes (a) CV, (b) MB, and (c) OII	73
31. Degradation efficiencies under visible light irradiation (8 h) by uncoated and coated amorphous TiO ₂ samples for dyes (a) MB and (b) OII	74
32. Effect of pH on photodegradation efficiency under visible light irradiation of 5Cur-TiO ₂ -P25 sample	76
33. Effect of pH on photodegradation efficiency under visible light Irradiation of 7.5Cur-AMO sample	76
34. Recyclability of (a) 5Cur-TiO ₂ -an, and (b) 5Cur-TiO ₂ -P25 under visible light irradiation (9 h)	79
35. Recyclability 7.5Cur-AMO under visible light irradiation (8 h)	80

Lists of Tables

Table	Page
1. X-ray data on TiO ₂ modifications	6
2. Properties of the three modifications of TiO ₂	7
3. Physicochemical properties and application of TiO ₂ prepared by the several methods	8
4. Characteristics of curcuminoids	15
5. Classification of dye on their chemical nature	20
6. The general properties of crystal violet, methylene blue, and orange II dyes TiO ₂	22
7. Doping moieties and preparation methods of metal doped-TiO ₂ photocatalysts	29
8. Doping moieties and preparation methods of nonmetal doped-TiO ₂ photocatalysts	31
9. Some physical properties of all TiO ₂ samples	47
10. IUPAC classification of the pore	49
11. Elemental analysis of TiO ₂ samples	61

Lists of Schemes

Scheme	Page
1. Probable interaction between curcumin and TiO ₂	60
2. Schematic mechanism pathway of curcumin-TiO ₂ system (a) under UV light irradiation, and (b) under visible light irradiation	65
3. Mechanism pathways of curcumin coated TiO ₂ under visible light Irradiation	82

Chapter 1

Introduction

1.1 Background and Rationale

Environmental pollution has become an issue of serious international concern in recent years. The presence of several organic pollutants results in serious environmental problems. Dye pollutants from the textile industry are an important source of environmental contamination. Large quantities of dyes are extensively used in the fundamental processing steps of textile industries. It was estimated that *ca.* 1–15 % of the dye is lost during the dyeing processes and was released as wastewater (Zainal, *et al.*, 2005). The color, generated by these waste synthetic dyes, is usually the first contaminant to be recognized in wastewater and up to 20–50% of the dye necessary to achieve the desired depth of color is discharged to the environment (Khatri, *et al.*, 2015). Considering both volume discharged and effluent compositions, the wastewater generated by the textile industry has been rated as one of the most polluting among all industry sectors. Given the great variety of fibers, dyes, process aids, and finishing products in use, the textile industry generated wastewater of great chemical complexity, diversity and volume (Bizani, *et al.*, 2006). Synthetic dyes are extensively used in the textile industries because of their simple dyeing procedure and good stability during washing process. The release of the wastewater into the ecosystem, for instance, as much as many million gallons discharged per year to wastewater treatment systems, is a dramatic source of aesthetic pollution, eutrophication, and perturbation in aquatic life. Therefore, the removal of colored wastewater is a necessary before being released to the environmental (Sauer, *et al.*, 2002).

The traditional techniques used for color removal are filtration, charcoal, and coagulation. Each method has few advantages and disadvantages. For example, the use of charcoal is technically easy but has high waste disposal cost. Coagulation using alums, ferric salts or limes is a low cost process, but all these methods have a major disadvantage of simply transferring the pollutants from one

phase to another phase rather than destroying them and sometime the by-products may be more toxic than the dye itself. Biological treatment is a proven method and cost effective. However, it has been reported that majority of dyes are adsorbed on the sludge and very long degraded times, due to the bio-recalcitrant nature of these dye molecules. This leads to the search for highly effective method to degrade the dye into environmentally compatible products (Toor, *et al.*, 2006).

In the last decade, there has been an extensive interest in heterogeneous photocatalysis using semiconductors for the treatment of recalcitrant chemical present in the wastewater. The main advantage of the method is that the pollutants are destroyed with no requirement for secondary disposal of concentrated wastes, providing a more environmentally sustainable solution. Among the semiconductors being studied, such as TiO_2 , ZnO , Fe_2O_3 , CdS , ZnS and so on, TiO_2 has been successfully used to decolorize and mineralize many organic pollutants including several dyes and their intermediates present in aqueous systems using both artificial light and under sunlight using solar technology (Muruganandham, *et al.*, 2005). TiO_2 is the most widely used as photocatalyst because of its good activity, chemical stability, commercial availability, and inexpensiveness. It is generally used as a photocatalyst for environmental applications such as air purification, water disinfection, hazardous waste remediation, and water purification (Nagaveni, *et al.*, 2004).

However, TiO_2 is active only under ultraviolet light (UV) because of its wide band gap, ~ 3.2 eV for anatase phase and ~ 3.0 eV for rutile phase, corresponding to wavelength 388 and 410 nm, respectively. In addition, the high rate of recombination of photogenerated electron-hole pairs resulted in low photo quantum efficiency. Several approaches have been applied to optimize the photocatalyst itself in order to improve the photocatalytic activity.

In the past decades, many efforts have been devoted to extending the spectral response of TiO_2 to visible light, including energy band modulation by doping with transition metal and non-metal elements. Transition elements have many valences, hence, trace transition metal ions doped in the TiO_2 matrix can be superficial potential trap of photogenerated electron-hole pairs which can help to lengthen the lifetime of electrons and holes and increase photocatalytic activity

(Yang, *et al.*, 2004). Doping with non-metal elements is claimed to produce generally more stable photocatalyst by the appearance of high energy HOMO levels above the valence band (Suib, 2013). Unfortunately, nearly all photocatalytic studies on TiO₂ have focused their studies on the crystalline forms, as it is commonly accepted that amorphous TiO₂ contains high concentration of defects that will invariably function as rapid electron-hole pairs recombination centers to render them inactive (Ohtani, *et al.*, 1997). However, amorphous TiO₂ has one interesting property: the high surface area which can lead to high adsorptivity. Up to date, there have been only a few reports that devoted interest in amorphous TiO₂.

We have had experience involving the synthesis of amorphous TiO₂ and studied its adsorptivity with metal ions (Mn(II), Fe(III), Cu(II), Pb(II)) with possible application in solid-phase extraction (SPE). We found that amorphous form which previously thought rather inactive also showed photocatalytic properties. Furthermore, these synthesized amorphous TiO₂ showed good adsorption property towards metal ions (Randorn, *et al.*, 2004; Kanna, *et al.*, 2005).

In 2011, we successfully improved an inert amorphous TiO₂ to photoactive powder under both UV and visible light irradiation by doping with trivalent Cr and Fe ions using incipient wetness impregnation method and tested for decolorization of methylene blue, model dye pollutant. During that period, our group was also studying the metal-curcumin complexes and it was curcumin that interested us as the dye to investigate by means of dye sensitized TiO₂. Besides having been used as food coloring agent, curcumin can also be used in cloth dyeing and it would be interesting if it can be used as dye sensitizer to improve the TiO₂ performance under sunlight.

In this work, we further investigated on the photoreactivity improvement of TiO₂ under visible light irradiation particularly with the amorphous form by coating it with curcumin using impregnation method and tested it by degradation of dye pollutants.

1.2 Objectives

The objective of this work is concentrated on the improvement of photocatalytic activity under visible light irradiation of all TiO₂ forms by coating it with curcumin. The aims of this study referring are as follows:

1.2.1 To study the optimum conditions for preparing curcumin coated on all forms of TiO₂ powder by incipient wetness impregnation method.

1.2.2 To characterize the physical properties of all products using XRD, DRS, BET, TGA, SEM-EDS, and TEM techniques.

1.2.3 To evaluate the photocatalytic activity under visible light irradiation by monitoring the decolorization of methylene blue, crystal violet, and orange II which are used as model dye pollutants.

1.2.4 To study the effect of various factors, such as acidity, initial concentration of dyes solution on the photocatalytic degradation of the as-prepared coated TiO₂ powders.

1.2.5 To investigate the recyclability of coated TiO₂ products.

The results from this entire work were splitted into two parts each of which has been published as follows:

Paper I. Curcumin-sensitized crystalline TiO₂ for enhanced photodegradation of dyes under visible light irradiation published in *Journal of Nanoparticles Research*.

Paper II. Curcumin-sensitized amorphous TiO₂ for enhanced photodegradation of dyes under visible light irradiation published in *Journal of Sol-Gel Science and Technology*.

Chapter 2

Principles and literature reviews

2.1 Principles

2.1.1 Titanium dioxide

Titanium dioxide (TiO_2) also known as titanium(IV) oxide or titania, is the naturally occurring oxide of titanium. It exists in three polymorphous structures, namely, anatase, brookite, and rutile. The most common structures are anatase and rutile, since brookite is rather unstable. Both anatase and rutile are tetragonal, whereas brookite is orthorhombic. In all three oxide modifications, each titanium atom is coordinated to six almost equidistant oxygen atoms, and each oxygen atom to three titanium atoms (Clark, *et al.*, 1968). These polymorphic forms of TiO_2 are shown in Figure 1. The structure of anatase, brookite, and rutile can be discussed in term of (TiO_6^{2-}) octahedral. The three crystal structures differ by the distortion of each octahedral and by the assembly patterns of the octahedral chains. In the case of anatase, the TiO_6^{2-} octahedron is slightly distorted, with two Ti-O bonds slightly greater than the other four, and with some of the O-Ti-O bond angles deviating from 90° . The distortion is greater in anatase than rutile. The third form of TiO_2 , brookite, the interatomic distances and the O-Ti-O bond angles are similar to those of rutile and anatase. The essential difference is that there are six different Ti-O bonds ranging from 1.87 to 2.04 Å. Accordingly, there are 12 different O-Ti-O bond angles ranging from 77° to 105° . Brookite is formed by joining together the distorted TiO_6^{2-} octahedral sharing three edges. All three oxide modifications are birefringent; anatase is uniaxial negative, brookite is biaxial positive and rutile is uniaxial positive. Crystallographic data on the three oxide modifications are summarized in Table 1. Properties of the three modifications of TiO_2 are given in Table 2.

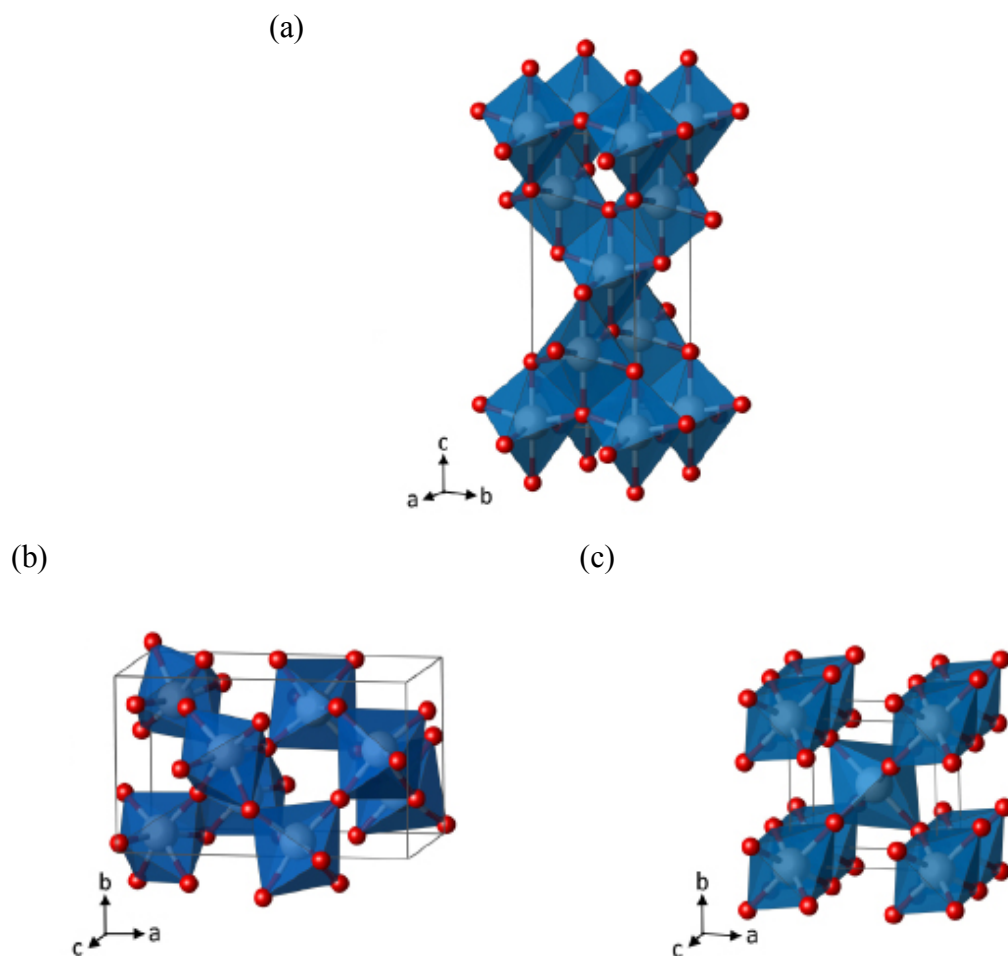


Figure 1 Crystal structures of TiO₂ (a) anatase, (b) brookite, and (c) rutile.

Table 1 X-ray data on TiO₂ modifications (Clark, *et al.*, 1968 : 268).

	Space group	Z	Cell parameters (Å)			Ti-O (Å) ^a
			A	B	C	
Anatase	$C_{4h}^{19} = C4/amc$	8	5.36	9.53		1.91(2)
						1.95(4)
Brookite	$D_{2h}^{15} = Pbca$	8	9.15	5.44	5.14	1.84-2.03
Rutile	$D_{4h}^{14} = P4_2/mnm$	2	4.954		2.959	1.944(4)
						1.988(2)

^aThe numbers in parentheses refer to the number of equivalent oxygen atoms at the stated distance from a titanium atom.

Table 2 Properties of the three modifications of TiO₂ (Clark, *et al.*, 1968 : 270).

	Anatase	Brookite	Rutile
Density (g/cm ³)	3.90	4.13	4.27
Hardness (Mohs' scale)	5.5-6.0	5.5-6.0	6.0-6.5
Melting Point (°C)	change to rutile	change to rutile	1840 ± 10
Entropy $S_{298.16}^{\circ}$ (cal/deg/m)	11.93	-	12.01
Refractive Index (25 °C) ($\lambda = 5893 \text{ \AA}$)	n_{ω} 2.5612 n_{ϵ} 2.4880	n_{α} 2.5831 n_{β} 2.5843 n_{γ} 2.7004	n_{ω} 2.6124 n_{ϵ} 2.8993
Dielectric Constant	$\epsilon = 48$ (powder)	$\epsilon = 78$	$\epsilon_{av} \approx 110$ $\epsilon_{II} = 180$ $\epsilon_{\perp} = 89$

2.1.2 Synthesis of TiO₂

TiO₂ can be prepared in various forms including powder, crystal, or thin film. Generally, TiO₂ may be manufactured by either older sulfate or newer chloride processes. On a laboratory scale, TiO₂ has been prepared by various methods, such as sol-gel method, hydrothermal method, combustion synthesis, inert-gas conversion, impregnation, and so on. The different preparation routes and the experimental conditions of TiO₂ result in products with different structures, morphology, particle size and contaminants. The physicochemical properties and application of TiO₂ prepared by several methods are summarized in Table 3.

Table 3 Some physicochemical properties and applications of TiO₂ prepared from several methods.

TiO ₂	Particle size ^a (nm)	Phase	surface area (m ² /g)	Tested application	Preparing method	Reference
TiO ₂ films	27	Anatase	43	Trichloroethylene degradation	Sol-Gel	Arconada, <i>et al.</i> , 2009
Ag/TiO ₂ films	10–40	Anatase	-	Methyl orange degradation	Sol-Gel	Hou, <i>et al.</i> , 2009
CuO-TiO _{2-x} N _x	56.8	Anatase	24	CO ₂ conversion	Sol-Gel	In, <i>et al.</i> , 2012
Fe/Nb/TiO ₂	10–13	Anatase	118-180	Methyl orange degradation	Sol-Gel	Estrellan, <i>et al.</i> , 2009
B/Ni/Ce/TiO ₂	12.7	Anatase	-	Phenol degradation	Sol-Gel	Zhang and Liu, 2008
TiO ₂ -HS ^b	500–800	Anatase	168	Rhodamine B degradation	Hydrothermal	Liu, <i>et al.</i> , 2007
TiO ₂ fibers	10–26	anatase	39-55	Sulforhodamine B degradation	Hydrothermal	Yang, <i>et al.</i> , 2009
Ag/TiO ₂ rods	L ^c : 2 μm	Rutile	-	CO ₂ conversion	Hydrothermal	Kong, <i>et al.</i> , 2013
Graphene/TiO ₂	15–30	Anatase	190	Rhodamine B degradation	Hydrothermal	Liang, <i>et al.</i> , 2010
F/Ce/TiO ₂	9	Anatase	61	Acid orange II degradation	Sonochemical	Yu, <i>et al.</i> , 2012
F/TiO ₂	1.5 μm	Anatase	160	Methylene blue degradation	Sonochemical	Yu, <i>et al.</i> , 2009
N/TiO ₂	11	Anatase	-	Direct sky blue 5B degradation	Sonochemical	Wang, <i>et al.</i> , 2011
N/TiO ₂ films	32	Anatase	-	Rhodamine B degradation	CVD ^d	Guo, <i>et al.</i> , 2007
Fe ₂ O ₃ /TiO ₂	300	Anatase	-	Methyl orange degradation	CVD ^d	Zhang and Lei, 2008

Table 3 Some physicochemical properties and applications of TiO₂ prepared from several methods. (continued)

TiO ₂	Particle size ^a (nm)	Phase	surface area (m ² /g)	Tested application	Preparing method	Reference
TiO ₂ HS ^b	2.2 μm	Anatase	174	Methyl orange degradation	Hard template	Yu, <i>et al.</i> , 2008
TiO ₂ fibers	5 μm	Anatase	79	Acetone degradation	Hard template	Yuan, <i>et al.</i> , 2006
TiO ₂ films	9–16	Anatase	-	Stearic acid degradation	Microwave	Simonsen, <i>et al.</i> , 2009
N/TiO ₂	10–20	Anatase	110-170	Phenol degradation	Microwave	Ou, <i>et al.</i> , 2011
Ag/TiO ₂ HS ^b	500	Anatase	105-130	Rhodamine B degradation	Microwave	Xiang, <i>et al.</i> , 2010
TiO ₂ HS ^b	10 μm	Anatase	28	Methyl orange degradation	Solvothermal	Lü, <i>et al.</i> , 2011
ZnO/TiO ₂ rods	L ^c : 60 μm	Rutile	225	CO ₂ conversion	Solvothermal	Xi, <i>et al.</i> , 2011
C/N/TiO ₂	9–15	Anatase	102	Bisphenol A degradation	Solvothermal	Wang and Lim, 2010
Polypyrrole/TiO ₂	20–40	Anatase	-	Methyl orange degradation	microemulsion	Sun, <i>et al.</i> , 2013
Pt/TiO ₂	50–5000	Anatase	105	Phenol degradation	microemulsion	Jiao, <i>et al.</i> , 2011

^a The particle size refers to the diameter of the prepared TiO₂ materials.

^b HS refers to the hollow sphere of prepared TiO₂.

^c L refers to length of the prepared TiO₂ materials.

^d CVD refers to the chemical vapor deposition method.

In this work the sol-gel based on base-catalysis through precipitation processes and incipient wetness impregnation method were employed for the preparation of amorphous TiO_2 and curcumin coated TiO_2 powder, respectively

(a) Sol-Gel method

The aqueous sol-gel process can shortly be defined as the conversion of a precursor solution into an inorganic solid via inorganic polymerization reactions induced by water. In general, the sol-gel process consists of the following steps as shown in Figure 2 : i) preparation of a homogeneous solution either by dissolution of metal organic precursors in an organic solvent that is miscible with water, or by dissolution of inorganic salts in water; ii) conversion of the homogeneous solution into a sol by treatment with a suitable reagent (generally water with or without any acid/base); iii) aging; iv) shaping; and v) thermal treatment/sintering. The first step in a sol-gel reaction is the formation of an inorganic polymer by hydrolysis and condensation reactions, i.e., the transformation of the molecular precursor into a highly cross linked solid. Hydrolysis leads to a sol, a dispersion of colloidal particles in a liquid, and further condensation results in a gel, an interconnected, rigid and porous inorganic network enclosing a continuous liquid phase. This transformation is called the sol-gel transition. There are two possibilities to dry the gels. Upon removal of the pore liquid under hypercritical conditions, the network does not collapse and aerogels are produced. When the gel is dried under ambient conditions, shrinkage of the pores occurs, yielding a xerogel. One of the highly attractive features of the sol-gel process is the possibility to shape the material into any desired form such as monoliths, films, fibers, and monosized powders, and subsequently to convert it into a ceramic material by heat treatment (Niederberger and Pinna, 2009).

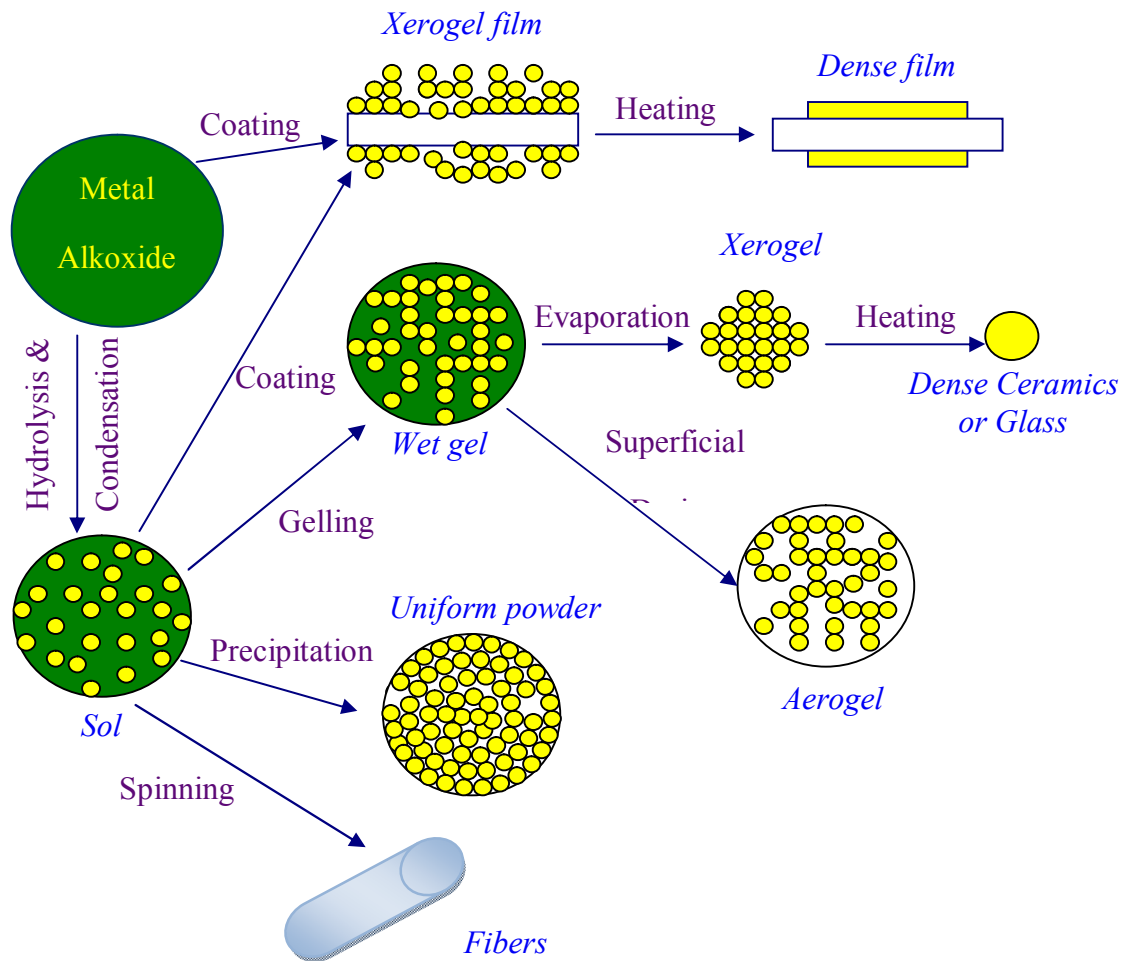
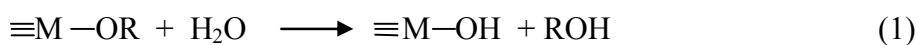


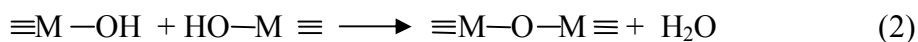
Figure 2 Various steps in the sol-gel process to control the final morphology of the product (Niederberger and Pinna, 2009).

The sol-gel conversion of metal alkoxides involves two main reaction types: hydrolysis and condensation. During hydrolysis, the alkoxide groups (-OR) are replaced via the nucleophilic attack of the oxygen atom of a water molecule under release of alcohol and the formation of a metal hydroxide, Eq. (1). Condensation reactions between two hydroxylated metal species leads to M-O-M bonds under release of water (oxolation), Eq. (2), whereas the reaction between a hydroxide and an alkoxide leads to M-O-M bonds under release of an alcohol (alkoxolation), Eq. (3).

Hydrolysis



Condensation



Alkoxolation



(b) Impregnation method

Preparative chemistry has for many years been critical to heterogeneous catalysis, defining as it does the number and type of active sites produced. One frequently used route to real heterogeneous catalysts involves impregnation of a porous solid support, using a solution of a precursor to the active phase. Impregnation is technically and superficially simple, but is in fact rather complex and multistep, involving:

- (i) Support wetting,
- (ii) Drying, and
- (iii) Calcination or reduction

Within the first of these, (i) ion-exchange/adsorption, (ii) ligands exchange reactions, and (iii) support modification and dissolution may occur to an equilibrium extent or may be kinetically defined by (i) the previous state of the support and its surface chemistry, (ii) the concentration, pH, temperature and viscosity of the impregnating solution, (iii) the chemistry of the solution species present, and (iv) the presence of any competing ions (Alexiou and Sermon, 1993).

Two types of impregnation technology, for heterogeneous catalysts, are recognized: dry and diffusion. In the former, the baking carrier is mixed with the impregnating solution containing all the required constituents. In diffusion technology, most widely adopted industrially, the impregnating solution contacts with the carrier whose pores are already filled with the solvent. The process commences with the diffusion of substances dissolved in the external solution and in the pore body.

Catalyst production consists of some stages: carrier preparation, coating the active phase constituents, drying, and baking the catalyst. The first two stages proceed in one apparatus (impregnator) at 20–100 °C. Carrier preparation involves air removal from the pores under vacuum to prevent disintegration of granules and treating it with competing substances to create adsorption centers of chemical type. This stage extends for 30–60 min. The second stage involves the adsorption of one or more constituents of the active phase on the prepared carrier in the circulation regime of the impregnating solution. When producing low-percentage catalysts, the process is carried out in gradient-free conditions with gradual dosing of concentrated solutions of active constituents into the circulation system at a rate that ensures uniform chemical composition all through the stationary carrier bed. This process extends for 30–90 min at 20–40 °C. At the end of sorption, the catalyst obtained is charged into the drying and baking system by conventional methods (Duplyakin, *et al.*, 1991).

2.1.3 Curcumin and dyes

Curcumin or diferuloylmethane, a polyphenolic diketone, is an active constituent of the spice turmeric which had long been used extensively in foods for both its flavor and color. Turmeric, in turn, was obtained from the dried rhizome of the perennial herb *Curcuma longa* L. cultivated extensively in Southeast Asia, India, China, and other countries with a tropical climate. The Latin name *Curcuma* is derived from the Arabic word, Kourkoum, which was the original name for saffron. As a consequence of its golden color and taste, *Curcuma* became known as “Indian Saffron” in Europe. *Curcuma longa* L. (German: Kurkuma, Gelbwurz(el), English: turmeric) is a member of the ginger family (Zingiberaceae), to which the genus *Zingiber*, ginger, also belongs. Curcumin is an orange-yellow pigment fraction of turmeric containing mixture of curcuminoids that are almost insoluble in water but highly soluble in organic solvents. The major components in the curcuminoid complexes are curcumin (approx. 77%), demethoxycurcumin (approx. 17%),

bisdemethoxycurcumin (approx. 3%) (Goel, *et al.*, 2008), and cyclocurcumin (Kiuchi, *et al.*, 1993) which are shown in Figure 3.

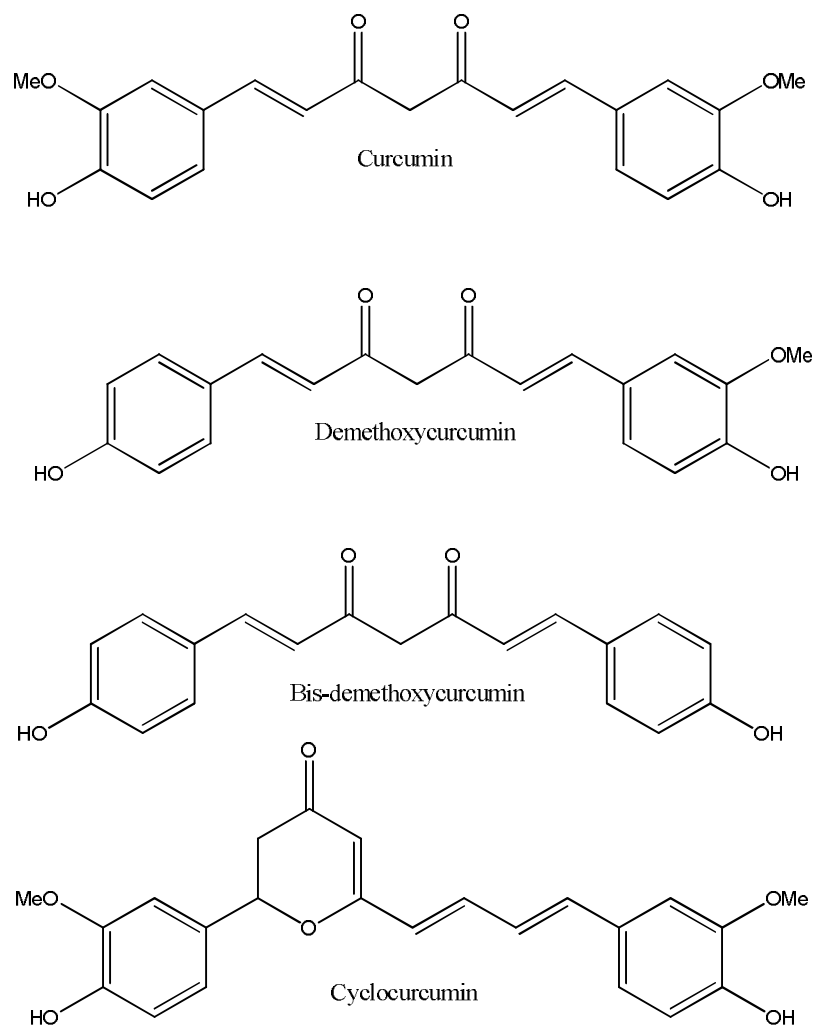
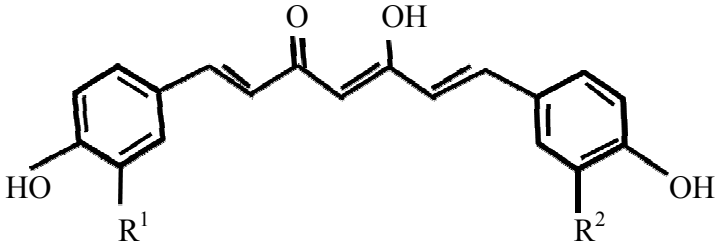


Figure 3 Structure of curcuminoids in turmeric.

The two symmetrically arranged chromophores of the structural motif $C=O-C=C$ and the conjugated double bond give curcumin its yellow color. Curcumin is most stable at pH 1–6, however, its solubility in aqueous solution is poor in this pH range. The characteristics of curcuminoid complexes are summarized in Table 4.

Table 4 Characteristics of curcuminoids.

chemical name	a) 1,7-bis-(4-hydroxy-3-methoxyphenyl)-hepta-1,6-dien-3,5-dione b) 1-(4-hydroxyphenyl)-7-(4-hydroxy-3-methoxyphenyl)-hepta-1,6-dien-3,5-dione c) 1,7-bis-(4-hydroxyphenyl)-hepta-1,6-dien-3,5-dione
C.A.S number	a) 458-37-7 b) 33171-16-3 c) 33171-05-0
molecular formula, molecular weight [g mol ⁻¹]	a) C ₂₁ H ₂₀ O ₆ , 368.39 b) C ₂₀ H ₁₈ O ₅ , 338.39 c) C ₁₉ H ₁₆ O ₄ , 308.39
chemical structure	 <p>a) curcumin : R¹ = R² = OCH₃ b) demethoxycurcumin : R¹ = H, R² = OCH₃ c) bisdemethoxycurcumin : R¹ = R² = H</p>
physical and chemical properties	
physical state	solid
color	orange-yellow (at neutral pH value)
odor	odorless
melting point	170–175 °C
flammability	nonflammable
light sensitivity	light sensitive
solubility	insoluble in water, diethyl ether acid soluble in ethanol, acetic

Turmeric has been used as a medicinal plant for thousands of years. Curcumin is well-known for its pharmaceutical applications with a potential use in therapy of many diseases such as cancer, cardiovascular disease, Alzheimer's disease, rheumatoid arthritis, and so on. Moreover, curcumin has also been used as a slow down ageing agent. Curcumin has a long history of use in food as a spice, mainly as an ingredient in many varieties of curry powders and sauces. Curcumin from turmeric is a main coloring substance known as C.I. Natural Yellow 3 which World Health Organization (WHO) and Food and Agriculture Organization (FAO) committees have approved it as a food additive (Govindarajan, 1980). Curcumin has high thermal and chemical stability, accompanied by the intense long wavelength absorption in the visible region of 420–580 nm with the extinction coefficient $20,000\text{--}50,000\text{ M}^{-1}\text{cm}^{-1}$ that would be certainly interesting as a natural dye sensitizer to extend visible light response of TiO_2 .

A dye is a colored substance that has an affinity to the substrate to which it is being applied. With regard to their solubility, organic colorants fall into two classes, dyes and pigments. The key distinction is that dyes are soluble in water and/or an organic solvent, while pigments are insoluble in both types of liquid media. Dyes are used to color substrates to which they have affinity. Pigments can be used to color any polymeric substrate but by a mechanism quite different from that of dyes. The dye is generally applied in an aqueous solution, and requires a mordant to improve the fastness of the dye on the fiber (Sharma, 2015).

Dyes can be separated as natural and synthetic dye. Natural dye covers all the dyes derived from the natural sources like plants, animal, and minerals. The first human-made (synthetic) organic dye, mauveine, was discovered by William Henry Perkin in 1856 (Holme, 2006). Many thousands of synthetic dyes have since been prepared. Synthetic dyes quickly replaced the traditional natural dyes. They cost less, they offered a vast range of new colors, and they imparted better properties upon the dyed materials.

Synthetic dyes, classified by their chromophores, have different and stable chemical structures to meet various coloring requirements (Toor, *et al.*, 2006). Dyes are now classified according to how they are used in the dyeing process (Garfield, 2000).

(a) Acid dyes

Acid dyes are water-soluble anionic dyes that are applied to fibers such as silk, wool, nylon and modified acrylic fibers using neutral to acid dye baths. Attachment to the fiber is attributed, at least partly, to salt formation between anionic groups in the dyes and cationic groups in the fiber. Acid dyes are not substantive to cellulosic fibers. Most synthetic food colors fall in this category.

(b) Basic dyes

Basic dyes are water-soluble cationic dyes that are mainly applied to acrylic fibers, but find some use for wool and silk. Usually acetic acid is added to the dye bath to help the uptake of the dye onto the fiber. Basic dyes are also used in the coloration of paper.

(c) Direct dyeing

Direct or substantive dyeing is normally carried out in a neutral or slightly alkaline dye bath, at or near boiling point, with the addition of either sodium chloride (NaCl) or sodium sulfate (Na₂SO₄). Direct dyes are used on cotton, paper, leather, wool, silk and nylon. They are also used as pH indicators and as biological stains.

(d) Mordant dyes

Mordant dyes require a mordant, which improves the fastness of the dye against water, light and perspiration. The choice of mordant is very important as different mordants can change the final color significantly. Most natural dyes are mordant dyes and there is, therefore, a large literature base describing dyeing techniques. The most important mordant dyes are the synthetic mordant dyes, or chrome dyes, used for wool; these comprise some 30% of dyes used for wool, and are especially useful for black and navy shades. The mordant, potassium dichromate, is

applied as an after-treatment. It is important to note that many mordants, particularly those in the heavy metal category, can be hazardous to health and extreme care must be taken in using them.

(e) Vat dyes

Vat dyes are essentially insoluble in water and incapable of dyeing fibres directly. However, reduction in alkaline liquor produces the water soluble alkali metal salt of the dye, which, in this leuco form, has an affinity for the textile fibre. Subsequent oxidation reforms the original insoluble dye. The color of denim is due to indigo, the original vat dye.

(f) Reactive dyes

Reactive dyes utilize a chromophore attached to a substituent that is capable of directly reacting with the fibre substrate. The covalent bonds that attach reactive dye to natural fibers make them among the most permanent of dyes. "Cold" reactive dyes, such as Procion MX, Cibacron F, and Drimarene K, are very easy to use because the dye can be applied at room temperature. Reactive dyes are by far the best choice for dyeing cotton and other cellulose fibers at home or in the art studio.

(g) Disperse dyes

Disperse dyes were originally developed for the dyeing of cellulose acetate, and are substantially water insoluble. The dyes are finely ground in the presence of a dispersing agent and then sold as a paste, or spray-dried and sold as a powder. Their main use is to dye polyester but they can also be used to dye nylon, cellulose triacetate, and acrylic fibres. In some cases, a dyeing temperature of 130 °C is required, and a pressurised dyebath is used. The very fine particle size gives a large surface area that aids dissolution to allow uptake by the fibre. The dyeing rate can be significantly influenced by the choice of dispersing agent used during the grinding.

(h) Azo dyeing

Azo dyeing is a technique in which an insoluble azoic dye is produced directly onto or within the fibre. This is achieved by treating a fibre with both diazoic and coupling components. With suitable adjustment of dye bath conditions the two components react to produce the required insoluble azo dye. This technique of dyeing is unique, in that the final color is controlled by the choice of the diazoic and coupling components.

(i) Sulfur dyes

Sulfur dyes are the most commonly used dyes manufactured for cotton in terms of volume. They are cheap, generally have good wash-fastness and are easy to apply. The dyes are absorbed by cotton from a bath containing sodium sulfide or sodium hydrosulfite and are made insoluble within the fiber by oxidation.

There are several ways for classification of commercial dyes. It can be classified in terms of structure, color and application methods. However, due to the complexities of the color nomenclature from the chemical structure system, the classification based on application is often favorable. Other than the above, dyes are also usually classified based on their particle charge upon dissolution in aqueous application medium such as cationic (all basic dyes), anionic (direct, acid, and reactive dyes), and non-ionic (dispersed dyes).

The classification and the different applications based on chemical nature for the common class of the dyes are presented in Table 5.

Table 5 Classification of dye on their chemical nature (Yagub, *et al.*, 2014).

Class	Substrate	Method of application	Chemical types
Acid	Wool, nylon, silk, inks, and paper	Generally from neutral to acidic bath.	Anthraquinone, wanthene, azo (including, nitroso, premetallised), nitro, and triphenylmethane.
Basic	Inks, paper, polyacrylonitrile, treated nylon, and polyester	Applied from acidic dye baths.	Hemicyanine, azo, cyanine, diazahemicyanine, xanthenes, triarylmethane, and acridine,
Direct	Nylon, rayon, paper, leather and cotton	Applied from neutral or a little alkaline bath containing additional electrolyte.	Phthalocyanine, azo, oxazine and stilbene.
Disperses	Polyamide, acrylic polyester, acetate, and plastics	Fine aqueous dispersions often applied by high temperature/pressure or lower temperature carrier methods; dye may be padded on cloth and thermo fixed.	Benzodifuranone, azo, nitro, anthraquinone, and styryl.
Reactive	Wool, cotton, silk, inks, and nylon	Reactive site on dye reacts with functional group on fiber to bind dye covalently under influence of heat and pH.	Anthraquinone, formazan, phthalocyanine, azo, oxazine and basic.
Sulphur	Rayon and cotton	Aromatic substrate vatted with sodium sulphide and reoxidised to insoluble sulphur-containing products on fiber.	Indeterminate structures
Vat	Wool and cotton.	Water-insoluble dyes solubilised by dropping in sodium hydrogen sulphite, then exhausted on reoxidised and fiber.	Indigoids and anthraquinone.

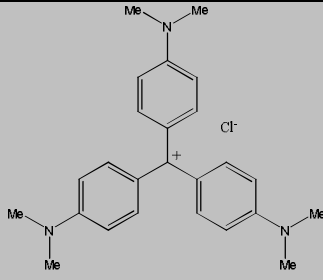
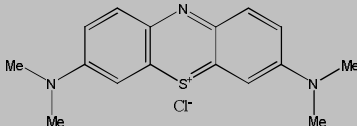
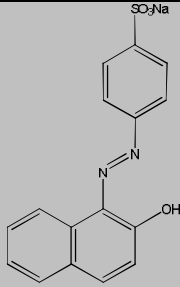
In the present entire work, crystal violet, methylene blue, and orange II were selected as a model of the dye pollutant with which the degradation efficiencies of the as-prepared catalysts are to be investigated. For publication, all three dyes were selected for degradation testing in **Paper I**, whereas in **Paper II** was used methylene blue and orange II for degradation testing.

Crystal violet (CV) is a triarylmethane dye. The dye is used as a histological stain and in Gram's method of classifying bacteria. CV has antibacterial, anti fungal, and anthelmintic properties and was formerly important as a topical antiseptic. The medical use of the dye has been largely superseded by more modern drugs, although it is still listed by the World Health Organization. When dissolved in water, the dye has a blue-violet color with an absorbance maximum at 590 nm and an extinction coefficient of $87,000 \text{ M}^{-1}\text{cm}^{-1}$. The color of the dye depends on the acidity of the solution. At a pH of 1.0 the dye is green with maximum absorption at 420 nm and 620 nm while in a strongly acidic solution (pH of -1), the dye is yellow with maximum absorption at 420 nm.

Methylene blue (MB), is a brightly colored blue cationic thiazine dye, with λ_{max} values at 665, 614 and 292 nm. It has many uses in a range of different fields such as biology and chemistry. The uses of MB include being an antidote for cyanide poisoning in humans, antiseptic in veterinary medicine and, most commonly, in vitro diagnostic in biology, cytology, hematology and histology, it used as redox indicators in analytical chemistry. At room temperature it appears as a solid, odorless, dark green powder that yields a blue solution when dissolved in water (Mills and Wang, 1999).

Orange II (OII), synonymous with Acid Orange, is an anionic mono-azo dye of acid class with the molecular formula $\text{C}_{16}\text{H}_{11}\text{O}_4\text{N}_2\text{SNa}$ which is soluble in water with a maximum absorbance at 483 nm and it has a tautomeric structure, azo and hydrazone forms (Daneshvar, *et al.*, 2008). OII is widely used in dyeing, weaving, tanning and paper industries causing a lot of healthy and environmental problems. The general properties of the selected dyes in this work are summarized in Table 6.

Table 6 The general properties of crystal violet, methylene blue, and orange II dyes.

	Crystal violet	Methylene blue	Orange II
Molecular structure			
Structure type	Cationic dye	Cationic dye	Anionic dye
Chemical name	Tris(4-(dimethylamino)phenyl) methylum chloride	3,7-bis(Dimethylamino)-phenothiazin-5-ium chloride	Sodium 4-[(2-hydroxy-1-naphthyl)azo]benzene sulfonate
Molecular formula	$C_{25}H_{30}ClN_3$	$C_{16}H_{18}N_3SCl$	$C_{16}H_{11}O_4N_2SNa$
Molecular weight (g mol⁻¹)	407.98	319.85	350.32
λ_{max} (nm)	590	665	483
Melting point (°C)	205	100-110	164
Physical state	odorless, dark-blue powder	odorless, dark green powder	odorless, orange powder
Solubility	water soluble, 16 g/L (25°C)	water soluble, 40 g/L (20°C)	water soluble, 116 g/L

(2) Treatments of dye pollutant

Traditional wastewater treatment technologies have proven to be markedly ineffective for handling wastewater of synthetic textile dyes because of the chemical stability of these pollutants. A wide range of methods has been developed for the removal of synthetic dyes from waters and wastewaters to decrease their impact on the environment. Removal of color in wastewater generated by the textile industries is color issue of discussion and regulation all over the world. Among the relative dyes, the textile azo dyes with synthetic intermediates as contaminant and its degradation products have undoubtedly attracted the most attention with regard to high environmental impact, because of their widespread use, their potentiality to form toxic aromatic products (carcinogenicity and mutagenicity properties) and their low removal rate during primary and secondary treatment. They represent about 50% of the worldwide production and correspond to an important source of contamination considering that a significant part of the synthetic textile dyes are lost in waste streams during manufacturing or processing operations. Therefore, it is important to develop effective wastewater remediation technologies for these compounds (Senthikumaar, *et al.*, 2005).

Various chemical and physical treatment processes are currently proposed for these dyes. These largely fall into the categories of direct precipitation or elimination by adsorption, flocculation, membrane separation, coagulation and chlorination (Da browski, 2001; Fu and Viraraghavan, 2001). These methods have been largely incomplete and ineffective because the problem is not completely resolved, still being required further treatment. A number of biological processes, such as sequenced anaerobic/aerobic digestion, have been proposed in the treatment of textile wastewater, but they are limited due to the fact that many of the dyes are xenobiotic and non-biodegradable. Alternative methods based on advanced oxidation processes combining ultraviolet irradiation and oxidative agents for dye treatment have been also investigated, but the presence of intermediates arising from the photodegradation reaction could be more harmful than the pollutant itself (Robinson, *et al.*, 2001). The treatment processes of synthetic dye from wastewater are summarized in Figure 4.

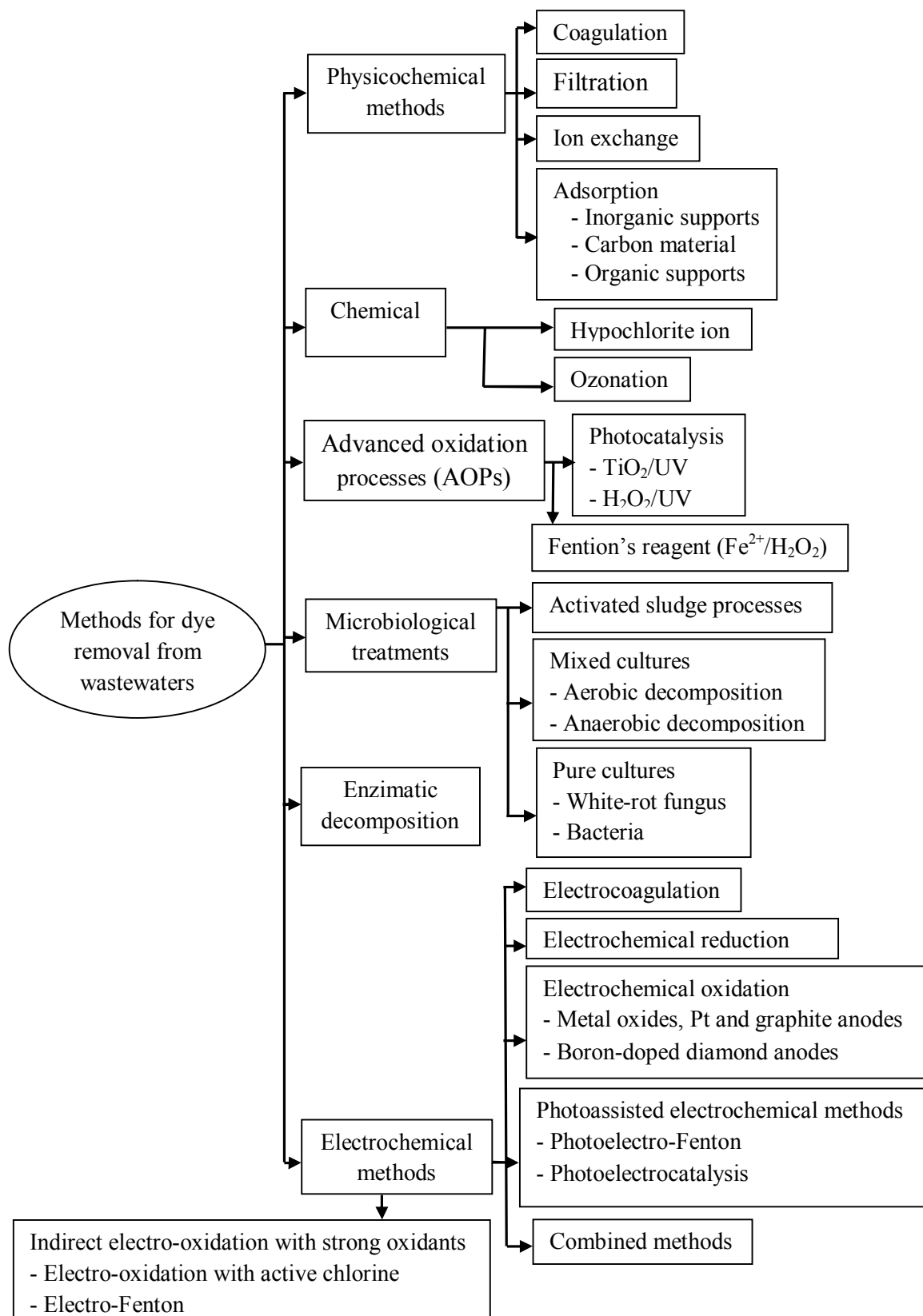


Figure 4 Main methods applied to the removal of synthetic dyes from wastewaters (Brillas and Martínez-Huitle, 2015).

In recent years attention has been focused on heterogeneous photocatalysis for the treatment of recalcitrant chemical present in the wastewater. Among these heterogeneous photocatalysis in the presence of irradiated semiconductors (TiO_2 , WO_3 , SnO_2 , ZnO , CdS , and others), TiO_2 has been successfully used to decolorize and mineralize many organic pollutants including several dyes and their intermediates present in aqueous systems using both artificial light and under sunlight using solar technology (Muruganandham, *et al.*, 2005). TiO_2 is the most widely used photocatalyst because of its good activity, chemical stability, commercial availability and inexpensiveness. It is generally used as a photocatalyst for environmental applications such as air purification, water disinfection, hazardous waste remediation and water purification (Nagaveni, *et al.*, 2004).

The efficiency of advanced oxidation processes for degradation of recalcitrant compounds has been extensively documented. Photochemical processes are used to degrade toxic organic compounds to CO_2 and H_2O without the use of additional chemical oxidants, because the degradation is assisted by high concentrations of hydroxyl radicals (OH^\bullet) generated in the process. In this case, the photoexcitation of TiO_2 particles promotes an electron from the valence band to the conduction band, generating an electron/hole pair. Both reductive and oxidative processes can occur at or near the surface of the photoexcited TiO_2 particle. In general, oxygen is used to scavenge the conduction band electron, producing a superoxide anion radical ($\text{O}_2^{\bullet-}$), effectively preventing electron/hole recombination, and prolonging the lifetime of the hole. The photogenerated hole has the potential to oxidize several substrates by electron transfer. In aqueous solutions, oxidation of water to hydroxyl radical by the photogenerated hole appears to be the predominant pathway. Hydroxyl radicals and, to a lesser extent, superoxide anion can act as oxidants, ultimately leading to the mineralization of organic compounds (Gomes de Moraes, *et al.*, 2000).

The mineralization of most of the organic pollutants could be degraded following the usually proposed mechanism, Eqs. (4)-(12) (Houas, *et al.*, 2001), for the heterogeneous photocatalytic oxidation processes as shown in Figure 5.

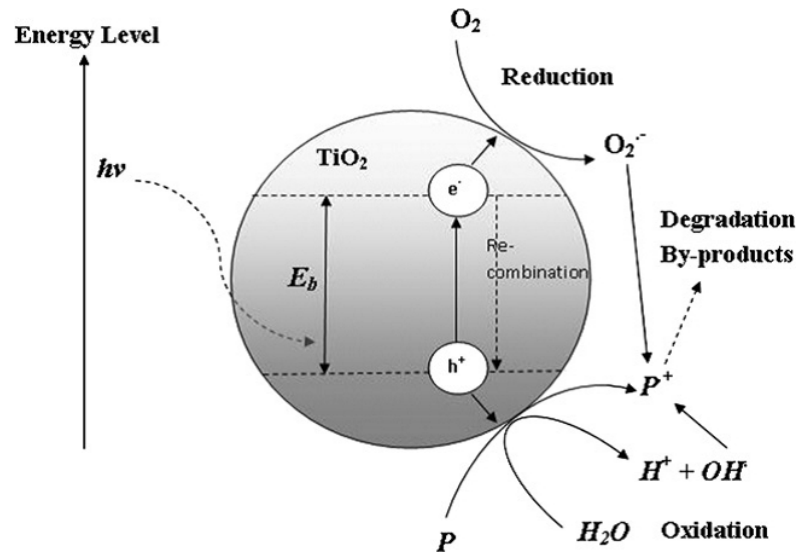


Figure 5 Mechanism of electron-hole pair formation in a TiO₂ particle in the presence of pollutant in water (Umar and Aziz, 2013).

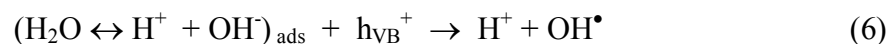
1. Absorption of efficient photons ($h\nu > E_g = 3.2 \text{ eV}$) by titania



2. Oxygen ionosorption (first step of oxygen reduction; oxidation state of oxygen changes from 0 to -1/2)



3. Neutralization of OH⁻ groups by photoholes which produces OH[•] radicals



4. Neutralization of O₂^{•-} by protons



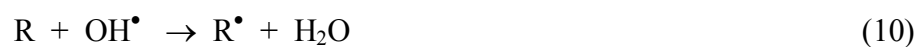
5. Transient hydrogen peroxide formation and dismutation of oxygen



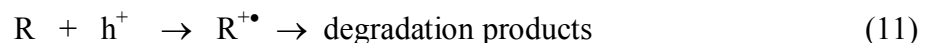
6. Decomposition of H₂O₂ and second reduction of oxygen



7. Oxidation of the organic reactant via successive attacks by OH[•] radicals



8. Direct oxidation by reaction with holes



As an example of the last process, holes can react directly with carboxylic acid generating CO_2



In most cases, the degradation is conducted for dissolved compounds in water with UV-illuminated TiO_2 . The possible extents of the technique concern the irradiation source and the physical state of the pollutant. Recently, many works have been reported on the degradation of organic dyes induced by visible light by photosensitization. The interest is to use solar visible light which is free and inexhaustible (Houas, *et al.*, 2001).

2.2 Literature reviews

In the many decades, since Fujishima and Honda discovered the possibility of water splitting by means of photoelectrochemical cell using TiO_2 (Fujishima and Honda, 1972) and Frank and Bard first examined the possibilities of using TiO_2 to decompose cyanide in water (Frank and Bard, 1977), there has been an increasing interest in environmental applications. Photocatalytic reactions at the surface of TiO_2 have been attracting much attention in view of their practical applications to environmental cleaning. Despite TiO_2 shows relatively high reactivity and chemical stability under UV light, $\lambda < 388 \text{ nm}$, whose energy exceeds the band gap of 3.20 eV in the anatase crystalline phase, the efficiency of solar energy harvesting is substantially limited due to its wide band gap, which allows only a small fraction of the solar spectrum to be absorbed. Due this, various semiconductors with smaller band gaps have been studied as potential candidates for visible light photocatalysis but so far TiO_2 remains as the benchmark for photocatalysts. A major advantage of TiO_2 is its good stability. Usually the smaller band gap materials are less stable and more prone to photocorrosion. In addition, the locations of the valence and conduction band edges in TiO_2 are suitable for photocatalysis. Several approaches attempts to change the spectral response of TiO_2 into the visible range by: metal-ion implanted TiO_2 (using transition metals: Cu, Co, Ni, Cr, Mn, Mo, Nb, V, Fe, Ru, Au, Ag, Pt),

non-metal doped-TiO₂ (N, S, C, B, P, I, F). In order to the photoreactivity of metal-doped TiO₂ can be explained by a new energy level produced in the band gap of TiO₂ by the dispersion of metal nanoparticles in the TiO₂ matrix. Additional benefit of transition metal doping is the improved trapping of electrons to inhibit electron-hole recombination during irradiation. Decrease of charge carriers recombination results in enhanced photoactivity (Zaleska, 2008).

The modification mechanism of anatase doped with nonmetals was also analyzed by Zhao and Liu (Zhao and Liu, 2008). They investigated N-TiO₂ and concluded that TiO₂ doped with substitutional nitrogen has shallow acceptor states above the valence state. In contrast, TiO₂ doped with interstitial nitrogen has isolated impurity states in the middle of the band gap. These impurity energy levels are mainly hybridized by N 2p states and O 2p states.

There are three different main opinions regarding modification mechanism of TiO₂ doped with nonmetals. (1) Band gap narrowing, (2) Impurity energy levels, and (3) Oxygen vacancies (Zaleska, 2008).

(1) Band gap narrowing: Asashi, *et al.*, (2001) found N 2p state hybrids with O 2p states in anatase TiO₂ doped with nitrogen because their energies are very close, and thus the band gap of N-TiO₂ is narrowed and able to absorb visible light.

(2) Impurity energy level: Irie, *et al.*, (2003) stated that TiO₂ oxygen sites substituted by nitrogen atom form isolated impurity energy levels above the valence band. Irradiation with UV light excites electrons in both the VB and the impurity energy levels, but illumination with visible light only excites electrons in the impurity energy level.

(3) Oxygen vacancies: Ihara, *et al.*, (2003) concluded that oxygen-deficient sites formed in the grain boundaries are important to emerge visible-activity and nitrogen doped in part of oxygen-deficient sites are important as a blocker for reoxidation.

Some doping moieties and preparation methods of doped-TiO₂ photocatalysts are given in Tables 7–8.

Table 7 Doping moieties and preparation methods of metal doped-TiO₂ photocatalysts.

Dopant	Preparation method	Potential application	References
Au	Titanium (IV) butoxide dissolved in absolute ethanol was added to solution containing tetrachloroauric acid, acetic acid, and ethanol. The resulting suspension was aged (2 days), dried under vacuum, ground and calcinated at 650°C.	Wastewater decoloring	Li, <i>et al.</i> , 2001
Pt	Photoreduction process: TiO ₂ was suspended in a mixture of hexachloroplatinic acid in methanol. The suspension was irradiated with a 125 W mercury lamp (60 min.). Pt-TiO ₂ was separated by filtration, washed with distilled water, and dried at 100°C for 24 h.	Wastewater decoloring	Li, <i>et al.</i> , 2002
V	Sol-gel method: Solution 1 (vanadyl acetylacetonate dissolved in n-butanol) was mixed with solution 2 (acetic acid in titanium butoxide) and hydrolyzed (24 h) by the water generated via the esterification of acetic and butanol. The suspension as dried at 150°C, pulverized, and calcined at 400°C for 0, and 5 h.	Wastewater decoloring	Wu and Chen, 2004
Fe	The reactive magnetron sputtering method: 99.99% titanium target and 99.9% iron pieces were placed in the reaction chamber and mixture of argon and oxygen was introduced into the chamber during discharging.	Wastewater decoloring	Carneiro, <i>et al.</i> , 2005

Table 7 Doping moieties and preparation methods of metal doped-TiO₂ photocatalysts (continued).

Dopant	Preparation method	Potential application	References
Ag	Silver nitrate was mixed with reduction agent (sodium citrate tribasic dihydrate) and the temperature was raised to 80°C with continuous stirring. Then TIP and HNO ₃ were added and the reaction was maintained at 50°C for 24 h. The prepared sol was dried at 105°C for 24 h and calcined at 300°C.	Degradation of nitrophenol in aqueous phase	Lee, <i>et al.</i> , 2005
V, Mn, Fe, Cu, Ce, W	Sol-gel processes; titanium isopropoxide was used as TiO ₂ precursor. Surface-doped TiO ₂ powders were prepared by coating the as-dried TiO ₂ powders with a thin doped TiO ₂ film. The TiO ₂ powders were dispersed in a coating solution that contains TTIP and transition metal ions in IPA at a molar ratio of M/TTIP/IPA= 0.2/1.0/1200.	Wastewater decoloring	Chang and Liu, 2014
V, Cr, Mn, Rh Co, Mo,	TiO ₂ nanowire catalysts were prepared using a molten-salt synthesis method at 825°C. Eutectic salt mixtures with appropriate compositions were used to prepare the catalysts. Transition metal dopants were added during the synthesis of the TiO ₂ nanowires to tune the catalytic activities of the TM-doped TiO ₂ (TM-TiO ₂) nanowires.	Catalytic oxidative coupling of methane	Yunarti, <i>et al.</i> , 2014
Sr	Ultrasonic-hydrothermal method and post calcination treatments of Ti(BuO) ₄ and Sr(NO ₃) ₂ at 450°C for 2 h.	Wastewater decoloring	Sood, <i>et al.</i> , 2015

Table 8 Doping moieties and preparation methods of nonmetal doped-TiO₂ photocatalysts.

Dopant	Preparation method	Potential application	References
N	Treating anatase TiO ₂ powder ST01 in the NH ₃ (67%)/Ar atmosphere at 600°C for 3 h.	Photooxidation of acetaldehyde	Asahi, <i>et al.</i> , 2001
	Titanium nitride (TiN) oxidation : Heating of TiN at 450–550°C for 2h in air (heating and cooling temperature rate: 2°C/min).	Photooxidation of aromatic compounds	Wu, <i>et al.</i> , 2008
	Mixture of Ti(OPr) ₄ , dodecylamine, and ethanol was refluxed for 4 h at 70°C to provide a clear solution. Then cooled to room temperature and CH ₃ COOH was added to neutralize the excess of dodecylamine.	Dye-sensitized solar cell	Kusumawardani, <i>et al.</i> , 2010
S	Oxidation annealing of titanium disulfide (TiS ₂) at 300–600°C.	Wastewater decoloring	Takeshita, <i>et al.</i> , 2006
N, S	Hydrolysis of Ti(SO ₄) ₂ in NH ₃ solution. Precipitate was centrifuged, washed with distilled water and alcohol. Obtained gels were dried under vacuum at 80 °C for 10 h and were ground to xerogel then calcinated at 400–800°C, 3 h.	Photooxidation of volatile compounds in gas phase	Yu, <i>et al.</i> , 2006
	TiCl ₄ and CS(NH ₂) ₂ or CO(NH ₂) ₂ were mixed with deionized water in a sealed Pyrex autoclave. The autoclave was heated up to 190 °C, and kept for 24 h, Finally, the products were separated by centrifugation, and washed with deionized water and alcohol three times, then dried at 80°C for 4 h.	Wastewater decoloring	Asiri, <i>et al.</i> , 2014

Table 8 Doping moieties and preparation methods of nonmetal doped-TiO₂ photocatalysts (continued).

Dopant	Preparation method	Potential application	References
N-F, S, C	Implantation and sol-gel method using a nonionic fluorosurfactant Zonyl (FS) and fluorine source combined with ethylenediamine as nitrogen source.	Wastewater decoloring	Likodimos, <i>et al.</i> , 2013
B	Anatase TiO ₂ powder (ST01) was grinding with boric acid triethyl ester and calcinated in air at 450°C.	Photooxidation of phenol compounds in aqueous phase	Zaleska, <i>et al.</i> , 2007
C	Acid-catalyzed sol-gel process. Alkoxidide precursor was dissolved in corresponding alcohol, mixed with hydrochloric acid aqueous solution. Obtained gel was aged for several days and calcinated in air (3 h at 65°C and 3 h at 250°C) and grounded.	Photooxidation of phenol compounds in aqueous phase	Lettmann, <i>et al.</i> , 2001
	Sol-gel method : TBOT was hydrolyzed in the presence of ethanol, water and nitric acid; precipitated titanium hydroxide was dried at 110°C and calcinated in air at 150-200°C.	Degration of Nox; wastewater decoloring	Treschev, <i>et al.</i> , 2008
N, F	Hydrothermal method; Ti(SO ₄) ₂ was dissolved in HF solution and then a certain amount of 25–28% NH ₃ ·H ₂ O was added under strong stirring for 1 h until it was well distributed, then centrifuged, washed, and dried at 80 °C.	Wastewater decoloring	Cheng, <i>et al.</i> , 2015

All of prior photocatalytic studies on TiO₂ focused on the crystalline forms, as it has been commonly accepted that amorphous TiO₂ contains high concentration of defects that will invariably function as rapid electron-hole pairs recombination centers to render them inactive (Ohtani, *et al.*, 1997). However, amorphous TiO₂ has one interesting property: the high surface area which can lead to high adsorptivity.

Up to date, there have been only a few reports that showed interest in amorphous TiO₂.

Randorn, *et al.*, (2004) prepared hydrated TiO₂ (h-TiO₂) powder by hydrolysis of TiCl₄ with concentrated NH₃ solution and studied the photocatalytic activity with MB dye under UV light irradiation. Moreover, investigation was extended to the effect of H₂O₂ on photodecomposition of MB. The synthesized powder was studied using XRD, FT-IR, BET, and TGA techniques. The results indicated that TiO₂ existed in amorphous form with some hydrated molecules. Due to its considerably high surface area, h-TiO₂ could adsorb a large amount of MB on its surface, about nine times as much of Degussa P25. It could photocatalyze the decomposition of MB, albeit slightly inferior to Degussa P25 if adsorption is excluded. In the presence of dilute H₂O₂ and with UV light, h-TiO₂ bleached methylene blue as good as Degussa P25. However, under similar conditions, but without UV light, h-TiO₂ bleached methylene blue much better than Degussa P25.

Kanna, *et al.*, (2005) studied the adsorptivity of some transition metal ions (Mn(II), Fe(III), Cu(II), and Pb(II)) on amorphous TiO₂ powder. TiO₂ was prepared from TiCl₄ and diluted ammonia solution at low temperature. The product obtained was characterized by XRD, EDXRF, TGA, DSC, and FT-IR techniques. It was found that the product was in the form of hydrated amorphous TiO₂, TiO₂·1.6H₂O (ha-TiO₂). The ha-TiO₂ exhibits high BET surface area at 449 m²/g. Adsorptions of metal ions onto the ha-TiO₂ surface were investigated in the batch equilibrium experiments, using Mn(II), Fe(III), Cu(II), and Pb(II) solutions. The concentrations of metal ions were determined by atomic absorption spectrometer. The adsorption isotherms of all metal ions were studied at pH 7. The adsorption of Mn(II), Cu(II), and Pb(II) ions on ha-TiO₂ conformed to the Langmuir isotherm while that of Fe(III) fit equally well to both Langmuir and Freundlich isotherms.

Zhang and Maggard, (2007) investigated photocatalytic activity of amorphous TiO₂ powder by measuring the H₂ produced in methanol solutions under Xe arc lamp. TiO₂ has obtained starting from Ti(*n*-butoxide)₄ in ethanol, acetone, hexane or tetrahydrofuran solutions by either slow evaporation (TiO₂-A1) or from rapid precipitation in an aqueous HCl solution using ammonia (TiO₂-A2). The samples were characterized by using PXRD, SEM, TGA, DRS, GC, and FT-IR techniques. The washed products lost/reabsorbed water up to a maximum of 19 wt% for samples of TiO₂-A1 and 9.9 % for TiO₂-A2, and exhibited an optical band gap of ~3.5 eV. Under full spectrum irradiation in aqueous of methanol solutions, the photocatalytic rates for H₂ production reached a maximum of 314 and 1,158 μmol h⁻¹ g⁻¹ for bare and platinized (0.5 wt%) samples of TiO₂-A1, respectively, and 210 and 170 μmol h⁻¹ g⁻¹ for TiO₂-A2. The photocatalytic rates measured at a slightly elevated temperature of 58 °C were up to 2 times greater than those measured nearer room temperature, while these rates were independent of the amount or type of solvent used in their preparation. The UV-vis diffused reflectance, post irradiation, indicated a higher concentration of Ti³⁺ sites in TiO₂-A1 compared to TiO₂-A2, and thus a higher density of active sites and reduced electron–hole recombination.

Li, *et al.*, (2008) studied adsorption and degradation of the cationic dyes over Co doped amorphous mesoporous titania–silica catalyst under UV and visible light irradiation. Undoped and Co doped TiO₂ were prepared as follows: 5.0 g of cetyltrimethyl-ammonium bromide (CTAB) was added to 66 mL solution containing 1.0 g sodium hydroxide. Then, 10 mL of tetraethylorthosilicate (TEOS) was added to it slowly to yield a clear gel, finally, the cobalt precursor (Co(NO₃)₂•6H₂O) and titanium tertraisopropoxide (TTIP) were alternatively and slowly added to the above gel and stirred for 2 h. The resulting gel was transferred into a Teflon bottle and treated under autogenous pressure without stirring at 363 K for 7 days. The final solid product was filtered, dried, and calcined at 723 K for 24 h. The final product was denoted as Co-TiO₂-SiO₂. The catalyst was characterized by a combination of various physicochemical techniques, such as N₂ physisorption, diffused reflectance UV-vis, X-ray diffraction, and FT-IR. The photodegradation of six cationic dyes (gentian violet, methyl violet, methylene blue, fuchsin basic, safranin T, and Rhodamine B) were studied under UV and visible light illumination.

Co-TiO₂-SiO₂ exhibited activity under UV light and had better activity under visible light when compared with that of Degussa P25. The activity of Co-TiO₂-SiO₂ was also compared with that of Co-MCM-41, Co doped mesoporous titania with a crystalline framework (Co-MTiO₂) and titania-loaded Co doped MCM-41 (TiO₂/Co-MCM-41) for the degradation of gentian violet under visible light irradiation. It was also found that the degradation rates of Co-TiO₂-SiO₂ for gentian violet, methyl violet, methylene blue, fuchsin basic and safranin T were greater in alkaline media than in acid and neutral media, while it did not exhibit any significant activity for the photodegradation of Rhodamine B in alkaline media or in acid media under visible light irradiation.

Recently, we reported doped amorphous TiO₂ with either Cr(III) or Fe(III) and studied photoreactivity with dye degradation under visible light irradiation with aimed application in environmental remediation (Buddee, *et al.*, 2001). During that period, some members of our group were studying metal-curcumin complexes and it was curcumin that interested us as the next dye to investigate.

However, reports of curcumin as sensitizer are scarce. Among those few, Ganesh, *et al.*, 2010 reported that curcumin-derived dye could be used as a sensitizer in dye sensitized solar cells. Furthermore, at the same time, Singh *et al.*, 2010 studied on the use of TiO₂ nanoparticles to photodegrade curcumin stain on fabric. In the most recent report, Shao, *et al.*, 2015 doped amorphous TiO₂ with carbon using benzyl alcohol as source of carbon. The method required heating to destroy benzyl alcohol to carbon which was believed to interstitially mixed with amorphous TiO₂.

In this entire work, we focused on trying to turn inactive amorphous TiO₂ to an active form (**Paper II**) and to improve photoreactivity of crystalline TiO₂ by coating with curcumin molecules (**Paper I**) by the sol-gel and incipient wetness impregnation processes. The surface morphology was studied by using scanning electron microscopy (SEM) and transmission electron microscopy (TEM). The X-ray diffraction (XRD) was used to study crystalline phase identification and confirmed structures of TiO₂ samples. The effect of various parameters such as coating agent concentrations was studied to optimize the preparation of curcumin coated TiO₂ for maximum photocatalytic degradation of the selected dyes in aqueous solutions under

visible light irradiation. We hoped that the inclusion of this coating agent might improve the photocatalytic properties of TiO₂ when activated with visible light which is more preferred as it would be useful in real life applications with lower cost of operation.

Chapter 3

Results and Discussion

3.1 Syntheses of products

Amorphous TiO₂

In the present study, the fresh uncoated amorphous TiO₂ was synthesized from reaction between TiCl₄ and diluted NH₃ solution via base-catalyzed sol-gel method at low temperature. Amorphous TiO₂ exists as a white powder solid as shown in Figure 6 while the commercial TiO₂, anatase (Carlo Erba), rutile (R706, TOA), and Degussa P25, which were also used as uncoated TiO₂ powders represented crystalline TiO₂ are shown in Figure 7(a)-(c).



Figure 6 The photograph of synthesized TiO₂ powder.

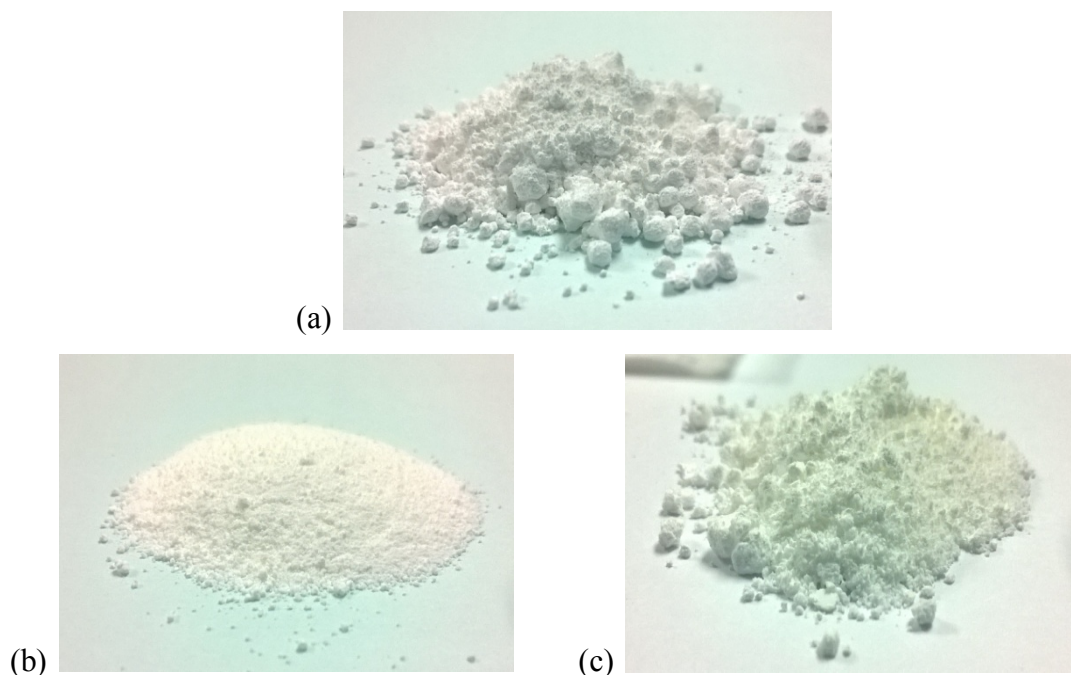
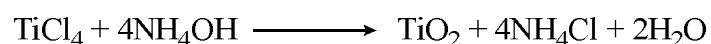


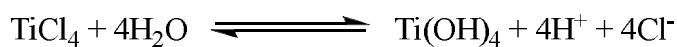
Figure 7 The photograph of uncoated commercial TiO_2 powders (a) anatase (Carlo Erba), (b) rutile (R706, TOA), and (c) Degussa P25.

During the synthesis process by sol-gel route, white precipitate formed and large amount of white smoke due to the formation of HCl were observed. The synthesis can be described by the following chemical reaction (Kanna, 2002);

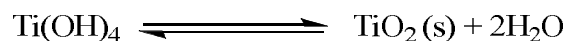


Generally, the sol-gel process consists of two sub-reactions, hydrolysis and condensation reactions. The hydrolysis reaction leads to the formation of original nuclei of TiO_2 whereas the condensation reaction leads to the growth of network system of original nuclei (Kumar, *et al.*, 1999). In the present work, the synthesis of TiO_2 route base-catalyzed sol-gel method can be explained in term of the hydrolysis and the condensation reactions as (Suwanachawalit, 2005);

The hydrolysis reaction :



The condensation reaction :



The resulting powder existed in an amorphous form because the condensation started before completion of the hydrolysis (Tang, *et al.*, 2002). Along the hydrolysis reaction, white smoke of HCl and heat occurred. Then the thermal from hydrolysis reaction accelerated condensation reaction. The reaction was carried out at low temperature, in the ice-bath, to avoid and reduce the strong reactions between TiCl₄ and NH₄OH.

Curcumin coated TiO₂

Curcumin coated TiO₂ samples were prepared by modified wet impregnation method using freshly prepared curcumin solution and TiO₂ powder. For **Paper I**, which interested in crystalline TiO₂, the resulting products designated as *x*Cur-TiO₂-an, *x*Cur-TiO₂-ru and *x*Cur-TiO₂-P25, for curcumin coating on anatase, rutile, and Degussa P25-TiO₂ (80% anatase and 20% rutile), respectively. In **Paper II**, the obtained powders designated as *x*Cur-AMO for curcumin coating on synthesized amorphous TiO₂ where *x* represents nominal curcumin content, 0.5–7 wt% and 1–10 wt% for curcumin coated crystalline TiO₂ (Cur-TiO₂) and curcumin coated amorphous TiO₂ (Cur-AMO), respectively. The photographs of prepared products are shown in Figure 8(a)-(d).

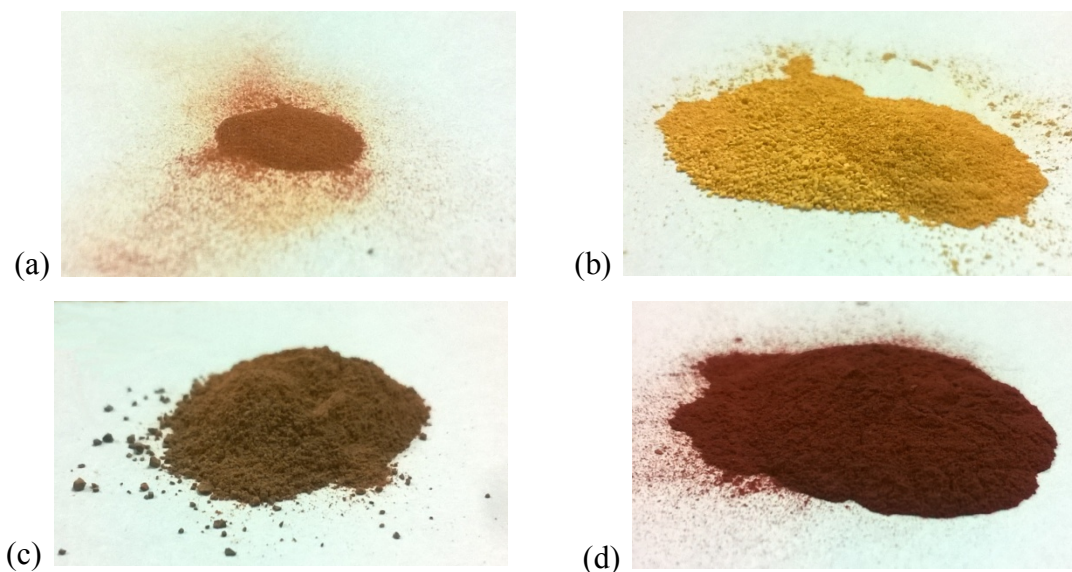


Figure 8 The photographs of coated TiO_2 powders; (a) 5Cur- TiO_2 -an, (b) 5Cur- TiO_2 -ru, (c) 5Cur-P25, and (d) 7.5Cur-AMO.

It can be seen that the coated TiO_2 products appear as yellowish to brownish powders due to an impregnation of curcumin onto TiO_2 surface. Comparison of products at the same curcumin content, Cur- TiO_2 -ru sample exhibited lighter yellowish color.

3.2 Characterizations of products

X-ray diffraction patterns

XRD technique was used to follow the phase transformation of TiO_2 samples. XRD measurements were carried out with the Philips PW 3710 powder diffractometer (PHILIPS X'Pert MPD, the Netherlands) using $\text{CuK}\alpha$ radiation ($\lambda = 1.5406 \text{ \AA}$) and equipped with a Ni filter over the range of $2\theta = 10\text{--}90^\circ$ at room temperature with the acceleration voltage, the applied current, and the scan rate were 40 kV, 30 mA, and 3° min^{-1} , respectively. The identification of a species from its powder diffraction pattern is based upon the position of the lines (in terms of 2θ) and

their relative intensities (Skoog and Leary, 1992). XRD patterns of curcumin, uncoated-TiO₂, and coated-TiO₂ samples are shown in Figures 9–11.

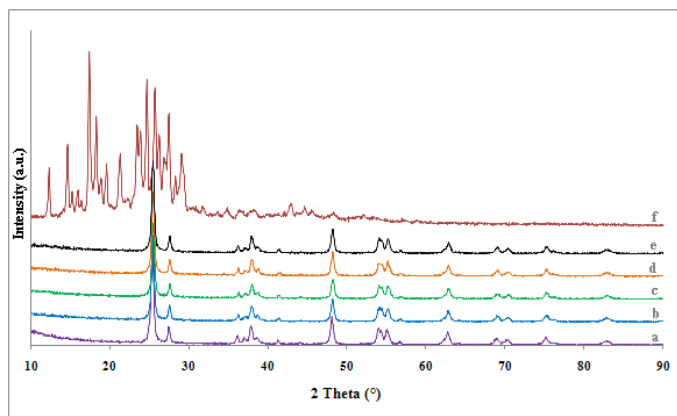


Figure 9 X-ray diffraction patterns of Cur-TiO₂-P25 for (a) uncoated P25-TiO₂, (b) 0.5Cur-TiO₂-P25, (c) 3Cur-TiO₂-P25, (d) 5Cur-TiO₂-P25, (e) 7Cur-TiO₂-P25, and (f) curcumin.

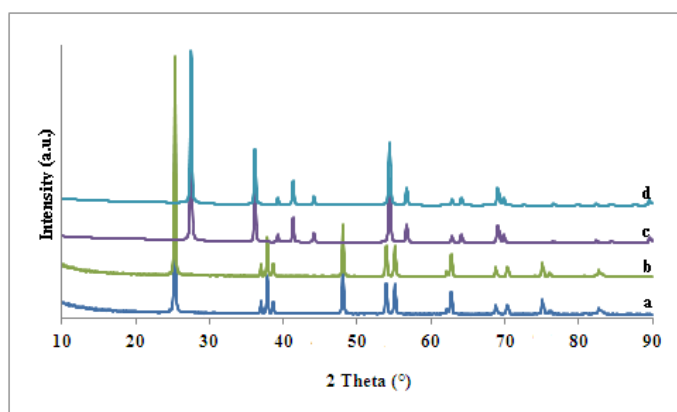


Figure 10 X-ray diffraction patterns of Cur-TiO₂-an and Cur-TiO₂-ru for (a) uncoated anatase TiO₂, (b) 5Cur-TiO₂-an, (c) uncoated rutile TiO₂, and (d) 5 Cur-TiO₂-ru.

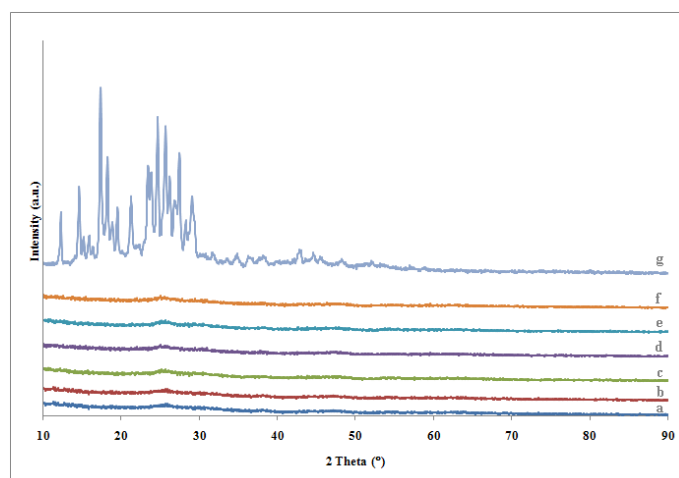


Figure 11 X-ray diffraction patterns of Cur-AMO for (a) uncoated amorphous TiO₂, (b) 1Cur-AMO, (c) 2.5Cur-AMO, (d) 5Cur-AMO, (e) 7.5Cur-AMO, (f) 10Cur-AMO, and (g) curcumin.

In case of Cur-TiO₂-P25, Figure 9, all show patterns of both anatase ($2\theta = 25.4^\circ$) and rutile ($2\theta = 27.5^\circ$) phases in the ratio of *ca.* 4:1, calculated by the intensities obtained from the area of the most intense diffraction peaks of these two modifications, Figure 10 shows the XRD patterns of curcumin coated anatase TiO₂ (Figure 10(b)) with only anatase phase ($2\theta = 25.4^\circ$) and XRD patterns of curcumin coated rutile TiO₂ (Figure 10(d)) showed only the rutile phase ($2\theta = 27.5^\circ$). It can be seen, from Figures 9–10, that the curcumin coating in this study range, 0.5–7 wt% as reported in **Paper I**, did not affect the TiO₂ nature. In case of amorphous samples, Figure 11 (**Paper II**), only flat base line was detected in synthesized TiO₂ sample which is shown in Figure 11(a), confirming the amorphous nature of product. Samples in Figure 11(b)-(f) with coating of 1–10 wt% curcumin content, did not show any differences in XRD patterns from Figure 11(a) indicating that all synthetic TiO₂ exist in an amorphous form.

The XRD pattern of crystalline curcumin powder (Figure 9(f)) shows the characteristic crystalline peaks at 2θ of 20° – 30° (Anitha, *et al.*, 2011). However, the coated samples in Figures 9 and 11 showed no XRD diffraction patterns of

curcumin which could be due to: (1) the amount of curcumin was too small to be detectable in XRD and (2) curcumin had lost its crystallinity after dissolution in the coating process. As mentioned above, evidence from XRD confirmed no phase transformation of TiO_2 occurred by the curcumin coating.

UV-vis diffused reflectance spectroscopy (DRS)

Diffused reflectance studies were obtained on a UV-vis absorption spectrophotometer, Shimadzu UV 2401, in the scan range 200–800 nm with a 2.0 nm slit width and using BaSO_4 as reference sample. Diffused reflectance spectra (DRS) of curcumin coated TiO_2 in this work can be divided into 2 parts: DRS of coated crystalline TiO_2 samples which reported in **Paper I** are shown in Figures 12–14, DRS of curcumin coated amorphous TiO_2 samples which appeared in **Paper II** is shown in Figure 15.

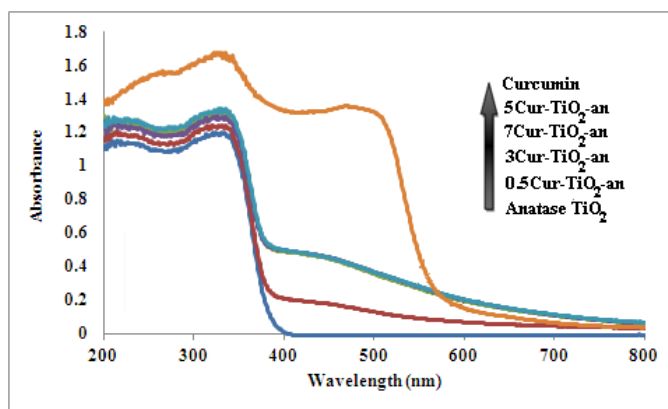


Figure 12 DRS spectra of curcumin coated anatase TiO_2 .

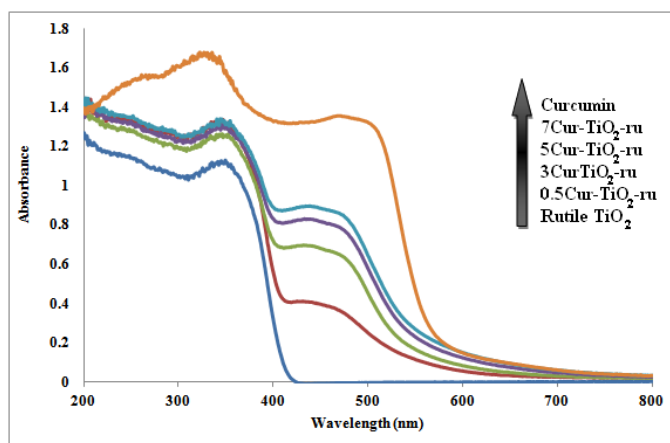


Figure 13 DRS spectra of curcumin coated rutile TiO_2 .

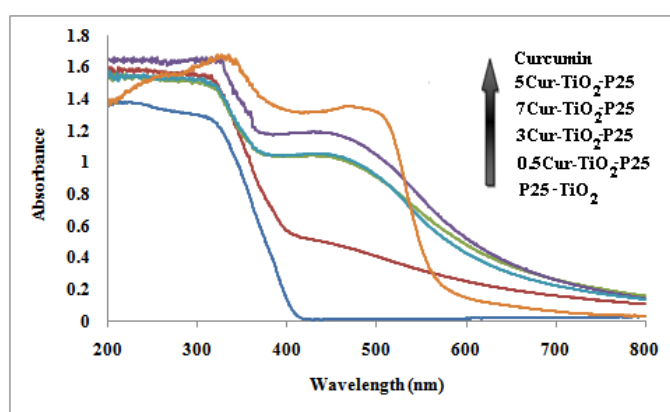


Figure 14 DRS spectra of curcumin coated P25- TiO_2 .

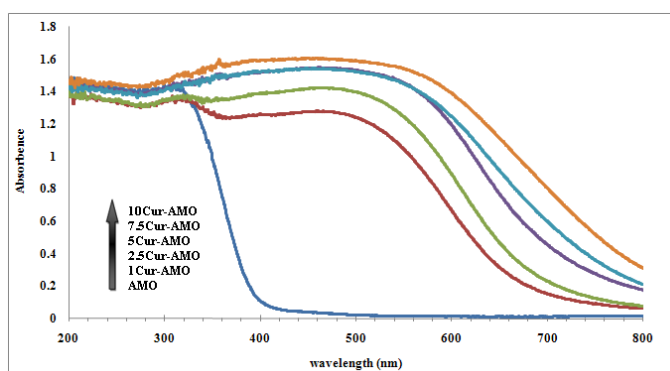


Figure 15 DRS spectra of curcumin coated amorphous TiO_2 .

From Figures 12–14, curcumin powder exhibited a broad absorption band around 200–600 nm with distinct absorption in visible region at 567 nm. This characteristic of curcumin absorption was attributed to the electronic transition of π – π^* type which was observed when curcumin dissolved in mixed methanol/water solvent (Waranyoupalina, *et al.*, 2009). After loading curcumin onto TiO₂ surface, the yellowish powder was obtained. The yellow color was certainly that of curcumin which adhered to the TiO₂ surface. The characteristic absorption peak of curcumin at 450–550 nm which appeared in each figure was an evidence confirming the presence of curcumin on surface of TiO₂. Furthermore, this absorption peak appeared only in all coated-TiO₂ samples and it can be seen that its intensity in all coated-TiO₂ samples increased with increasing of curcumin contents until reaching the saturated concentration which was around 5–7 wt% of curcumin. The absorption edge of uncoated TiO₂ was found at the shorter wavelength than that of the coated samples. This is because the uncoated TiO₂ has no absorption in the visible light region (>400 nm) whereas curcumin coated TiO₂ displays a wide absorption band in the range 400–700 nm.

In order to study the optical property of sample, the band gap energies of all TiO₂ samples were determined from their diffused reflectance spectra and calculated using Eq. (13):

$$E_g = h \frac{c}{\lambda} = \frac{1240}{\lambda} \quad (13)$$

where E_g is the band gap energy (eV), h is the Planck's constant (6.63×10^{-34} J.s), c is the light velocity (3.0×10^8 m/s), and λ is the wavelength at onset of absorption (nm) determined by the linear extrapolation of the steep part of the UV absorption toward the baseline.

By using Eq. (13), all uncoated TiO₂ exhibited higher band gap energy than the coated ones. The coated TiO₂ samples showed the bathochromic shift caused by curcumin. **Paper I** reported the decreasing of band gap energy from 3.21, 3.02, and 3.07 to 3.15, 2.78, and 2.67 for the series of Cur-TiO₂-an, Cur-TiO₂-ru, and Cur-TiO₂-P25, respectively. **Paper II** reported the decreasing of band gap energy from 3.20 to

1.66 eV for curcumin coated amorphous TiO₂ samples. It is clearly seen that the coating of curcumin onto TiO₂ surface affected the light absorption edge toward to longer wavelength. The summaries of calculated band gap energy of all samples are shown in Table 9.

Table 9 Some physical properties of all TiO₂ samples.

Sample	Phase	S _{BET} (m ² /g)	Particle size ^{a,b} (nm)	DRS		pH _{pzc}
				λ _{onset} (nm)	E _g ^c (eV)	
Curcumin	-	9.64	-	567	2.19	-
Anatase TiO₂	Anatase (A)	10.72	32.46	386	3.21	6.6
5Cur-TiO₂-an	A	14.22	36.28	394	3.15	4.9
Rutile TiO₂	Rutile (R)	16.08	55.38	410	3.02	6.9
5Cur-TiO₂-ru	R	19.73	57.22	446	2.78	6.1
P25 TiO₂	A+R	51.41	22.68	404	3.07	6.7
0.5Cur-TiO₂-P25	A+R	52.97	23.63	422	2.94	5.2
3Cur-TiO₂-P25	A+R	54.69	23.64	437	2.84	4.4
5Cur-TiO₂-P25	A+R	53.51	27.57	464	2.67	4.7
7Cur-TiO₂-P25	A+R	53.99	27.57	440	2.82	4.1
Amorphous TiO₂	Amorphous	322.49	4.99	388	3.20	6.3
1Cur-AMO	Amorphous	313.39	5.13	605	2.05	5.9
2.5Cur-AMO	Amorphous	299.06	5.38	626	1.98	5.8
5Cur-AMO	Amorphous	297.48	5.41	674	1.84	5.7
7.5Cur-AMO	Amorphous	268.35	6.00	721	1.72	5.5
10Cur-AMO	Amorphous	241.86	6.65	747	1.66	5.4

^a Calculated using Eq. (14) for coating on crystalline TiO₂.

^b Calculated using Eq. (15) for coating on amorphous TiO₂.

^c Calculated using Eq. (13).

Surface area and surface morphology

The specific surface area of TiO₂ samples was measured for observing an adsorption behavior of dye on TiO₂ surface. The surface area is an average measurement of the external surface of a large number of particles and expressed in term of the area per unit mass (m²/g). There are two main analysis techniques for measuring surface area; gas adsorption and gas permeability. In this work gas adsorption surface area analysis was used.

The Brunauer–Emmett–Teller (BET) specific surface areas (S_{BET}) were characterized by analyzing the N₂ adsorption isotherms obtained at 77 K of pressed powder in sample holder using the SA 3100 (Beckman Coulter, USA) equipment for **Paper I** and BELSORP-max (BEL, Japan) equipment for **Paper II**. Before measurement, the samples were degassed with helium at 553 K for 3 h. The S_{BET} and some physical properties of all TiO₂ samples are summarized in Table 9.

The specific surface areas of uncoated TiO₂ and curcumin coated all TiO₂ are shown in Table 9. In **Paper I**, surface areas of crystalline TiO₂ were of 10.72, 16.08, and 51.41 m²/g for anatase, rutile, and P25-TiO₂, respectively. Coating of curcumin onto TiO₂ did not show significant effect to surface area of the TiO₂ host. Among the surface areas of all TiO₂ samples in Table 9, the synthesized amorphous TiO₂ which reported in **Paper II** had the highest value of 322.49 m²/g which gradually decreased as the amount of curcumin increased. The lowest value was 241.86 m²/g for 10Cur-AMO. The relation between particle size, surface area, and band gap energy in Table 9 agree with the remark that band gap energy and surface area decrease with the increasing particle size (Lin, *et al.*, 2006). The larger surface area of sample could be attributed to highly network system from condensation reaction which was caused by the high volume of water in amorphous sample (Zhang, *et al.*, 2001).

The method to determine the crystallize and particle size of TiO₂, in this work, depended on the TiO₂ nature to be described below.

In case of crystalline TiO₂, **Paper I**, the crystallize size can be calculated using the Scherrer's equation, Eq. (14)

$$D_{\text{XRD}} = \frac{0.9\lambda}{\beta \cos\theta} \quad (14)$$

where D_{XRD} is the average crystallite sizes (nm), λ the X-ray wavelength ($\lambda = 1.5406 \text{ \AA}$), β the full-width at half-maximum (FWHM) of the highest intensity peak in radians, and θ the diffraction peak angle (Baiju, *et al.*, 2007).

In case of non-crystalline TiO_2 , **Paper II**, assuming all the particles have the same spherical size and shape, the particle size can be calculated by Eq. (15)

$$\text{Particle size (nm)} = \frac{6000}{S_{\text{BET}} \cdot \rho} \quad (15)$$

where S_{BET} is the BET specific surface area (m^2/g) and ρ is the density of TiO_2 . The density of the amorphous TiO_2 is 3.73 g/cm^3 . (Prasai, *et al.*, 2012)

The porous nature of TiO_2 was studied by nitrogen adsorption isotherm. In order to utilize the information within the adsorption isotherms, it is necessary to inspect the shape of physisorption isotherm and the identification of the principle mechanism of adsorption. The majority of physisorption isotherms could be grouped into six types, as shown in Figure 16 and Table 10.

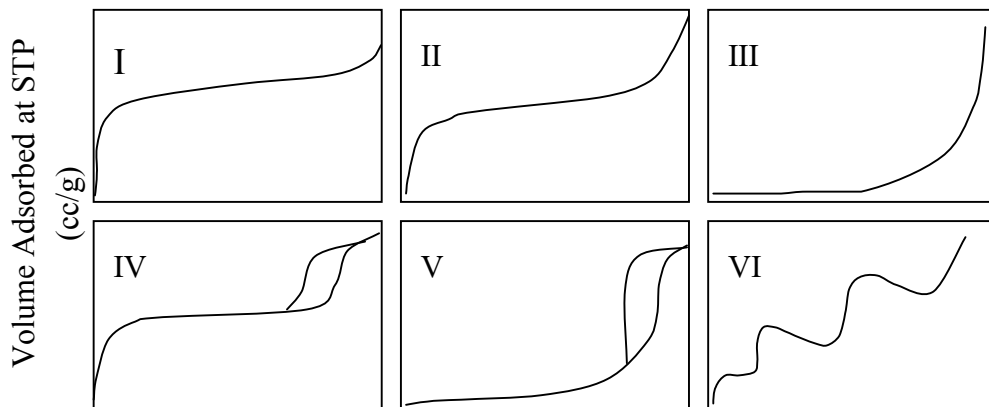


Figure 16 IUPAC classification of adsorption isotherms (Ryu, *et al.*, 1999).

Table 10 IUPAC classification of the pore (Khalil, *et al.*, 2001).

Porosity type	Diameter (d)
Ultramicropores	< typical molecule diameter of the adsorptive about 0.6 nm
Micropores	$d < 2 \text{ nm}$
Mesopores	$2 \text{ nm} < d < 50 \text{ nm}$
Macropores	$d > 50 \text{ nm}$

The Type I isotherm is given by microporous solids. The very steep region at low P/P_0 is due to the filling of very narrow pores and limiting uptake is dependent on the accessible micropore volume rather than on the internal surface area.

The Type II isotherm is normally given by a non-porous solids which unrestricted monolayer-multilayer adsorption can occur.

The Type III isotherm is generally associated with weak adsorbent-adsorbate and relatively strong adsorbate-adsorbate interactions. In this case cooperative effects lead to the development of patches of multilayer before a uniform monolayer has been formed.

The Type IV isotherm with hysteresis loop is the characteristic features of the adsorbate-adsorbate interactions which is associated with capillary condensation. Some microporous or mesoporous solids are amongst the few adsorbents to give Type V isotherm.

The Type VI isotherm is relatively rare, it presents stepwise multilayer adsorption on a uniform non-porous surface. (Ryu, *et al.*, 1999).

The adsorption isotherms of uncoated-, coated-TiO₂, and curcumin powder are shown in Figure 17.

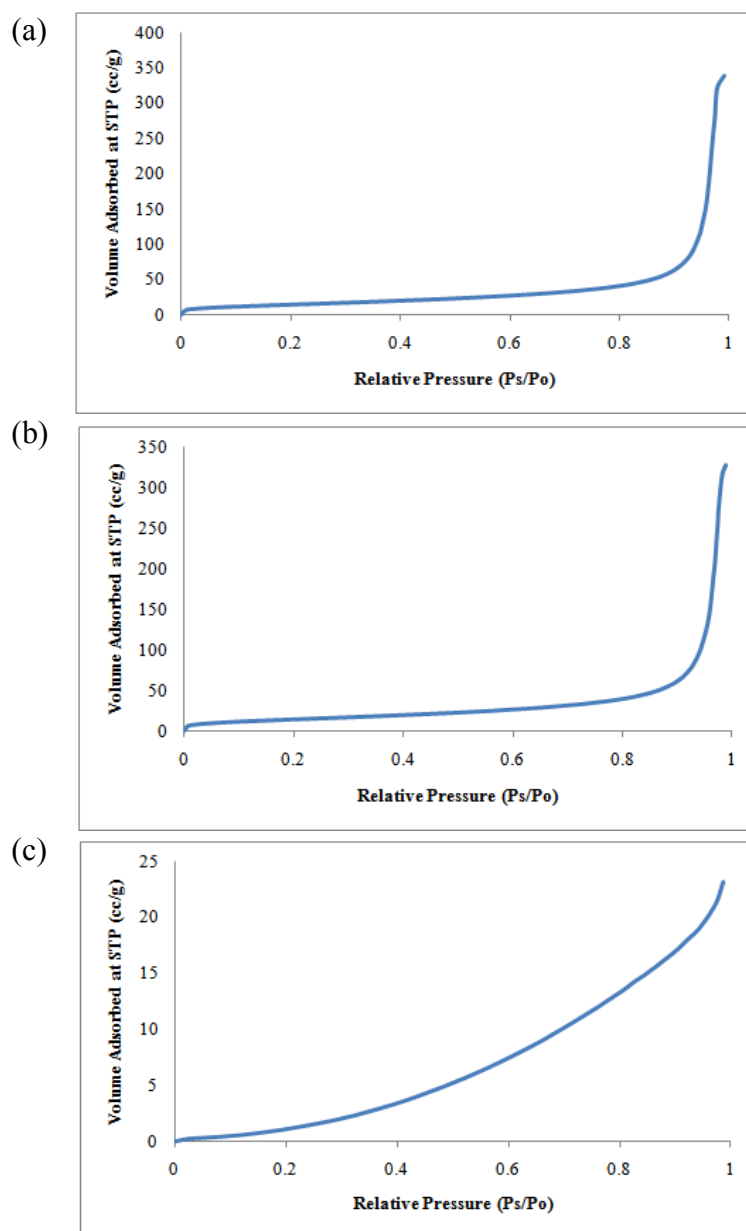


Figure 17 The N₂ adsorption isotherms of samples for (a) uncoated P25-TiO₂, (b) 5Cur-TiO₂-P25, and (c) curcumin powder.

From Figure 17(a), uncoated P25-TiO₂ showed type II isotherm indicating the nature of adsorbent as being either non-porous or macro-porous adsorbent with strong adsorbate-adsorbent interactions (Shim and Kim, 2008). The adsorption isotherm of coated sample with 5 wt% curcumin content also showed

typical type II isotherm as shown in Figure 17(b). The isotherm in Figure 17(c) exhibited by curcumin powder belonged to type III resulting from weak interaction between adsorbent and adsorbate (Sing, *et al.*, 1985). When curcumin was coated onto TiO₂ in the range of 0.5–7 wt% the resulting isotherms were identical to that of uncoated TiO₂ (Figure 17(a)-(b)), implying that curcumin coating did not affect the N₂ adsorption isotherm of TiO₂.

The surface morphologies and microstructures of the uncoated and coated TiO₂ samples were investigated through the SEM and TEM images which performed on the JSM-5800 LV scanning electron microscope and the transmission electron microscope (JEM-2010, JEOL Apparatus). The sample for SEM was prepared by coating the specimen with thin layer of gold. The sample for TEM was prepared by sonication and dropping the sample solution onto the Cu grid holder. The SEM study gives the information about the morphology and aggregation of particle. The surface morphologies at 10,000 times magnification of uncoated and coated TiO₂ samples are shown in Figures 18–20.

In the case of coating on crystalline TiO₂, **Paper I**, Figures 18–19, the results appeared as lower aggregation of spherical shape of small particles. The SEM images revealed uniform spherical structures with quite smooth surface of all Cur-TiO₂ samples. There were no distinct differences between uncoated- and coated samples suggesting that curcumin coating did not affect the morphology and aggregation of crystalline TiO₂.

For the coating on amorphous TiO₂, shown in Figure 20, the uncoated amorphous TiO₂ (Figure 20(a) and 20(b)) appeared as round shape particles with no sharp edges or smooth surfaces characteristic of crystallinity. Similar results were observed with the coated TiO₂ samples (Figure 20(c)-(f)).

The XRD and SEM results revealed that the coating agent, curcumin, did not affect the morphology and aggregation of the prepared TiO₂ samples in this work.

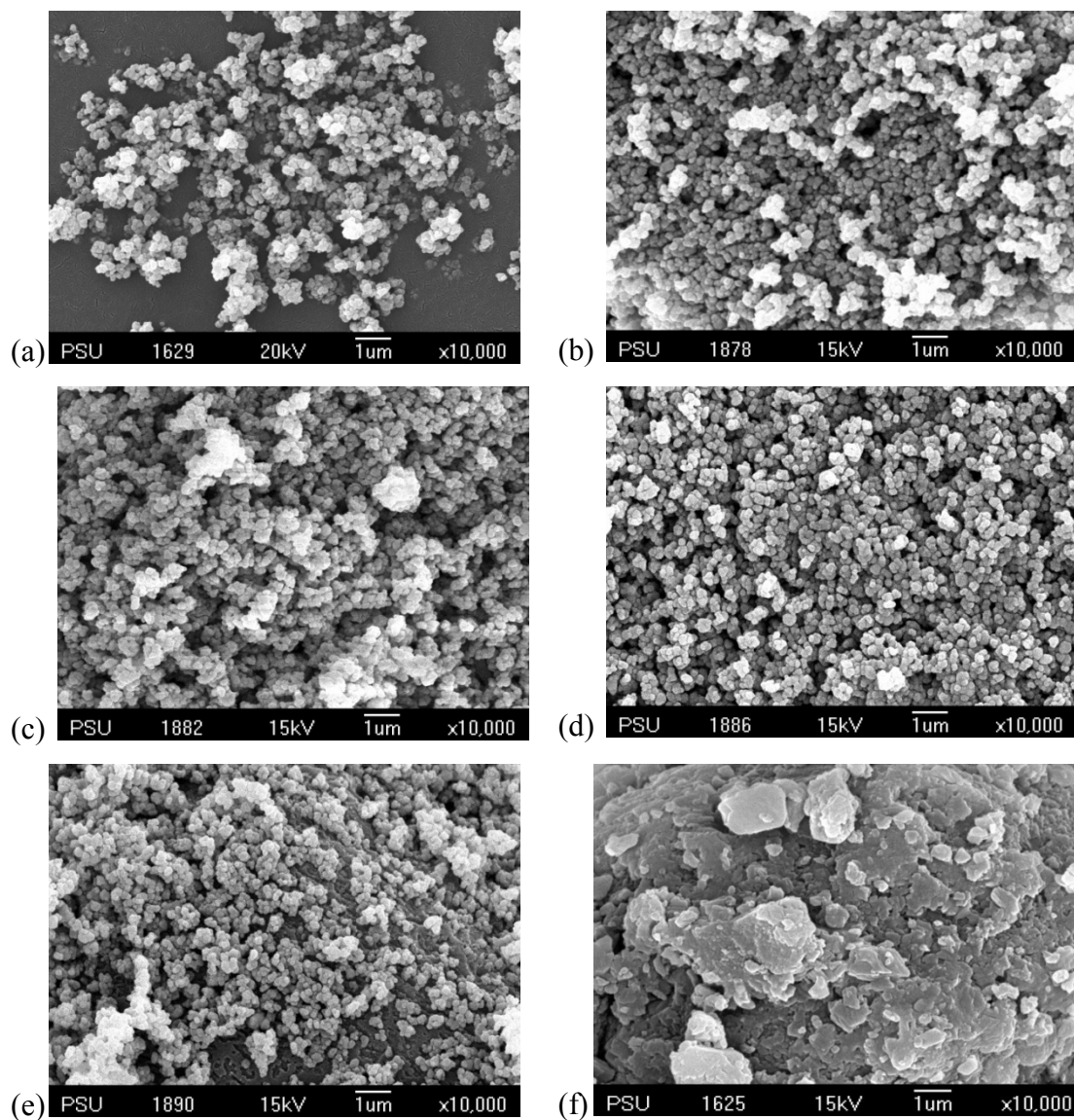


Figure 18 SEM images (10,000x) of samples for: (a) uncoated anatase TiO₂, (b) 0.5Cur-TiO₂-an, (c) 3Cur-TiO₂-an, (d) 5Cur-TiO₂-an, (e) 7Cur-TiO₂-an and (f) curcumin powder.

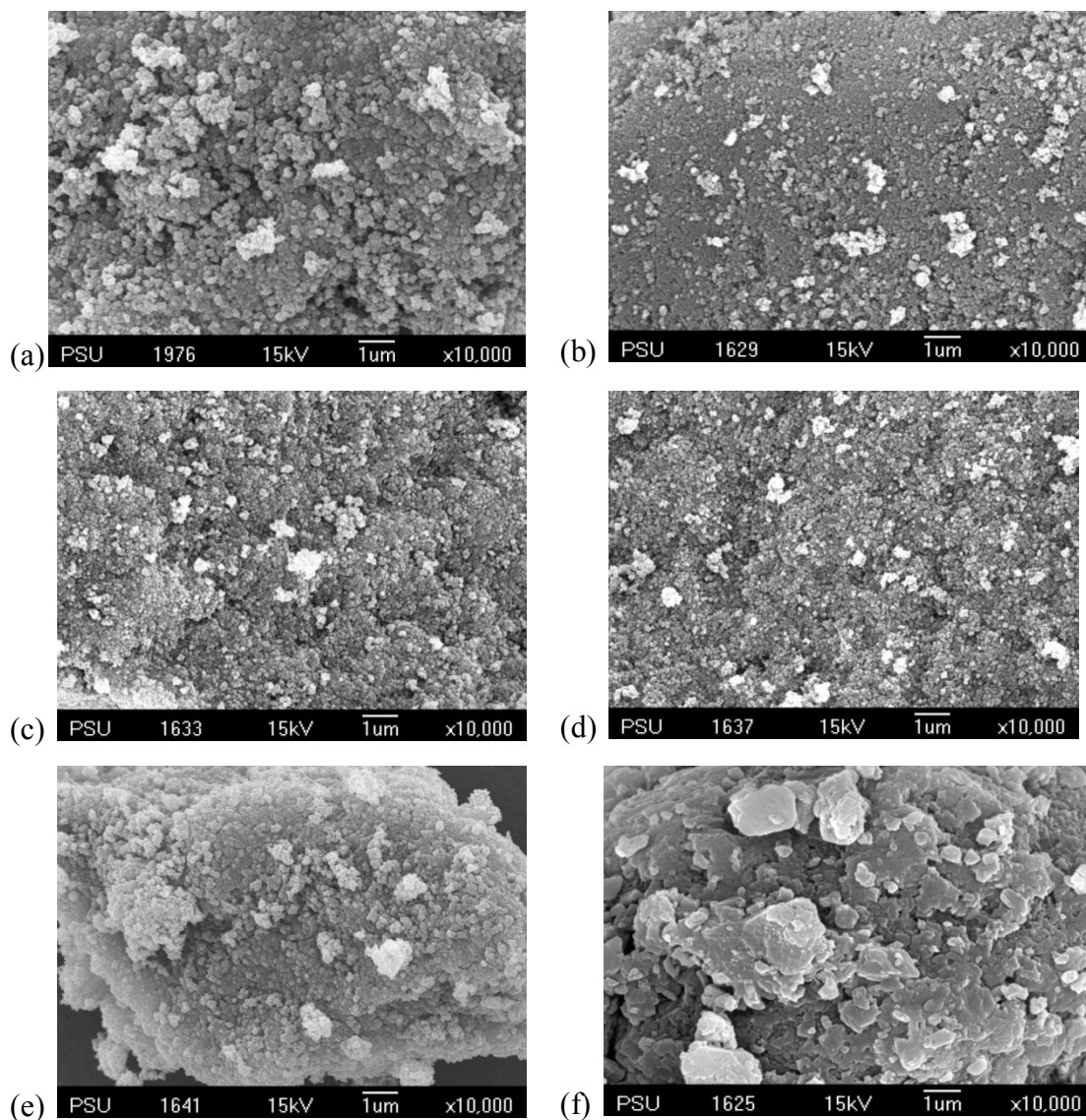


Figure 19 SEM images (10,000x) of samples for: (a) uncoated P25-TiO₂, (b) 0.5Cur-TiO₂-P25, (c) 3Cur-TiO₂-P25, (d) 5Cur-TiO₂-P25, (e) 7Cur-TiO₂-P25, and (f) curcumin powder.

A comparison between uncoated and coated amorphous TiO₂ samples at 15,000 and 50,000 times of magnification are shown in Figure 20. The high agglomeration of many small spherical particles could be seen, however, no obvious difference in SEM images between uncoated and coated amorphous TiO₂ powders was detected implying that curcumin did not affect the morphologies of TiO₂.

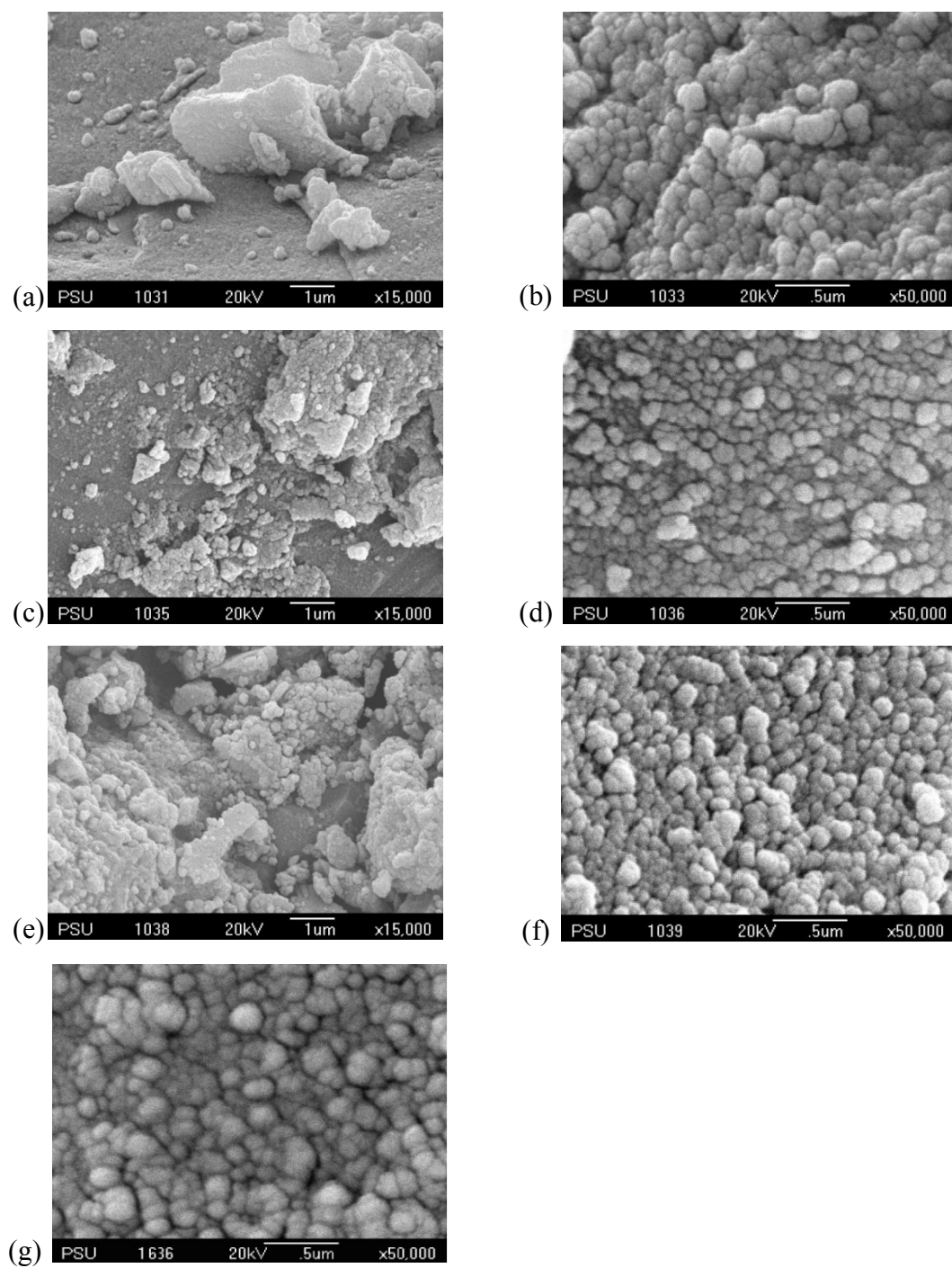
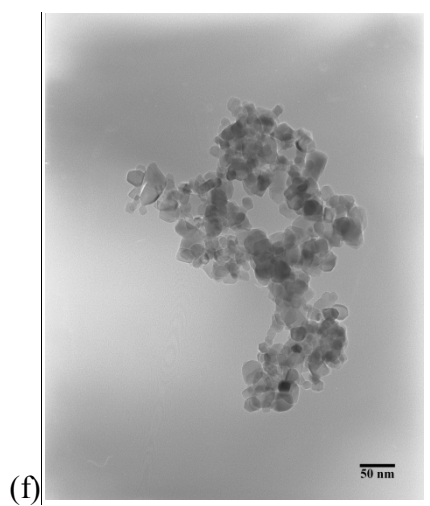
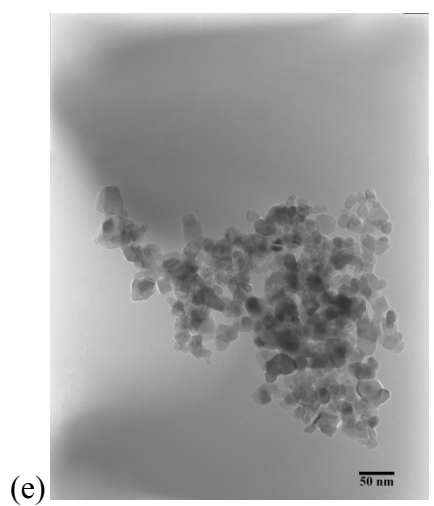
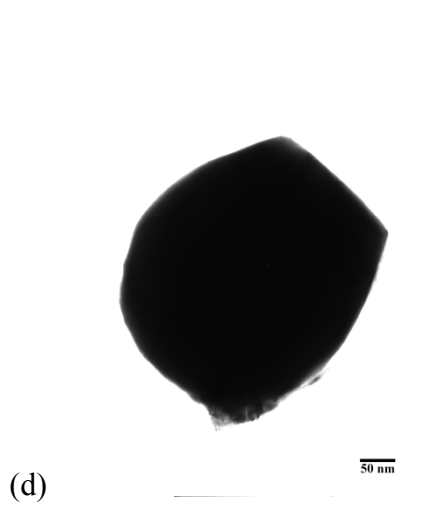
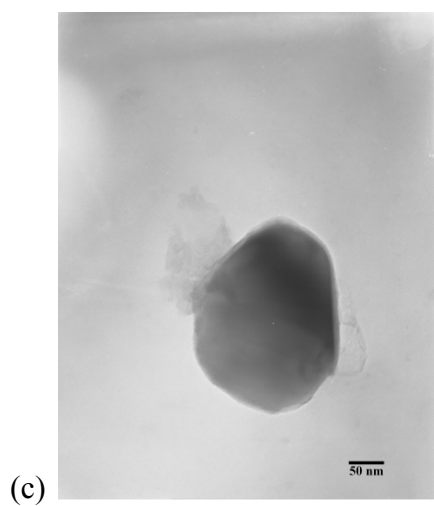
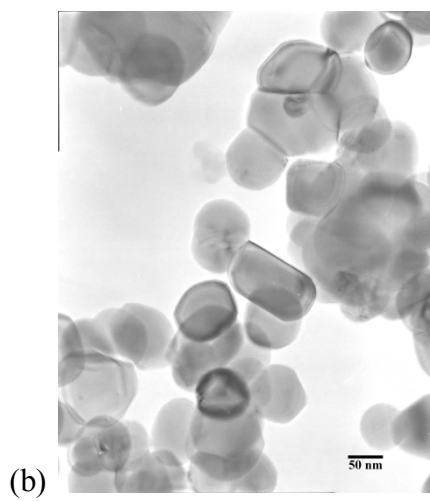
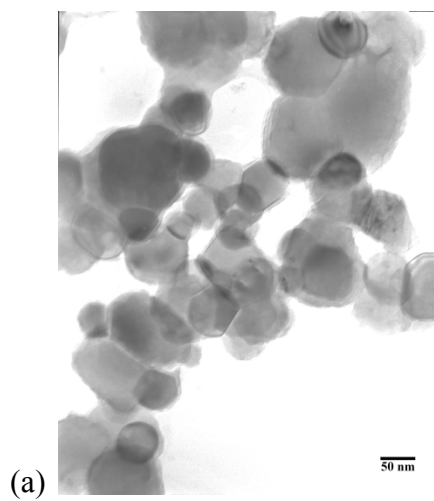


Figure 20 SEM images of samples at various magnification for: (a) uncoated amorphous TiO_2 (15,000x), (b) uncoated amorphous TiO_2 (50,000x), (c) 1Cur-AMO (15,000x), (d) 1Cur-AMO (50,000x), (e) 10Cur-AMO (15,000x), (f) 10Cur-AMO (50,000x), and (g) curcumin powder (50,000x).

The particle size, size distribution, and morphology were investigated with TEM. The TEM images of uncoated TiO₂, coated TiO₂, and curcumin powder are shown in Figure 21. From Figure 21(a)-(f), **Paper I**, the uncoated TiO₂ and 5 wt% coated samples have similar appearances with spherical particle size of around 50–200 nm for Cur-TiO₂-an (Figure 21(a)-(b)), 100–250 nm for Cur-TiO₂-ru (Figure 21(c)-(d)), and 10–50 nm for Cur-TiO₂-P25 (Figure 21(e)-(f)). Figure 21(i) shows TEM image of curcumin in non-dissolving solvent (distilled water), it can be seen that curcumin had uniform spherical shape with different size of average diameter 50–150 nm. The crystallite sizes from XRD calculation of coated TiO₂ samples seem to be slightly larger than the uncoated samples. The TEM sizes of anatase and rutile, both coated and uncoated, are significantly larger than the XRD sizes which could be due to aggregation of these powders.

Figures 21(g)-(h), show TEM images of uncoated and coated amorphous TiO₂ powders. Both uncoated and coated samples appeared as agglomerated particles with particle size of 100–200 nm assembled from small particles. The coated samples (Figure 21(h)) showed slightly larger particle size than the uncoated ones (Figure 21(g)). This result was supported by the particle size which calculated from Eq. (16). TEM image of curcumin is also shown in Figure 21(i) for the sake of particle size comparison.

Combining with SEM result, larger particle observed with TEM caused by agglomeration of many small TiO₂ particles.



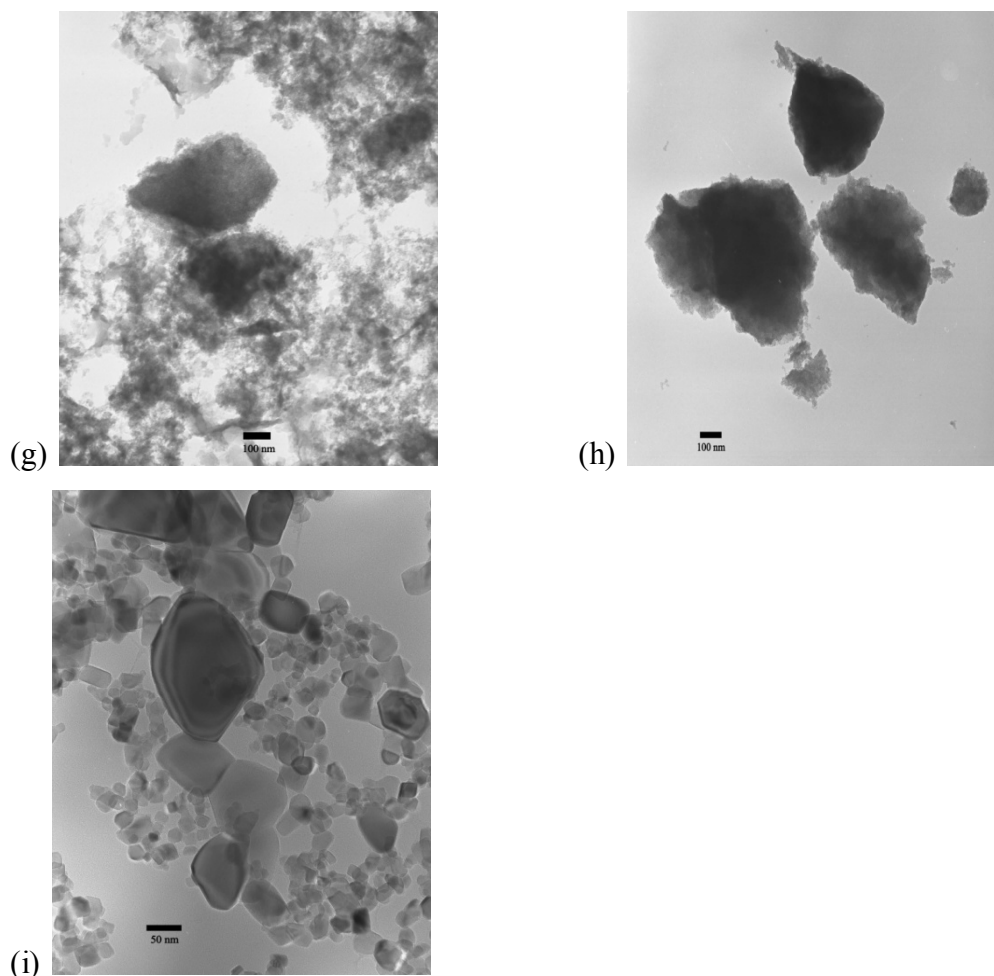


Figure 21 TEM images of samples for: (a) uncoated anatase TiO_2 , (b) 5Cur- TiO_2 -an, (c) uncoated rutile TiO_2 , (d) 5Cur- TiO_2 -ru, (e) uncoated P25- TiO_2 , (f) 5Cu- TiO_2 -P25, (g) uncoated amorphous TiO_2 , (h) 10Cur-AMO, and (i) curcumin powder.

Fourier-transformed infrared spectroscopy (FT-IR)

Infrared spectroscopy is a technique for determining the functional groups within the compounds. Fourier-transformed spectroscopy is a measurement technique whereby spectra are collected based on measurements of the temporal coherence of a radiative source, using time-domain measurements of the electromagnetic radiation or other type of radiation. It can be applied to a variety of

types of spectroscopy including optical spectroscopy, infrared spectroscopy (FT-IR), and electron spin resonance spectroscopy. The FT-IR spectrum range of the usage in the mid-infrared region, which covers the frequency from 400 to 4,000 cm^{-1} (Skoog and Leary, 1992).

In **Paper I**, FT-IR spectroscopy (Perkin Elmer, Model Spectrum BX, USA) was used to investigate the interaction of curcumin in TiO_2 through the fingerprint vibrations of both curcumin and TiO_2 as shown in Figure 22. Prior to the spectrum acquisition, the sample for FT-IR was ground with KBr and pressed into pellet by applying a pressure of 300 kg cm^2 . The FT-IR spectra of uncoated- and coated- TiO_2 were not distinctively different from each other (Figure 22(a)-(e)) attributable to TiO_2 being the major part and the very small amount of add-in curcumin in each sample. Uncoated P25- TiO_2 (Figure 22(a)) showed strong and broad absorption peak below 800 cm^{-1} which is the characteristic of Ti–O stretching vibration. This broad band, unfortunately, did not give a clear usable information. The characteristic Ti–O vibration in anatase and rutile phases which usually appears at 682 and 503 cm^{-1} , respectively (Zhang and Reller, 2001), were not detectable as they should be masked under this broad region. A broad band at 3,433 cm^{-1} is the O–H stretching vibration peak of the hydroxyl functional group and the peak at 1,634 cm^{-1} is attributed to the bending vibration of the surface H–OH (Zhou, *et al.*, 2012).

In the case of coated- TiO_2 samples (Figure 22(b)-(e)), they all looked similar to the uncoated spectrum except the strong broad peak at 400–800 cm^{-1} became broader. Since this region is characterized by the Ti–O stretching vibration it is possible that the broadening effect may be due to the weak chemical interaction between curcumin and TiO_2 . Curcumin molecule has one of the most prominent functional group—the β -diketone group— at the center which has high driving force to form chelation with metal ion. In this respect, it is not surprising to anticipate the interaction—be it weak or strong—of this β -diketone moiety with Ti atom at the bulk surface, as shown in Scheme 1. Figure 22(f) shows characteristic band of curcumin at 3,447 cm^{-1} due to the phenolic O–H stretching vibration. Moreover, absorption bands at 1,605 cm^{-1} can be assigned to the stretching vibration of benzene ring of curcumin, sharp band at 1,502 cm^{-1} to the C=O and C=C vibration, a band at 1,430 cm^{-1} to the

olefinic C–H bending vibration, a band around 1,200–1,300 cm^{-1} to the aromatic C–O stretching vibration, and a weak band at 850 cm^{-1} to the C–O–C stretching vibration (Yallapu, *et al.*, 2010). The very weak band around 2,350 cm^{-1} (in all samples) is the vibration mode from atmospheric CO_2 in the surroundings.

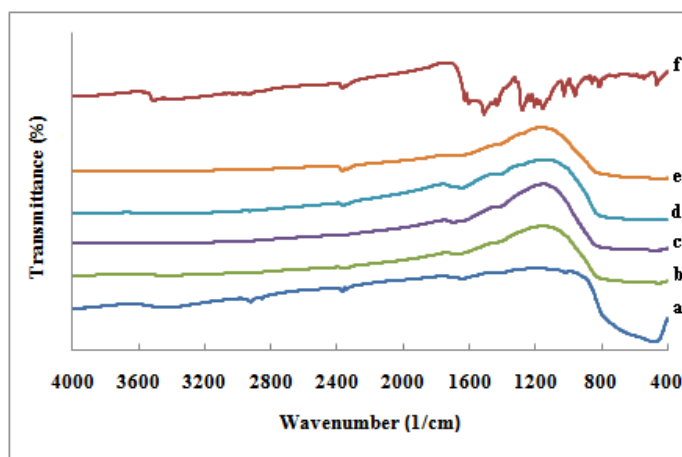


Figure 22 FT-IR spectra for: (a) uncoated P25 TiO_2 , (b) 0.5Cur- TiO_2 -P25, (c) 3Cur- TiO_2 -P25, (d) 5Cur- TiO_2 -P25, (e) 7Cur- TiO_2 -P25, and (f) curcumin powder.

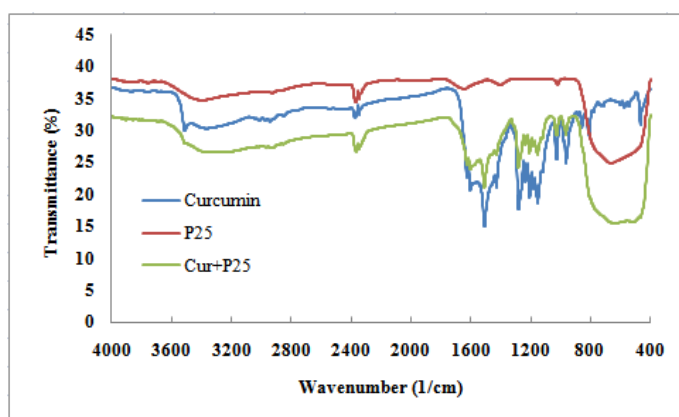
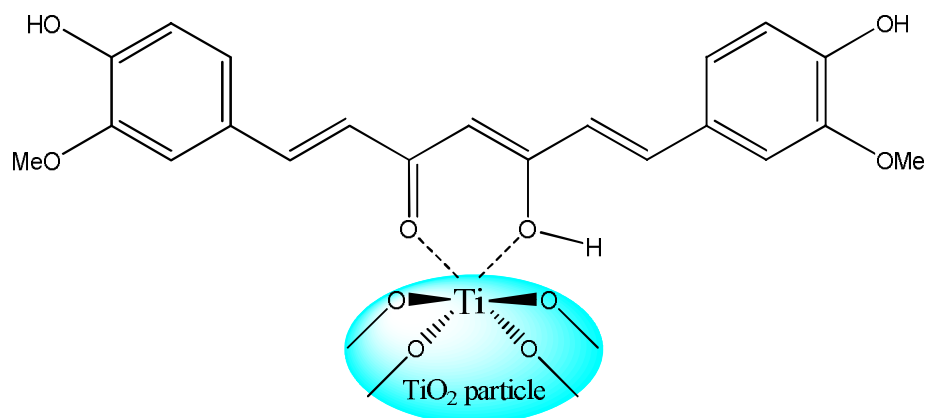


Figure 23 FT-IR spectra of neat curcumin, neat P25, and mixture of curcumin + P25- TiO_2 (1:1 w/w).



Scheme 1 Probable interaction between curcumin and TiO_2 (adapted from Singh, *et al.*, 2010).

For comparison, a mixed powder of curcumin and P25- TiO_2 was prepared by physically mixing the two powders (1:1 w/w) together. The FT-IR spectra of this mixed powder, along with spectra of neat curcumin and neat P25- TiO_2 , are shown in Figure 23. It can be seen that the FT-IR spectrum of Cur + P25- TiO_2 mixture shows patterns of both pure curcumin and pure P25- TiO_2 . This result suggested that the curcumin contents in the coated samples are too low to be observed with FT-IR technique.

Elemental analysis and elemental mapping

The presence of curcumin in each sample was checked by calcinations of sample powder up to $1,450^\circ\text{C}$ using a CHN elemental analyzer (FlashEA 1112, Eager 300 Software). The content of carbon (C) and hydrogen (H) in the coated TiO_2 samples were determined with a CHN analyzer and are shown in Table 11. These data revealed that only small amount of curcumin was present in the TiO_2 bulk. Table 11 shows the very low percentage of C and H contents in Cur- TiO_2 -P25 samples. This result supports the results from XRD and FT-IR that only minute amount of curcumin was present in these samples. Although the percentage of C and H contents were very small, they did vary linearly with increasing curcumin loadings. A rationale for low

adsorption of curcumin by the bulk TiO₂ is the mediocre surface area of P25-TiO₂ (51.41 m²/g) as well as its characteristic type II of adsorption isotherm which usually found in materials of low adsorption capacity (Shim and Kim, 2008).

Table 11 Elemental analysis of TiO₂ samples.

Sample	Element (%)	
	C	H
Curcumin	69.03	5.54
0.5Cur-TiO₂-P25	0.48	0.12
3Cur-TiO₂-P25	1.04	0.15
5Cur-TiO₂-P25	1.61	0.18
7Cur-TiO₂-P25	1.91	0.20

Detailed analysis of the chemical composition on the surface of TiO₂ was investigated with energy dispersive X-ray spectroscopy (EDX) attached to the SEM, the result of which are shown in Figure 24. In Figure 24(a), elemental distribution of uncoated amorphous TiO₂ showed C, O, and Ti signal strength of 4, 7, and 106 with the respective atomic % of 2.37, 16.77, and 80.86, respectively, while the coated ones (Figure 24(b)) the same figure sets were 7, 6, 80 and 11.44, 19.48, 69.08, respectively. The information from these figures showed that the atomic % of C and O in the coated samples increased but decreased for Ti compared to the uncoated ones. Considering Figure 24(a) and 24(b), the bright area of C and O increased whereas it decreased for Ti corresponding to higher concentration of C and O but lower concentration of Ti atoms at the surface. This, of course, was the result of coating curcumin on the surface of amorphous TiO₂, hence, some of Ti atoms were masked by thin film of curcumin rendering less Ti atoms detectable by EDX.

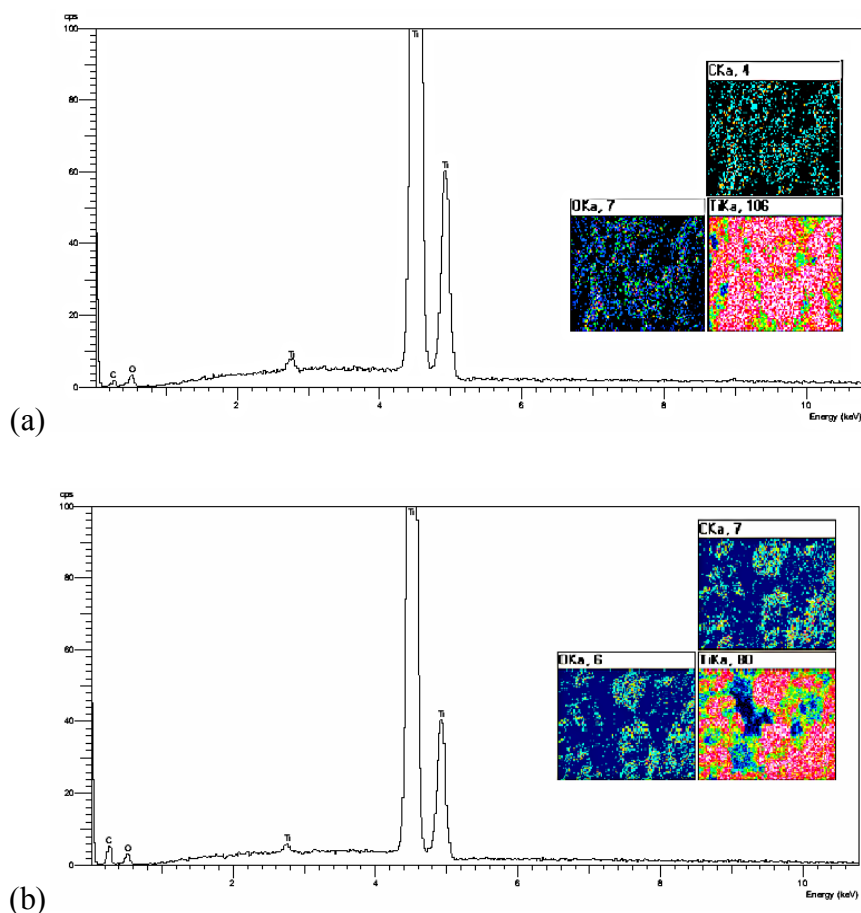


Figure 24 Elemental mapping of (a) amorphous TiO₂ and (b) 7.5Cur-AMO.

Thermogravimetric analysis

Thermogravimetric analysis (TGA7, Perkin Elmer) was used to observe the inclusion of moisture and curcumin in amorphous TiO₂ samples. The temperature program was set in the range 50–1300°C with the heating rate 10 °C/min in an air flow. In **Paper II**, TGA was used to study thermal stability of amorphous TiO₂ including its fraction of volatile components (moisture and curcumin) by monitoring the weight change while the specimen was heated. Figure 25 shows TGA thermograms of uncoated and coated amorphous TiO₂. The TGA curve of uncoated amorphous TiO₂ (Figure 25(a)) showed only one main weight loss state of 27% in the range from room temperature up to 500°C attributable to the elimination of physically

and/or chemically adsorbed water molecules (Kadam, *et al.*, 2014). While the curve of coated TiO₂ sample (Figure 25(b)) showed three weight loss states: first from room temperature to 500°C with 24.1 % weight loss occurring in the same way as uncoated one including decomposition of curcumin molecules (Kumar, *et al.*, 2014), the second weight loss of 1.3% in the range of 600–900°C was due to decomposition of residual fragments and transformation from amorphous to anatase phase of TiO₂, and finally, weight loss of 0.3% at 1,000–1,200°C could come from the completely transformation to rutile phase of TiO₂.

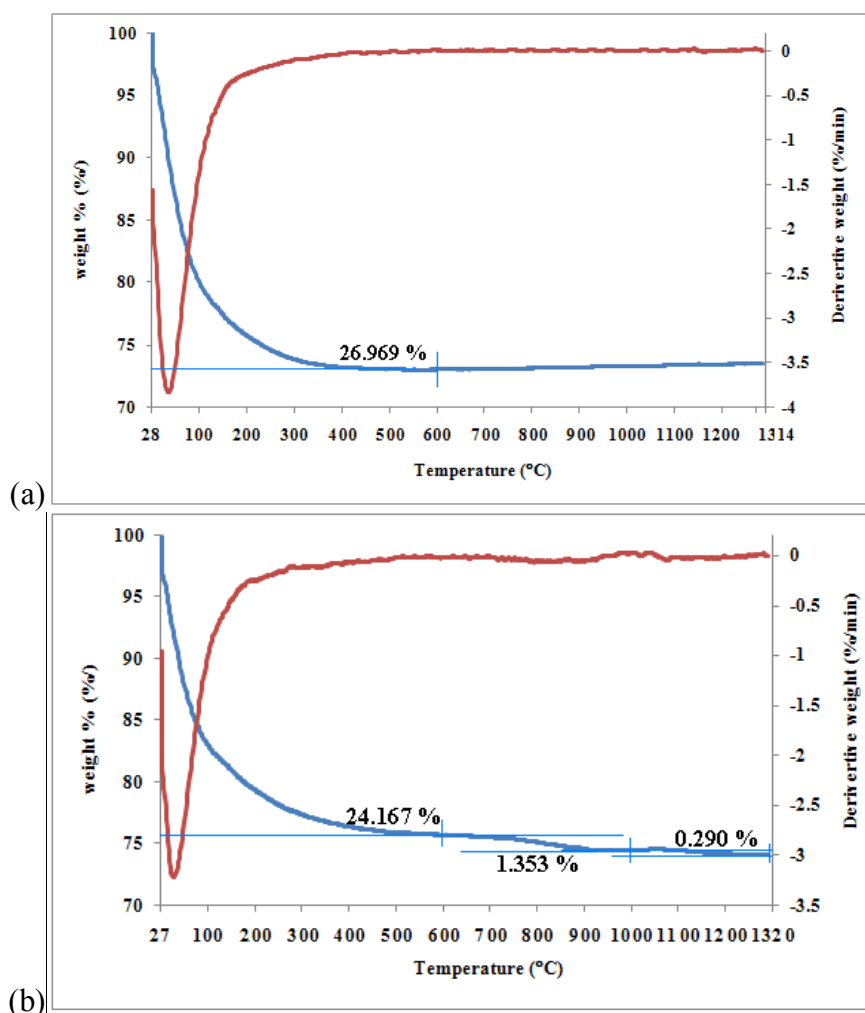


Figure 25 The thermograms of (a) amorphous TiO₂ and (b) 7.5Cur-AMO.

Calculation of energy levels

The redox potential of curcumin was measured using the cyclic voltammetry technique. Curcumin solution was prepared by dissolving specific amount of curcumin powder in MeOH and 0.1 M tetrabutylammonium hexafluorophosphate was used as electrolyte. The voltammograms were recorded with a PGSTAT 30 Autolab potentiostat system at room temperature between 1.00 and -2.50 V with glassy carbon electrode (GCE) as working electrode, Ag/AgCl as reference electrode, and platinum wire as auxillary electrode (Chaithanadul, 2011). To understand the charge transport properties and the electrochemical stability of curcumin, the redox properties of curcumin were studied and reported in **Paper I**. From these data, the energy levels of the highest occupied molecular orbital (HOMO) and lowest unoccupied molecular orbital (LUMO) were calculated by using the following relations (Zou, *et al.*, 2005),

$$E_{\text{HOMO}} = -[eE_{\text{ox}} + 4.37] \quad \text{eV} \quad (16)$$

and

$$E_{\text{LUMO}} = -[eE_{\text{red}} + 4.37] \quad \text{eV} \quad (17)$$

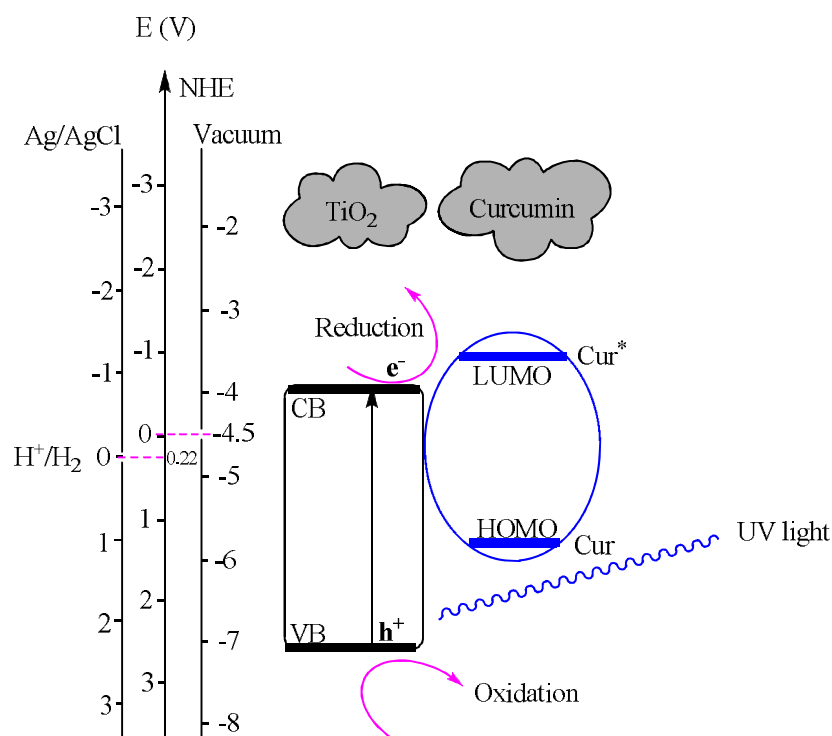
where E_{ox} and E_{red} are the oxidation and reduction onset potentials in the cyclic voltammogram, respectively. The difference between E_{LUMO} and E_{HOMO} yields the band gap energy (E_g),

$$E_g = E_{\text{LUMO}} - E_{\text{HOMO}} \quad \text{eV} \quad (18)$$

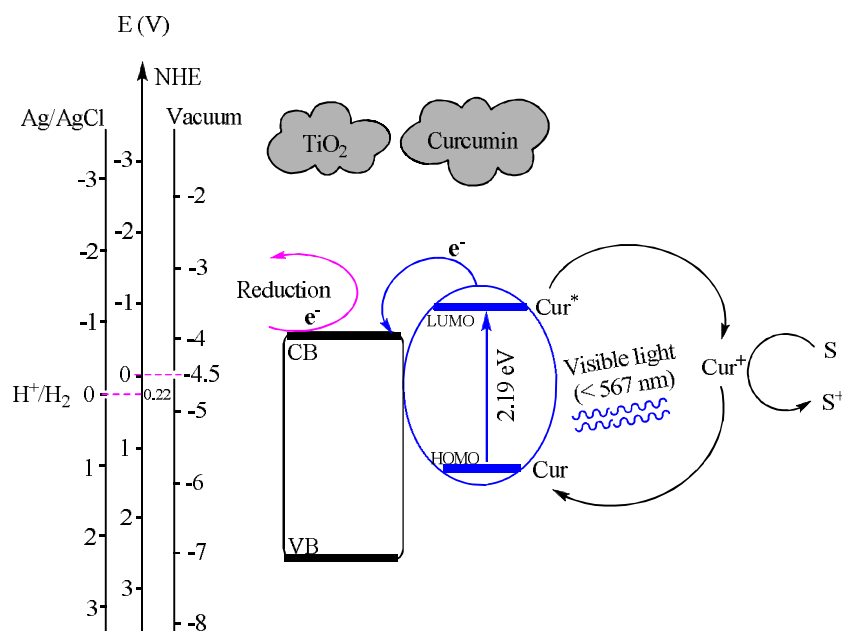
The values in these relations are referenced to Ag/AgCl electrode. Based on the cyclic voltammetry data, the E_{LUMO} of curcumin was calculated from Eq. (17) to obtain $E_{\text{LUMO}} = -3.65$ eV with the reduction onset potential of curcumin ($E_{\text{red}} = -0.72$ V (Ag/AgCl)) (Chaithanadul, 2011). In the voltammogram, the bottom of the reduction potential was -0.955 V with the reduction onset at -0.72 V. These were measured in dimethylsulfoxide (DMSO). Attempt was made to measure it in methanol/water mixed solvent but the signal was very weak albeit equal to that in

DMSO. The values of E_{LUMO} and E_{HOMO} of curcumin obtained here are not too far off from those estimated by Singh, *et al.*, 2010 using different approach based on data reported by other researchers. The value of E_{g} was estimated as 2.19 eV (Table 9) from the UV-vis absorption onset (Figures 12–14) and using Eq. (13). The E_{HOMO} was then calculated as $E_{\text{HOMO}} = -5.84$ eV using Eq. (18), after the E_{LUMO} and E_{g} had been known (Zou, *et al.*, 2005). These values were converted to be referenced with vacuum, recall that -4.5 V vacuum corresponding to 0 V NHE in aqueous solution and 0.22 V NHE as 0 V Ag/AgCl (Smestad, *et al.*, 2003). The redox potential including mechanism pathway of curcumin-TiO₂ system both under UV and visible light irradiation are shown in Scheme 2.

a) Under UV light irradiation



b) Under visible light irradiation



Scheme 2 Schematic mechanism pathway of curcumin-TiO₂ system (a) under UV light irradiation, and (b) under visible light irradiation (adapted from Hilal, *et al.*, 2007).

Point of zero charge determination

One of the most important characteristics of metal oxide surface is the pH_{pzc} which corresponds to the pH of the liquid surrounding metal oxide particles when the sum of surface positive charges balance the sum of surface negative charges. The pH_{pzc} value characterizes surface acidity: when metal oxide particles are introduced in an aqueous environment their surface charge is positive if $\text{pH}_{\text{solution}} < \text{pH}_{\text{pzc}}$ and is negative if $\text{pH}_{\text{solution}} > \text{pH}_{\text{pzc}}$ (Reymond and Kolenda, 1999). The pH at the point of zero charge (pH_{pzc}) can be measured by several methods. In this work, pH_{pzc} of all samples were determined by using the pH drift method (Bessekhouad, *et al.*, 2004). Prior to the measurement, 0.1 M of sodium chloride solution was prepared as an inert electrolyte. The pH of the solution was adjusted from 2 to 12 by adding

either diluted HCl or NaOH. The pH of the adjusted solution is known as an initial pH, pH_i . Then, 50 mg of TiO_2 sample was added to 50 mL of the electrolyte solution at each pH and stirred for 24 h to obtain the adsorption–desorption equilibrium and the final pH was measured as pH_f . The pH_{pzc} was obtained from the intersection point where the experimental data curve deviates from the ideal values measured at various concentrations of inert electrolytes.

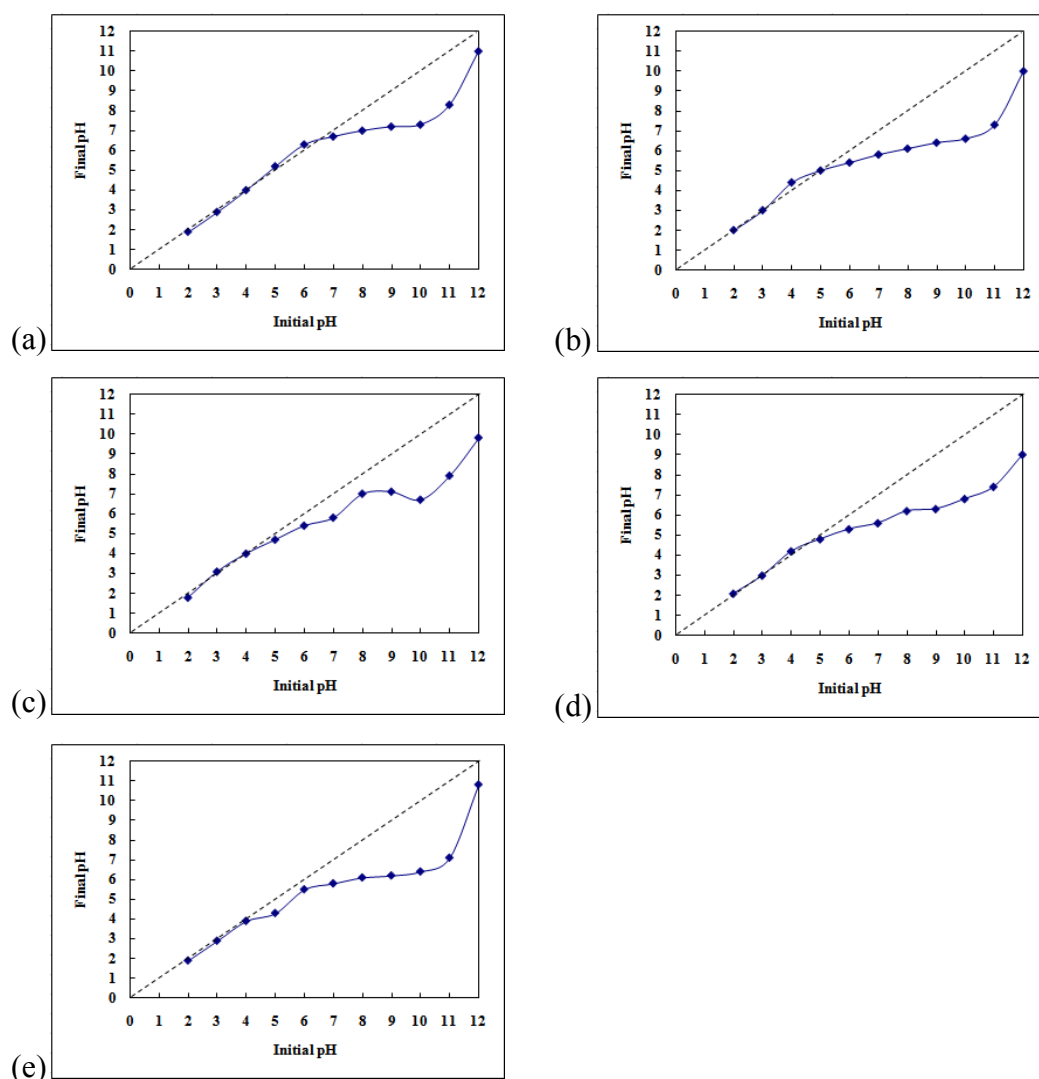


Figure 26 The pH_{pzc} graphs of samples (a) uncoated P25- TiO_2 , (b) 0.5Cur- TiO_2 -P25, (c) 3Cur- TiO_2 -P25, (d) 5Cur- TiO_2 -P25, and (e) 7Cur- TiO_2 -P25.

Figure 26 shows the graphs from the pH_{pzc} determinations constructed by plotting the initial pH (pH_i) versus the pH at equilibrium (pH_f). The pH_{pzc} then was obtained from the interception point between the data curve and the straight line of $\text{pH}_i = \text{pH}_f$ (dash line). With this method, the pH_{pzc} values of uncoated TiO_2 , 0.5Cur- TiO_2 -P25, 3Cur- TiO_2 -P25, 5Cur- TiO_2 -P25, and 7Cur- TiO_2 -P25 were obtained to be 6.7, 5.2, 4.4, 4.7, and 4.1, respectively. The value of uncoated TiO_2 sample was in the same range with values reported by several researchers in the range 6.25–6.90. The results revealed that curcumin coating affected the pH_{pzc} of TiO_2 by lowering the pH_{pzc} . Moreover, on increasing curcumin loading the pH_{pzc} value decreased. The pH_{pzc} values of all TiO_2 samples are given in Table 9.

3.3 Photocatalytic study

In this work, the photocatalytic activities of TiO_2 samples were evaluated using three model dyes, CV, MB, and OII under UV and visible light irradiation. **Paper I** reported the photoreactivity of crystalline TiO_2 on all three dyes both under UV and visible light irradiation at dyes concentration of 2.5×10^{-5} M while **Paper II** reported the photoreactivity of amorphous TiO_2 on MB and OII dyes which represented cationic and anionic dye, respectively, since high adsorptivity of amorphous TiO_2 , MB dye concentration which used in this part is four times higher than normal concentration, 1×10^{-4} M.

The photocatalytic study was performed using a UV-vis spectrophotometer (Specord S100, Analytik Jena GmbH, Germany) by measuring absorbance at wavelength 590, 665, and 485 nm for CV, MB, and OII dye, respectively. The percentage of dye decolorized (adsorption study) or degraded (photocatalytic study) was determined from the following equation;

$$\% \text{ dyes degradation} = \frac{C_o - C_t}{C_o} \times 100 \quad (19)$$

where C_o is the initial concentration of dye solution and C_t is the concentration of dye solution at specific time interval when the aliquot was collected.

Adsorption study

Prior to studying photoreactivity, the adsorption efficiency was measured by monitoring the decolorization of three model dyes (CV, MB, and OII) under dark condition for 1 h. The adsorption efficiencies of curcumin coated crystalline TiO₂ samples which appeared in **Paper I** are shown in Figure 27.

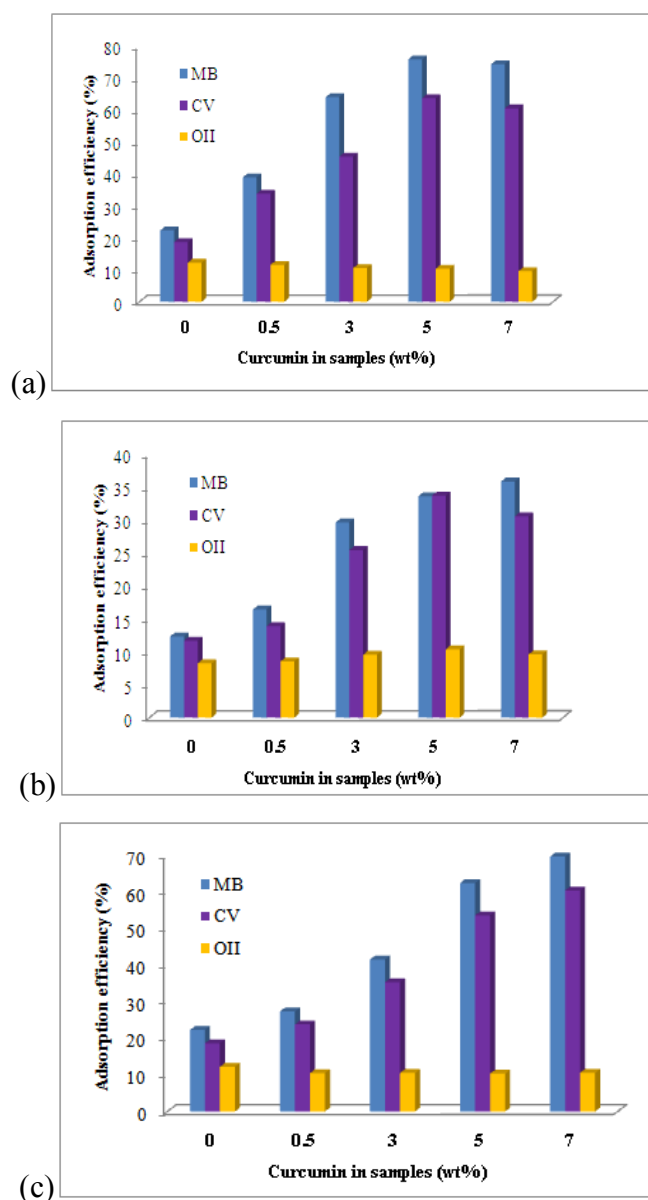


Figure 27 Adsorption efficiencies of TiO₂ samples for (a) Cur-TiO₂-an, (b) Cur-TiO₂-ru, and (c) Cur-TiO₂-P25 with three selected dyes (1h).

As shown in Figure 27(a)-(c), the catalysts showed the same trend of adsorption efficiency for MB and CV that the efficiency increased with increasing curcumin content. However, in the case of OII the opposite result was observed when increasing amount of curcumin yielded low adsorption efficiency throughout the study range. It is known that CV and MB are cationic azo dyes whereas OII is anionic dye after dissociation in an aqueous solution. The interpretation of adsorptivity on TiO₂ surface with curcumin coating can be explained in term of electrostatic interaction between charges of dye and the TiO₂ surface. As mentioned above, the pH_{pzc} of anatase, rutile, and uncoated P25-TiO₂ were 6.6, 6.9, and 6.7, respectively, and decreased to 5.2–4.1 with increasing curcumin loading. All experiments in this part were carried out at the natural pH of each dye solution, 6.7, 6.9, and 7.2 for CV, MB, and OII, respectively, which were higher than the pH_{pzc} of the coated TiO₂ samples. Under this condition, the catalyst surface would be more negative. For CV and MB, adsorption efficiencies increased due to stronger attraction between more negatively charged TiO₂ surface and positively charged cationic dye fragment (Sun, *et al.*, 2008). In the case of OII, the negatively charged dye fragment would repel with the negatively charged TiO₂ surface, hence, lowering the adsorption efficiency.

In **Paper II**, MB and OII were selected as target pollutants. At normal concentration, synthesized amorphous TiO₂ completely adsorbed MB dye within 1 h, therefore, high MB concentration is required in this part.

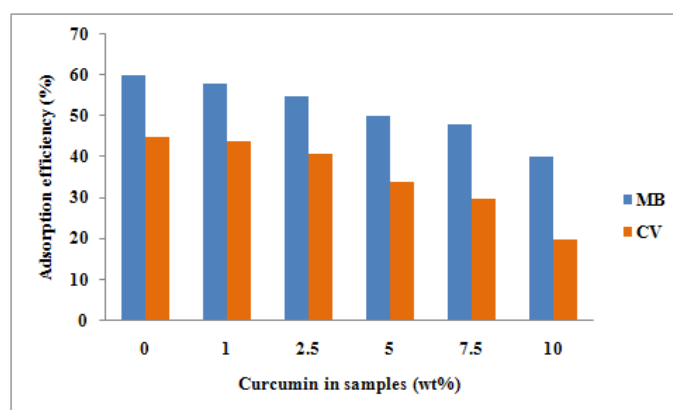


Figure 28 Adsorption efficiencies of curcumin coated amorphous TiO₂ samples with two selected dyes (1h).

It can be seen from Figure 28 that the adsorption efficiency of amorphous TiO₂ decreased after curcumin loadings attributed to the decreasing of BET surface areas of coated TiO₂ sample which showed in Table 9. Note that, MB concentration in Figure 28 is four times higher than OII concentration.

Photocatalytic study with UV light

Photocatalytic study under UV irradiation was evaluated from the degradation of the same set of dyes. In **Paper I**, the degradation efficiencies exhibited by all TiO₂ samples under 5 h of UV irradiation are shown in Figure 29 where uncoated TiO₂ (Degussa P25 and anatase) showed excellent photodegradation (100 %) and upon coating it with curcumin the degradation efficiency under UV excitation decreased. This result could be rationalized as due to decreasing of an active sites on TiO₂ surface as they were covered by curcumin molecules leading to decreasing of electron–hole pair generation, hence, hydroxyl radical or superoxide radical decreased and the photocatalytic efficiency decreased. The curcumin coated TiO₂ had brown color before being used in the photodegradation reaction and turned to light brown after the reaction. The uncoated- and coated-anatase TiO₂ also showed the same trend as that of P25-TiO₂ samples. On the other hand, the curcumin-coated rutile did not show any effect on the photoreactivity under UV irradiation as all of Cur-TiO₂-ru samples were still rather inert with poor photoreactivity. Therefore, the photoreactivity under UV irradiation of Cur-TiO₂-an and Cur-TiO₂-ru was not presented in this part.

The photoreactivities under UV activation of uncoated- and coated amorphous TiO₂ were not studied because from our previous study, it was inactive.

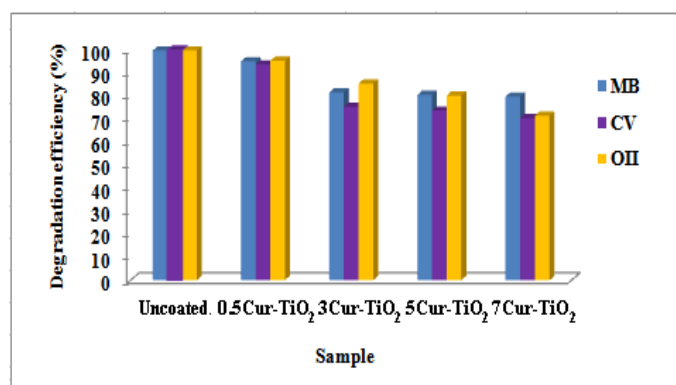


Figure 29 Degradation efficiencies of three selected dyes under UV irradiation (5h) by uncoated and coated P25-TiO₂ samples.

Photocatalytic study with visible light

The main target in this work is to improve the photocatalytic activity of TiO₂, both crystalline and amorphous phases, to response to visible light activation. The photocatalytic study under visible light irradiation was carried out by determining dyes degradation with 18 W fluorescence lamps as source of visible light. The photocatalytic activities of curcumin coated P25-TiO₂ samples under visible light irradiation are shown in Figure 30. It was readily seen that uncoated P25-TiO₂ showed the lowest photocatalytic activity under visible light compared to the coated ones. The irradiation time had to be extended to 8–9 h to have a more decisive conclusion. During the first 5 h of irradiation, the reaction rate increased slowly after which it dramatically increased. CV and MB dyes were nearly completely decolorized (including adsorption), but OII showed only *ca.* 70–80 % of decolorization efficiency. However, if irradiation was extended to 12 h, OII showed complete decolorization yielding a clear colorless solution. The curcumin coated anatase and rutile TiO₂ samples were also tested for comparison and the Cur-TiO₂-an samples showed the same result with Cur-TiO₂-P25 samples. However, the photodegradation under visible light irradiation of Cur-TiO₂-ru samples was not improved. Therefore, the photoreactivity under visible light irradiation of Cur-TiO₂-an and Cur-TiO₂-ru were

not included in this part. The inertness of curcumin coated rutile may be explained by means of high electron-hole pairs recombination rate (Jung and Kim, 2009).

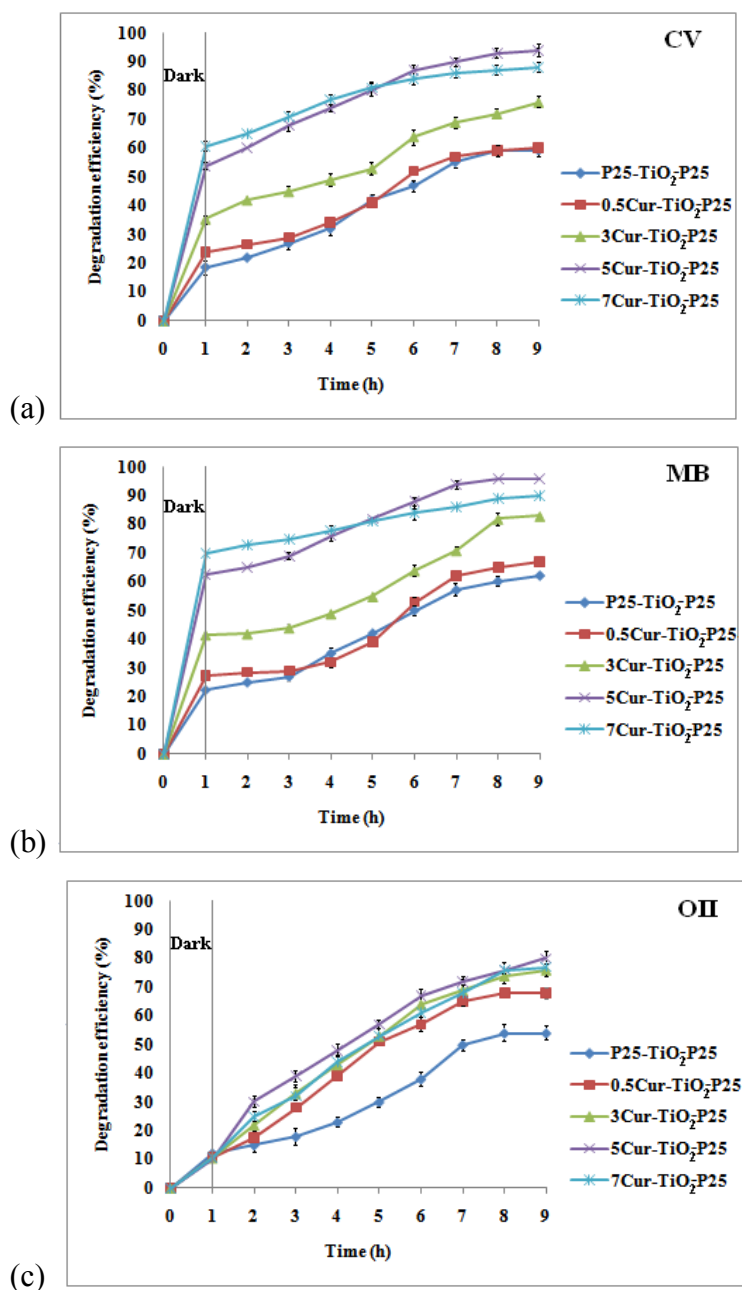


Figure 30 Degradation efficiencies under visible light irradiation (9 h) by uncoated and coated P25-TiO₂ samples for dyes (a) CV, (b) MB, and (c) OII.

In **Paper II**, the photoreactivity of all amorphous TiO₂ samples with 8 h of visible light irradiation are shown in Figure 31. From Figure 31(a) the photoreactivity at high MB concentration revealed that both uncoated and coated samples still had high adsorption efficiency in the range of 40–60 % while only 10% was observed for P25-TiO₂ (standard reference). After illumination, uncoated amorphous TiO₂ was not active whereas the activity of all coated TiO₂ samples increased. Figure 31(b) shows the photoreactivity at normal OII concentration with high adsorptivity about 20–45% compared to only 10 % exhibited by P25-TiO₂. Under visible light irradiation, all coated TiO₂ samples showed increasing degradation efficiency of OII. Increasing curcumin loadings from 1–7.5 wt% increased photoreactivity towards both MB and OII dyes. For the 10 wt%, it did show some photocatalytic activity roughly parallel to others but since it started with lower adsorption than others so at the end of 8 h its overall decolorization efficiency was still lower than the rest.

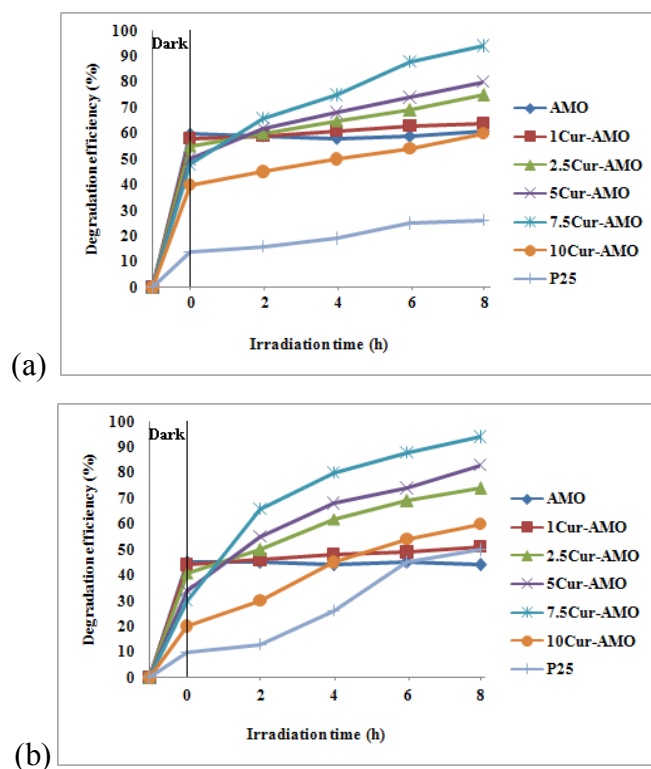


Figure 31 Degradation efficiencies under visible light irradiation (8 h) by uncoated and coated amorphous TiO₂ samples for dyes (a) MB and (b) OII.

As shown in Table 9, the uncoated amorphous TiO₂ has the highest BET surface area which decreases when coated with curcumin. The decrease of surface area in the coated samples was inevitably due to the masking by curcumin molecules which deposited on the surface of amorphous TiO₂. The support for this observation is that on a closer inspection of Figure 31 we can see the gradual lowering of adsorption (at 0 h irradiation) as the concentration of coating curcumin increased.

Effect of pH on photocatalytic activities

The effects of acidity and basicity of solution to the photocatalytic activity of the prepared TiO₂ samples were determined by varying the solution pH values to 3, 5, 7, 9 and 11. The natural pH of each dye (CV, MB, and OII) was 6.7, 6.9, and 7.2, respectively. Photodegradation efficiencies for CV, MB, and OII dyes by 5 wt% of curcumin coated on P25-TiO₂ under visible light irradiation at varying pH are shown in Figure 32 whereas Figure 33 presents the photodegradation efficiencies for MB and OII dyes by coated amorphous TiO₂. Since the prepared TiO₂ with 5 and 7.5wt% curcumin content onto crystalline TiO₂ (**Paper I**) and amorphous TiO₂ (**Paper II**), respectively, showed the highest photodegradation efficiency under visible light irradiation for all three dyes, the influence of acidic and basic solution on photodegradation efficiency was monitored by means of 5Cur-TiO₂-P25 sample (Figure 32) and 7.5Cur-AMO sample (Figure 33).

The results showed that the heterogeneous photocatalytic process under studied was strongly dependent on the pH of the solution. It has been known that the metal oxide particles suspended in water behave similarly to diprotic acids. For TiO₂, the surface hydroxyl groups undergo two acid–base equilibria (Sun, *et al.*, 2008):



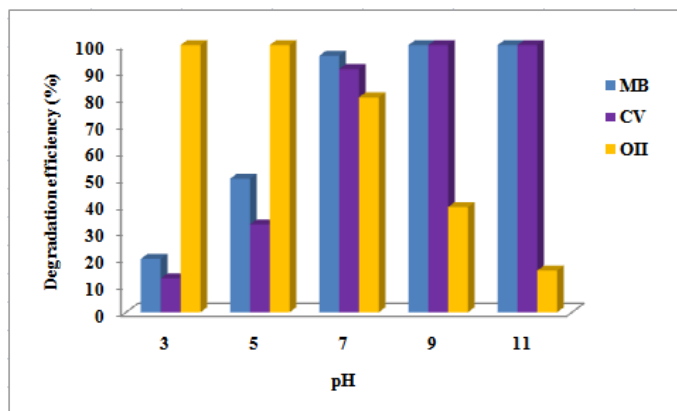


Figure 32 Effect of pH on photodegradation efficiency under visible light irradiation of 5Cur-TiO₂-P25 sample.

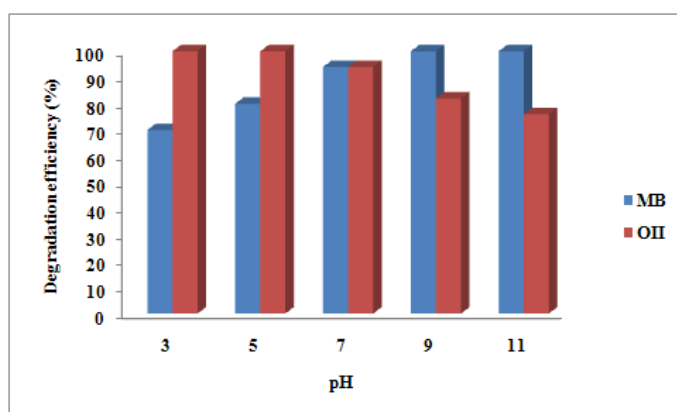


Figure 33 Effect of pH on photodegradation efficiency under visible light irradiation of 7.5Cur-AMO sample.

In **Paper I**, the interpretation of pH effect on the photocatalytic process is rather complex because of its multiple roles such as electrostatic interactions between the semiconductor surface, solvent molecules, substrate, and charged radicals formed during the reaction process (Vijayabalan, *et al.*, 2009). The surface charge property of TiO₂ changes with the change of solution pH. The TiO₂ surface is

positively charged in acidic medium, i.e. when $\text{pH} < \text{pH}_{\text{pzc}}$, and negatively charged in alkaline medium when $\text{pH} > \text{pH}_{\text{pzc}}$ (Sun, *et al.*, 2008). Experiments in this section employed 5Cur-TiO₂-P25 (pH_{pzc} 4.4) as the catalyst, thus, its surface charge would be positively charged when the solution pH was less than 4.4 and would be negatively charged if $\text{pH} > 4.4$. Recall that CV and MB molecules when ionized the parent fragment carried positive charges while fragment of OII carried negatively charges. From Figure 32, at pH 3, the surface of TiO₂ became positively charge [Eq. (20)] which caused the electrostatic repulsion between the surface of TiO₂ and the dye cations and retarded the photodegradation activities. At pH 5 which was slightly higher than the pH_{pzc} 4.4, the photodegradation efficiencies of CV and MB increased slightly. At still higher pH, the surface of TiO₂ became more negative and electrostatic interaction between the negative surface and the dye cations led to strong adsorption with a corresponding high photodegradation activities reaching a maximum at pH 9 (at pH 11 the color of CV dye already turned to colorless due to its pH indicator properties) (Adak, *et al.*, 2005; Senthilkumar and Porkodi, 2005). The photoreactivity of both dyes fall in the order: $\text{pH } 11 \approx \text{pH } 9 > \text{pH } 7 > \text{pH } 5 > \text{pH } 3$. In case of OII which yields negative fragment after ionization, the photodegradation activities show a maximum at pH 3 up to pH 5 after which the activity decreased dramatically in the order: $\text{pH } 3 \approx \text{pH } 5 > \text{pH } 7 > \text{pH } 9 > \text{pH } 11$.

In the same way, **Paper II**, pH_{pzc} of 7.5Cur-AMO was 6.3, thus, its surface charge would be positively charged when the solution pH was less than 6.3 and would be negatively charged if $\text{pH} > 6.3$. The acid conditions were carried out at pH 3 and 5 while the basic ones were carried out at pH 9 and 11. The natural pH of MB and OII solutions were 6.9 and 7.2, respectively. Trends of photoreactivity of MB and OII appeared in opposite way due to MB giving cationic fragment while OII anionic fragment after dissociation in water. The photoreactivity of MB dye fell in the order: $\text{pH } 11 \approx \text{pH } 9 > \text{pH } 7 > \text{pH } 5 > \text{pH } 3$ and that of OII in the order: $\text{pH } 3 \approx \text{pH } 5 > \text{pH } 7 > \text{pH } 9 > \text{pH } 11$. Curcumin coatings decreased the pH_{pzc} of amorphous TiO₂ from 6.3 to 5.4. This means, roughly, around pH 5.4 the photoreactivities of MB dye should increase whereas OII dye should decrease with increasing pH solution. Note that MB dye concentration in this study was four times higher than that normally used

in other reports because of high adsorptivity enhances its overall decolorizing efficiency, i.e. adsorption + photodegradation instead of photodegradation alone.

Recyclability of curcumin coated TiO₂ catalysts

The curcumin coated TiO₂ in this work (except rutile TiO₂) can be reused in the photocatalytic degradation of CV and MB dyes under visible light several times. After the first use, the surface of coated P25-TiO₂ and coated anatase TiO₂ catalysts remained clean since the adsorbed dye molecules were destroyed by the photocatalytic mode whereas the surface of coated-rutile appeared “dirty” as it was covered with dye molecules. Attempt to regenerate the coated-rutile surface by using H₂O₂ as oxidizing agent under UV irradiation was not successful since its surface remained dirty. With their clean surfaces, the coated P25-TiO₂ and coated anatase TiO₂ photocatalysts could be used in the next recycling test immediately after the first use and the results are shown in Figure 34. The recycling tests were run up to five times of which the efficiencies drop from approximately 90–70 % were observed for both dyes. Among the two catalysts, the coated P25-TiO₂ exhibited slightly better performance than coated anatase samples. In the recycling study, the pH of solutions were kept at the corresponding natural pH of dye solutions. OII dye was not included in the recycling test since it showed rather low efficiency under visible light at slightly high pH.

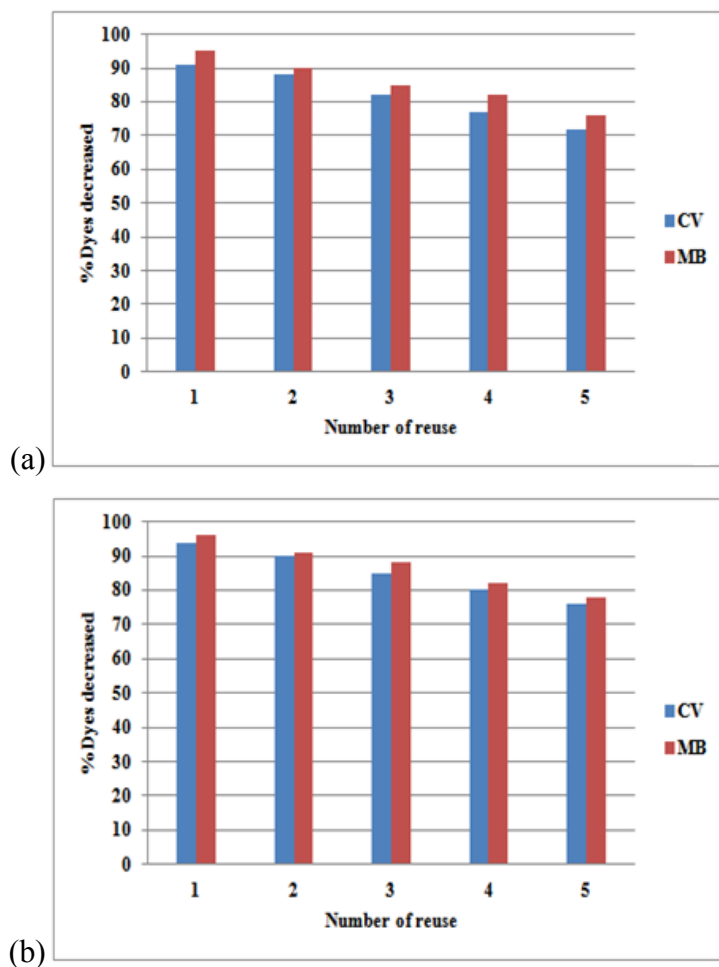


Figure 34 Recyclability of (a) 5Cur-TiO₂-an, and (b) 5Cur-TiO₂-P25 under visible light irradiation (9 h).

The recyclability of coated amorphous TiO₂ was tested to see its service life under visible light irradiation. After the first use, the surface of coated sample remained clean since the adsorbed dye molecules were destroyed by the photocatalytic process. This is different from the uncoated amorphous TiO₂ which also has high surface adsorptivity but low (almost negligible) photocatalytic activity. After having been used, the surface of uncoated TiO₂ became “dirty” since it was covered with dye molecules and required regeneration before the next recycle uses (Kanna, *et al.*, 2010). On the other hand, with clean surface, the curcumin coated photocatalyst in this work can be used in the next recycle test immediately after the

first use. The recycle tests were run up to five times (Figure 35) without any significant loss of efficiency.

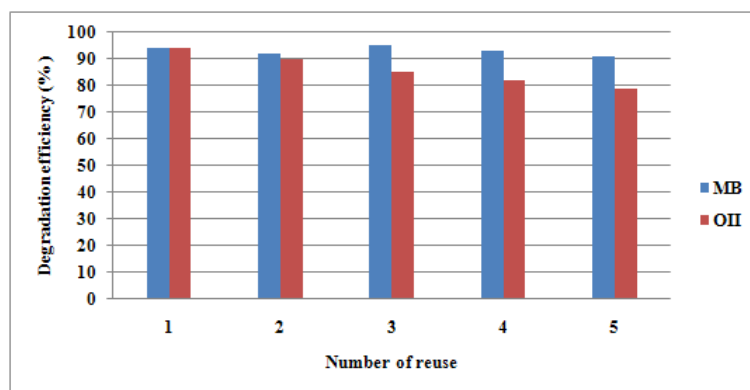
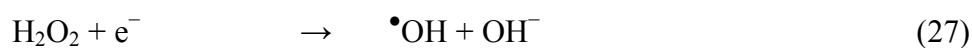
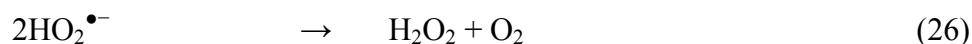
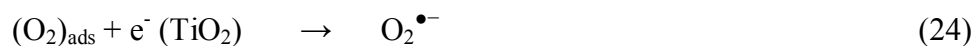
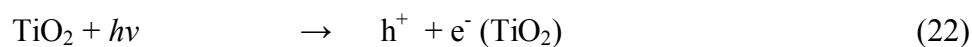


Figure 35 Recyclability 7.5Cur-AMO under visible light irradiation (8 h).

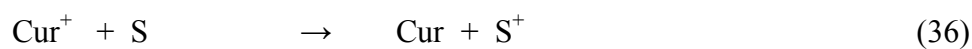
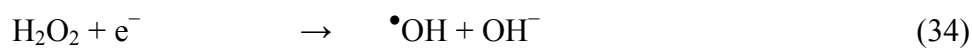
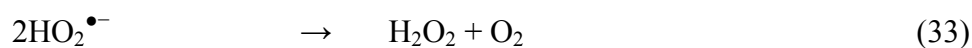
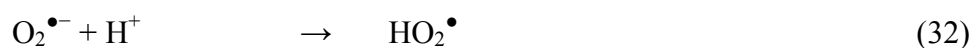
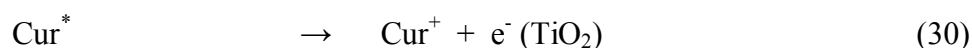
Mechanism pathways of photodegradation by TiO₂ catalysts

From the above photodegradation results and Scheme 2, the uncoated TiO₂ photodegraded dyes and the curcumin coating ones showed lower photodegradation efficiency under UV irradiation. The photodegradation mechanism under this condition should proceed through the accepted pathways as follows (Baiju, *et al.*, 2007; Matthews, *et al.*, 1996; Randorn, *et al.*, 2004; Houas, *et al.*, 2001).



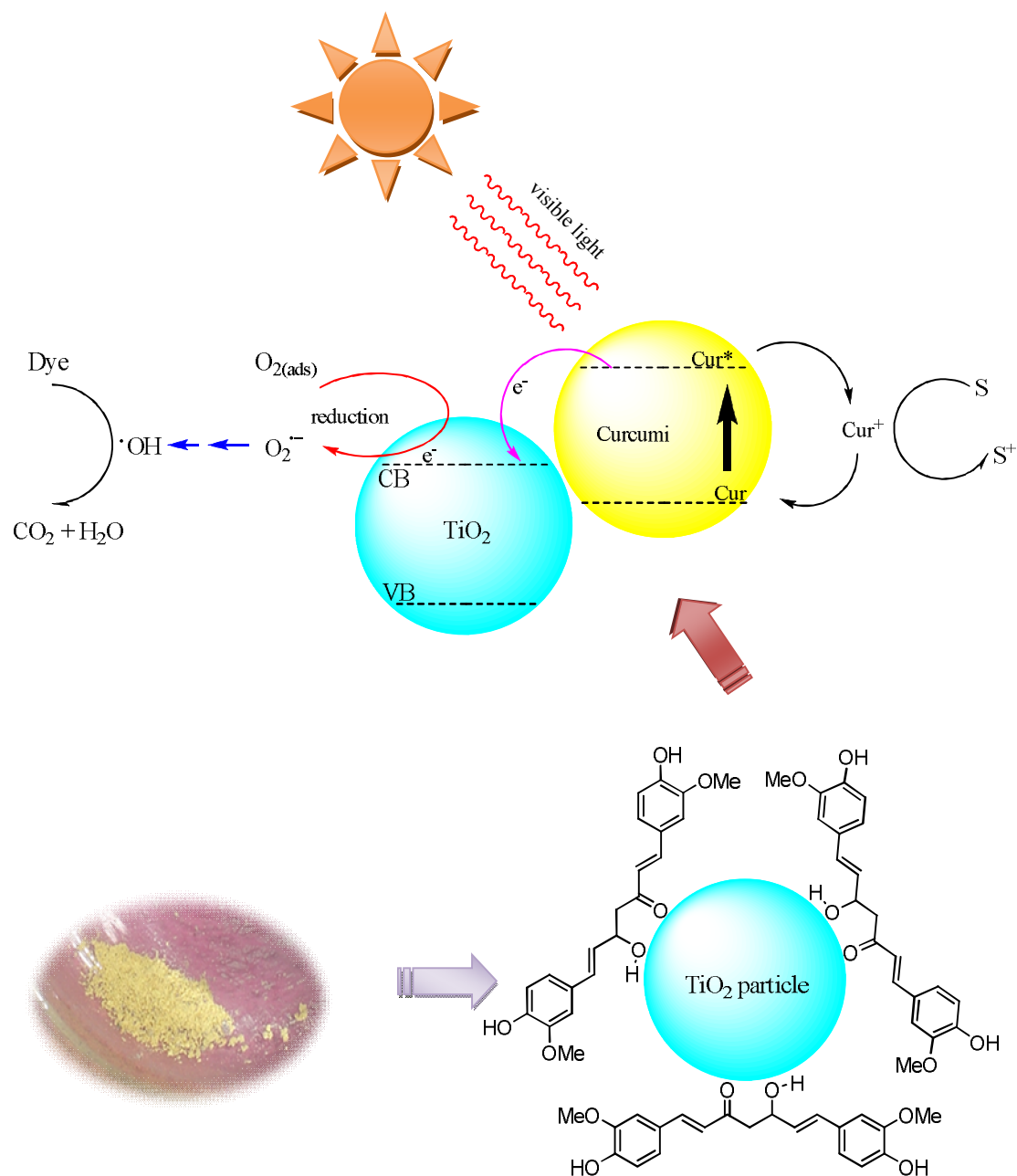
The main entities that induce the degradation are the e^- - h^+ pair generated in the bulk of TiO₂ by UV light having energy in excess of the band gap.

On the other hand, under visible light, curcumin coating boosted the photocatalytic activity, presumably, by means of the same process as that found as in the role of sensitizing agent in dye sensitized solar cell (DSSCs). The light absorption in the DSSCs takes place by dye molecules and the charge separation by electron injection from dye to TiO₂ at the semiconductor interface. The sensitizing molecule in this case is the curcumin molecules. The mechanism can be summarized in chemical reaction terminology as Eqs. (29)-(36)



The energy of the visible light is insufficient to create e⁻-h⁺ pair from TiO₂ but it is enough to cause some changes via curcumin. Curcumin adsorbed on TiO₂ surface was excited by the visible light (Eq. (29)), after which the excited electron was transferred to the conduction band of TiO₂ (Eq. (30)). The role of this electron was to reduce the adsorbed O₂ on the catalyst surface to become the superoxide anion (Eq. (31)), a precursor of Eqs. (32)-(34) in the degradation of model dyes, Eq. (35). The positively charged curcumin (Cur⁺) in Eq. (30) may interact with surrounding solvent molecules (S) and return to neutral stage, Eq. (36), ready for the next round of excitation by visible light again. Since the parent fragment of CV and MB carry positive charge, it should be favorably adsorbed to the negative sites of the TiO₂ surface and subsequently attacked by the very active •OH moiety (Ishibashi, *et al.*, 2000), leading to the destruction of the dyes molecule. For OII which yields negative fragment can be directly degraded by the very active •OH radical diffusing within the medium without having to be adsorbed on TiO₂ surface. The mechanism pathway for photodegradation by TiO₂ coating with curcumin molecule which play

mainly role as dye sensitizing agent under visible light illumination is given in Scheme 3.



Scheme 3 Mechanism pathways of curcumin coated TiO₂ under visible light irradiation.

Chapter 4

Concluding remarks

The preparation of TiO₂ coated with curcumin was achieved via the sol-gel process followed modified impregnation method. The optimal curcumin content at 5 wt% for crystalline TiO₂ and 7.5 wt% for amorphous TiO₂ coating showed better photoreactivity than other curcumin loadings. Incorporation of curcumin into all forms TiO₂ did not affect its nature phases but light absorption was extended to longer wavelength and the absorption intensities corresponded with curcumin content. Elemental analysis showed low percentages of C and H indicating only small amount of curcumin coating on the catalyst surface. For the photocatalytic studies, the coated on crystalline TiO₂ showed better adsorptivity than uncoated sample for cationic azo dyes, CV and MB, but no difference adsorptive activity of anionic dye due to the decreasing of pH_{pzc}, on the other hand, uncoated amorphous TiO₂ showed better adsorptivity than coated samples due to the lowering of BET surface area of coated samples. Under UV irradiation (only the crystalline TiO₂ was test), the coated TiO₂ showed photodegradation efficiency comparable to uncoated ones within 5 h of irradiation, however, under visible light the coated samples exhibited higher photodegradation efficiency than uncoated TiO₂ for all three dyes. Under visible light activation, curcumin acted as the sensitizer with the excited electron was injected into the conduction band of TiO₂ leading to the photocatalytic processes. In conclusion, this work was successfully turned the TiO₂ with low visible light response to highly photoactive by means of dye-sensitized pathway.

References

- Adak, A., Bandyopadhyay, M. and Pal, A. 2005. Removal of crystal violet dye from wastewater by surfactant-modified alumina. *Separation and Purification Technology*. 44: 139–144.
- Alexiou, M. S. and Sermon, P. A. 1993. Aspects of the preparation of heterogeneous catalysts by impregnation. *Reaction Kinetics and Catalysis Letters*. 51: 1–7.
- Anitha, A., Maya, S., Deepa, N., Chennazhi, K. P., Nair, S.V., Tamura, H. and Jayakumar, R. 2011. Efficient water soluble O-carboxymethyl chitosan nanocarrier for the delivery of curcumin to cancer cells. *Carbohydrate Polymers*. 83: 452–461.
- Arconada, N., Durán, A., Suárez, S., Portela, R., Coronado, J. M. and Sánchez, B. 2009. Synthesis and photocatalytic properties of dense and porous TiO₂-anatase thin films prepared by sol-gel. *Applied Catalysis B: Environmental*. 86(1–2): 1–7.
- Asahi, R., Morikawa, T., Ohwaki, T., Aoki, K. and Taga, Y. 2001. Visible-light photocatalysis in nitrogen-doped titanium dioxide. *Science*. 293: 269–271.
- Asiri, A. M., Al-Amoudi, M. S., Bazaid, S. A., Adam, A. A., Alamry, K. A. and Anandan, S. 2014. Enhanced visible light photodegradation of water pollutants over N-, S-doped titanium dioxide and n-titanium dioxide in the presence of inorganic anions. *Journal of Saudi Chemical Society*. 18: 155–163.
- Baiju, K. V., Shukla, S., Sandhya, K. S., James, J. and Warriar, K. G. K. 2007. Photocatalytic activity of sol-gel-derived nanocrystalline titania. *Journal of Physical Chemistry C*. 111: 7612–7622.
- Bessekhouad, Y., Robert, D., Weber, J. V. and Chaoui, N. 2004. Effect of alkaline-doped TiO₂ on photocatalytic efficiency. *Journal of Photochemistry and Photobiology A: Chemistry*. 167: 49–57.

- Bizani, E., Fytianos, K., Poullos, I. and Tsiridis, V. 2006. Photocatalytic decolorization and degradation of dye solutions and wastewaters in the presence of titanium dioxide. *Journal of Hazardous Materials*. 136: 85–94.
- Brillas, E. and Martínez-Huitle, C. A. 2015. Decontamination of wastewaters containing synthetic organic dyes by electrochemical methods. An updated review. *Applied Catalysis B: Environmental*. 166–167: 603–643.
- Buddee, S., Wongnawa, S., Sirimahachai, U. and Puetpaibool, W. 2011. Recyclable UV and visible light photocatalytically active amorphous TiO₂ doped with M (III) ions (M= Cr and Fe). *Materials Chemistry and Physics*. 126: 167–177.
- Carneiro, J. O., Teixeira, V., Portinha, A., Dupak, L., Magalhaes, A. and Coutinho, P. 2005. Study of the deposition parameters and Fe-dopant effect in the photocatalytic activity of TiO₂ films prepared by dc reactive magnetron sputtering. *Vacuum*. 78: 37–46.
- Chaithanadol, K. 2011. A study on complex formation between curcumin and chromium(III) ion. Master of Science Thesis, Prince of Songkla University, Songkhla, Thailand.
- Chang, S.-m. and Liu, W.-s. 2014. The roles of surface-doped metal ions (V, Mn, Fe, Cu, Ce, and W) in the interfacial behavior of TiO₂ photocatalysts. *Applied Catalysis B: Environmental*. 156–157: 466–475.
- Cheng, J., Chen, J., Lin, W., Liu, Y. and Kong, Y. 2015. Improved visible light photocatalytic activity of fluorine and nitrogen co-doped TiO₂ with tunable nanoparticle size. *Applied Surface Science*. 332: 573–580.
- Clark, R. J. H. 1968. *The chemistry of titanium and vanadium*. Elsevier: Amsterdam.
- Da browski, A. 2001. Adsorption-from theory to practice. *Advances in Colloid and Interface Science*. 93: 135–224.

- Daneshvar, N., Aber, S. and Hosseinzadeh, F. 2008. Study of C.I. acid orange 7 removal in contaminated water by photo oxidation processes. *Global NEST Journal*. 10(1): 16–23.
- Duplyakin, V. K., Belyi, A. S., Rodionov, A. V. and Alfeev, V. S. 1991. New impregnation process for producing coated catalysts. *Chemistry and Technology of Fuels and Oils*. 27: 39–42.
- Estrellan, C. R., Salim, C. and Hinode, H. 2009. Photocatalytic activity of sol-gel derived TiO₂ co-doped with iron and niobium. *Reaction Kinetics and Catalysis Letters*. 98(1): 187–192.
- Frank, S. N. and Bard, A. J. 1977. Heterogeneous photocatalytic oxidation of cyanide ion in aqueous solutions at titanium dioxide powder. *Journal of the American Chemical Society*. 99(1): 303–304.
- Fu, Y. and Viraraghavan, T. 2001. Fungal decolorization of dye wastewaters: a review. *Bioresource Technology*. 79: 251–262.
- Fujishima, A. and Honda, K. 1972. Electrochemical photolysis of water at a semiconductor electrode. *Nature*. 238(5358): 37–38.
- Ganesh, T., Kim, J. H., Yoon, S. J., Kil, B. H., Maldar, N. N., Han, J. W. and Han, S. H. 2010. Photoactive curcumin-derived dyes with surface anchoring moieties used in ZnO nanoparticle-based dyesensitized solar cells. *Materials Chemistry and Physics*. 123:62–66.
- Garfield, S. 2001. *Mauve: How One Man Invented a Color That Changed the World*. Norton: New York.
- Goel, A., Kunnumakkara A.B. and Aggarwal, B. B. 2008. Curcumin as “Curecumin”: from kitchen to clinic. *Biochemical Pharmacology*. 75: 787–809.

- Gomes de Moraes, S., Sanches Freire, R. and Duran, N. 2000. Degradation and toxicity reduction of textile effluent by combined photocatalytic and ozonation processes. *Chemosphere*. 40: 369–373.
- Govindarajan, V. S. 1980. Turmeric: chemistry, technology and quality. *Critical Reviews in Food Science and Nutrition*. 12: 199–301.
- Guo, Y., Zhang, X. W., Weng, W. H. and Han, G. R. 2007. Structure and properties of nitrogen-doped titanium dioxide thin films grown by atmospheric pressure chemical vapor deposition. *Thin Solid Films*. 515(18): 7117–7121.
- Hilal, H. S., Majjad, L. Z., Zaatar, N. and El-Hamouz, A. 2007. Dye-effect in TiO₂ catalyzed contaminant photo-degradation: sensitization versus charge-transfer formalism. *Solid State Sciences*. 9: 9–15.
- Holme, I. 2006. Sir William Henry Perkin: a review of his life, work and legacy. *Coloration Technology*. 122: 235–251.
- Houas, A., Lachheb, H., Ksibi, M., Elaloui, E., Guillard, C. and Hermann, J. M. 2001. Photocatalytic degradation pathway of methylene blue in water. *Applied Catalysis B: Environmental*. 31: 145–157.
- Huo, K. F., Zhang, X. M., Fu, J. J., Qian, G. X., Xin, Y. C. and Zhu, B. Q. 2009. Synthesis and field emission properties of rutile TiO₂ nanowires arrays grown directly on a Ti metal self-source substrate. *Journal of Nanoscience and Nanotechnology*. 9(5): 3341–3346.
- Ihara, T., Miyoshi, M., Triyama, Y., Marsumato, O. and Sugihara, S. 2003. Visible-light-active titanium oxide photocatalyst realized by an oxygen-deficient structure and by nitrogen doping. *Applied Catalysis B: Environmental*. 42: 403–409.
- In, S. I., Vaughn, D. D. and Schaak, R. E. 2012. Hybrid CuO-TiO_{2-x}N_x hollow nanocubes for photocatalytic conversion of CO₂ into methane under solar irradiation. *Angewandte Chemie International Edition*. 51(16): 3915–3918.

- Irie, H., Watanabe, Y. and Hashimoto, K. 2003. Nitrogen-concentration dependence on photocatalytic activity of $\text{TiO}_{2-x}\text{N}_x$ powders. *Journal of Physical Chemistry B* 107(23): 5483–5486.
- Ishibashi, K., Fujishima, A., Watanabe, T. and Hashimoto, K. 2000. Quantum yields of active oxidative species formed on TiO_2 photocatalyst. *Journal of Photochemistry and Photobiology A: Chemistry*. 134: 139–142.
- Jiao, Y. Z., Peng, C. X., Guo, F. F., Bao, Z. H. and Yang, J. H. 2011. Facile synthesis and photocatalysis of size-distributed TiO_2 hollow spheres consisting of {116} plane-oriented nanocrystallites. *Journal of Physical Chemistry C*. 115: 6405–6409.
- Jung, H. S. and Kim, H. 2009. Origin of low photocatalytic activity of rutile TiO_2 . *Electronic Materials Letters*. 5: 73–76.
- Kadam, A. N., Dhabbe, R. S., Kokate, M. R., Gaikwad, Y. B. and Garadkar, K. M. 2014. Preparation of N doped TiO_2 via microwave-assisted method and its photocatalytic activity for degradation of malathion. *Spectrochimica Acta Part A: Molecular Spectroscopy*. 133: 669–676.
- Kanna, M. 2002. Adsorption behavior of some metal ions on titanium dioxide surface. Master of Science Thesis, Prince of Songkla University, Songkhla, Thailand.
- Kanna, M., Wongnawa, S., Sherdshoopongse, P. and Boonsin, P. 2005. Adsorption behavior of some metal ions on hydrated amorphous titanium dioxide surface. *Songklanakarinn Journal of Science and Technology*. 27: 1017–1026.
- Khalil, T., Abou El-Nour, F., El-Gammal, B. and Boccaccini. 2001. Determination of surface area and porosity of sol-gel derived ceramic powders in the system $\text{TiO}_2\text{-SiO}_2\text{-Al}_2\text{O}_3$. *Powder Technology*. 114: 106–111.
- Khatri, A., Peerzada, M. H., Mohsin, M. and White, M. 2015. A review on developments in dyeing cotton fabrics with reactive dyes for reducing effluent pollution. *Journal of Cleaner Production*. 87: 50–57.

- Kiuchi, F., Goto, Y., Sugimoto, N., Akao, N., Kondo, K. and Tsuda, Y. 1993. Nematocidal activity of turmeric: synergistic action of curcuminoids. *Chemical and Pharmaceutical Bulletin*. 41:1640–1643.
- Kong, D., Tan, J. Z. Y., Yang, F., Zeng, J. L. and Zhang, X. W. 2013. Electrodeposited Ag nanoparticles on TiO₂ nanorods for enhanced UV visible light photoreduction CO₂ to CH₄. *Applied Surface Science*. 277: 105–110.
- Kumar, S. R., Suresh, C., Vasudevan, A. K., Suja, N. R. and Mukundan, P. 1999. Phase transformation in sol-gel titania containing silica. *Materials Letters*. 38: 161–166.
- Kumar, S. S. D., Mahesh, A., Mahadevan, S. and Mandal, A. B. 2014. Synthesis and characterization of curcumin loaded polymer/lipid based nanoparticles and evaluation of their antitumor effects on MCF-7 cells. *Biochimica et Biophysica Acta*. 1840: 1913–1922.
- Kusumawardani, C., Indriana, K. and Narsito. 2010. Synthesis of nanocrystalline N-doped TiO₂ and its application on high efficiency of dye-sensitized solar cells. *Science Journal Ubon Ratchathani University*. 1(1): 1–8.
- Lee, M. S., Hong, S. S. and Mohseni, M. 2005. Synthesis of photocatalytic nanosized TiO₂-Ag particles with sol-gel method using reduction agent. *Journal of Molecular Catalysis A: Chemical*. 242: 135–140.
- Lettmann, C., Hildebrand, K., Kisch, H., Macyk, W. and Maier, W. 2001. Visible light photodegradation of 4-chlorophenol with a coke-containing titanium dioxide photocatalyst. *Applied Catalysis B: Environmental*. 32: 215–227.
- Li, J., Liu, S., He, Y. and Wang, J. 2008. Adsorption and degradation of the cationic dyes over Co doped amorphous mesoporous titania–silica catalyst under UV and visible light irradiation. *Microporous and Mesoporous Materials*. 115: 416–425.

- Li, X. Z. and Li, F. B. 2001. Study of Au/Au³⁺-TiO₂ photocatalysts towards visible photooxidation for water and wastewater treatment. *Environmental Science & Technology*. 35: 2381–2387.
- Li, X. Z. and Li, F. B. 2002. The enhancement of photodegradation efficiency using Pt-TiO₂ catalyst. *Chemosphere*. 48: 1103–1111.
- Liang, Y. Y., Wang, H. L., Casalongue, H. S., Chen, Z, and Dai, H. J. 2010. TiO₂ nanocrystals grown on graphene as advanced photocatalytic hybrid materials. *Nano Research*. 3(10): 701–705.
- Likodimos, V., Han, C., Pelaez, M., Kontos, A. G., Liu, G., Zhu, D., Liao, S., de la Cruz, A. A., O’Shea, K., Dunlop, P. S. M., Byrne, J. A., Dionysiou, D. D. and Falaras, P. 2013. Anion-doped TiO₂ Nanocatalysts for water purification under visible light. *Industrial & Engineering Chemistry Research*. 52: 13957–13964.
- Lin, H., Huang, C. P., Li, W., Ni, C., Shah, S. I. and Tseng Y.-H. 2006. Size dependency of nanocrystalline TiO₂ on its optical property and photocatalytic reactivity exemplified by 2-chlorophenol. *Applied Catalysis B: Environmental*. 68:1–11.
- Liu, Z. Y., Sun, D. D., Guo, P. and Leckie, J. 2007. One-step fabrication and high photocatalytic activity of porous TiO₂ hollow aggregates by using a low-temperature hydrothermal method without templates. *Chemistry: A European Journal*. 13(6): 1851–1855.
- Lü, X., Ding, S. J., Xie, Y. and Huang, F. Q. 2011. Non-aqueous preparation of high-crystallinity hierarchical TiO₂ hollow spheres with excellent photocatalytic efficiency. *The European Journal of Inorganic Chemistry*. 18: 2879–2883.
- Matthews, D., Infelta, P. and Gratzel, M. 1996. Calculation of the photocurrent-potential characteristic for regenerative, sensitized semiconductor electrodes. *Solar Energy Materials & Solar Cells*. 44: 119–155.

- Mills, A. and Wang, J. 1999. Photobleaching of methylene blue sensitised by TiO₂: an ambiguous system. *Journal of Photochemistry and Photobiology A: Chemistry*. 127: 123–134.
- Muruganandham, M., Shobana, N. and Swaminathan, M. 2005. Optimization of solar photocatalytic degradation conditions of Reactive Yellow 14 azo dye in aqueous TiO₂. *Journal of Molecular Catalysis A: Chemical*. 246: 154–161.
- Nagaveni, K., Sivalingam, G. and Heged, M. S. 2004. Solar photocatalytic degradation of dyes: high activity of combustion synthesized nano TiO₂. *Applied Catalysis B: Environmental*. 48: 83–93.
- Niederberger, M. and Pinna, N. 2009. *Metal Oxide Nanoparticles in Organic Solvents: Synthesis, Formation, Assembly, and Application*. Engineering Materials and Processes Series. Springer Verlag: London.
- Ohtani, B., Ogawa, Y. and Nishimoto, S. I. 1997. Photocatalytic activity of amorphous-anatase mixture of titanium(IV) oxide particles suspended in aqueous solutions. *The Journal of Physical Chemistry B*. 101: 3746–3752.
- Ou, H. H., Lo, S. L. and Liao, C. H. 2011. N-doped TiO₂ prepared from microwave-assisted titanate nanotubes (Na_xH_{2-x}Ti₃O₇): the effect of microwave irradiation during TNT synthesis on the visible light photoactivity of N-doped TiO₂. *Journal of Physical Chemistry C*. 115(10): 4000–4007.
- Prasai, B., Cai, B., Underwood, M. K., Lewis, J. P. and Drabold, D. A. 2012. Properties of amorphous and crystalline titanium dioxide from first principles. *Journal of Materials Science*. 47: 7515–7521.
- Randorn, C., Wongnawa, S. and Boonsin, P. 2004. Bleaching of methylene blue by hydrated titanium dioxide. *Science Asia*. 30: 149–156.
- Reymond, J. P. and Kolenda, F. 1999. Estimation of the point of zero charge of simple and mixed oxides by mass titration. *Powder Technology*. 103: 30–36.

- Robinson, T., McMullan, G., Marchant, R. and Nigam, P. 2001. Remediation of dyes in textiles effluent: a critical review on current treatment technologies with a proposed alternative. *Bioresource Technology*. 77: 247–255.
- Ryu, Z., Zheng, J., Wang, M. and Zhang, B. 1999. Characterization of pore size distributions on carbonaceous adsorbents by DFT. *Carbon*. 37: 1257–1264.
- Sauer, T., Neto, G. C., José, H. J. and Moreira R. F. P. M. 2002. Kinetics of photocatalytic degradation of reactive dyes in a TiO₂ slurry reactor. *Journal of Photochemistry and Photobiology A: Chemistry*. 149: 147–154.
- Senthilkumar, S. and Porkodi, K. 2005. Heterogeneous photocatalytic decomposition of crystal violet in UV-illuminated sol-gel derived nanocrystalline TiO₂ suspensions. *Journal of Colloid and Interface Science*. 288: 184–189.
- Shao, P., Tian, J., Zhao, Z., Shi, W., Gao, S. and Cui, F. 2015. Amorphous TiO₂ doped with carbon for visible light photodegradation of rhodamine B and 4-chlorophenol. *Applied Surface Science*. 324:35–43.
- Sharma, S. K. 2015. Green chemistry for dyes removal from wastewater: Research trends and applications. John Wiley & Sons: New Jersey.
- Shim, W. G. and Kim, S. C. 2008. Heterogeneity analysis of P-25 and carbon coated TiO₂ in liquid phase adsorption of methylene blue and bisphenol A, *Journal of Advanced Engineering and Technology*. 1: 291–295.
- Sing, K. S. W., Everett, D. H., Haul, R. A. W., Moscou, L., Pierotti, R. A., Rouquerol, J. and Siemie-niewska, T. 1985. Reporting physisorption data for gas/solid systems with special reference to the determination of surface area and porosity, *Pure and Applied Chemistry*. 57: 603–619.
- Simonsen, M. E., Li, Z. S. and Søgaaard, E. G. 2009. Influence of the OH groups on the photocatalytic activity and photoinduced hydrophilicity of microwave assisted sol-gel TiO₂ film. *Applied Surface Science*. 255(18): 8054–806.

- Singh, U., Verma, S., Ghosh, H. N., Rath, M. C., Priyadarsini, K. I., Sharma, A., Pushpa, K. K., Sarkar, S. K. and Mukherjee, T. 2010. Photo-degradation of curcumin in the presence of TiO₂ nanoparticles: fundamentals and application. *Journal of Molecular Catalysis A: Chemical*. 318: 106–111.
- Skoog, D. A. and Leary, J. J. 1992. *Principle of instrumental analysis*. Saunders Collage Publishing: Philadelphia.
- Smestad, G. P., Spiekermann, S., Kowalik, J., Grant, C. D., Schwartzberg, A. M., Zhang, J., Tolbert, L. M. and Moons, E. 2003. A technique to compare polythiophene solid-state dye sensitized TiO₂ solar cells to liquid junction devices. *Solar Energy Materials and Solar Cells*. 76: 85–105.
- Sood, S., Umar, A., Mehta, S. K., Sinha, A. S. K. and Kansal, S. K. 2015. Efficient photocatalytic degradation of brilliant green using Sr-doped TiO₂ nanoparticles. *Ceramics International*. 41: 3533–3540.
- Suib, S. L. 2013. *New and future developments in catalysis: Solar photocatalysis*. 1st edition. Elsevier: Amsterdam.
- Sun, J., Qiao, L., Sun, S. and Wang, G. 2008. Photocatalytic degradation of orange G on nitrogen-doped TiO₂ catalysts under visible light and sunlight irradiation. *Journal of Hazardous Materials*. 155: 312–319.
- Sun, L. B., Shi, Y. C., Li, B., Li, X. C. and Wang, Y. 2013. Preparation and characterization of polypyrrole/TiO₂ nanocomposites by reverse microemulsion polymerization and its photocatalytic activity for the degradation of methylorange under natural light. *Polymer Composites*. 34(7): 1076–1080.
- Suwanachawalit, C. 2005. *The metal-doping on the physical and photocatalytic properties of nanosized TiO₂ powder*. Master of Science Thesis, Prince of Songkla University, Songkhla, Thailand.

- Takeshita, K., Yamakata, A., Ishibashi, T., Onishu, H., Nishijima, K. and Ohno, T. 2006. Transient IR absorption study of charge carriers photogenerated in sulfur-doped TiO₂. *Journal of Photochemistry and Photobiology A: Chemistry*. 177: 269–275.
- Tang, Z., Zhang, J., Cheng, Z. and Zhang, Z. 2002. Synthesis of nanosized rutile TiO₂ powder at low temperature. *Materials Chemistry and Physics*. 9319: 1–4.
- Toor, A. P., Verma, A., Jotshi, C. K., Bajpai, P. K. and Singh, V. 2006. Photocatalytic degradation of Direct Yellow 12 dye using UV/TiO₂ in shallow pond slurry reactor. *Dyes and Pigments*. 68: 53–60.
- Treschev, S. Y., Chou, P. W., Tseng, T.H. Wang, J.B., Perevedentseva, E. V. and Cheng C. L. 2008. Photoactivities of the visible light-activated mixed phase carbon-containing titanium dioxide: The effect of carbon incorporation. *Applied Catalysis B: Environmental*. 79: 8–16.
- Umar, M. and Aziz, H. A. 2013. Photocatalytic degradation of organic pollutants in water. *Organic Pollutants-Monitoring, Risk and Treatment: Intech*.
- Vijayabalan, A., Selvam, K., Velmurugan, R. and Swaminathan, M. 2009. Photocatalytic activity of surface fluorinated TiO₂-P25 in the degradation of reactive orange 4. *Journal of Hazardous Materials*. 172: 914–921.
- Wang, X. K., Wang, C., Guo, W. L. and Wang, J. G. 2011. A novel single-step synthesis of N-doped TiO₂ via a sonochemical method. *Materials Research Bulletin*. 46(11): 2041–2044.
- Wang, X. P. and Lim, T. T. 2010. Solvothermal synthesis of C-N codoped TiO₂ and photocatalytic evaluation for bis phenol A degradation using a visible-light irradiated LED photoreactor. *Applied Catalysis B: Environmental*. 100(1–2): 355–364.
- Waranyoupalina, R., Wongnawa, S., Wongnawa, M., Pakawatchai, C., Panichayupakaranant, P. and Sherdshoopongse, P. 2009. Studies on complex

- formation between curcumin and Hg(II) ion by spectrophotometric method: A new approach to overcome peak overlap. *Central European Journal of Chemistry*. 7: 388–394.
- Wu, J. C. S. and Chen, C. H. 2004. A visible-light response vanadium-doped titania nanocatalyst by sol-gel method. *Journal of Photochemistry and Photobiology A: Chemistry*. 163: 509–515.
- Wu, Z., Dong, F., Zhao, W. and Guo, S. 2008. Visible light induced electron transfer process over nitrogen doped TiO₂ nanocrystals prepared by oxidation of titanium nitride. *Journal of Hazardous Materials*. 157(1): 57–63.
- Xi, G. C., Ouyang, S. X. and Ye, J. H. 2011. General synthesis of hybrid TiO₂ mesoporous “french fries” toward improved photocatalytic conversion of CO₂ into hydrocarbon fuel: a case of TiO₂/ZnO. *Chemistry: A European Journal*. 17(33): 9057–9061.
- Xiang, Q. J., Yu, J. G., Cheng, B. and Ong, H. C. 2010. Microwave-hydrothermal preparation and visible-light photoactivity of plasmonic photocatalyst Ag-TiO₂ nanocomposite hollow spheres. *Chemistry-An Asian Journal*. 5(6): 1466–1474.
- Yagub, M. T., Sen, T. K., Afroze, S. and Ang, H. M. 2014. Dye and its removal from aqueous solution by adsorption: A review. *Advances in Colloid and Interface Science*. 209: 172–184.
- Yallapua, M. M., Jaggi, M. and Chauhana, S. C. 2010. β-Cyclodextrin-curcumin self-assembly enhances curcumin delivery in prostate cancer cells. *Colloids and Surfaces B: Biointerfaces*. 79: 113–125.
- Yang, D. J., Liu, H. W., Zheng, Z. F., Yuan, Y., Zhao, J. C. and Waclawik, E. R. 2009. An efficient photocatalyst structure: TiO₂ (B) nanofibers with a shell of anatase nanocrystals. *Journal of the American Chemical Society*. 131(49): 17885–17893.

- Yang, Y., Li, X.-J., Chen, J.-T. and Wang, L.-Y. 2004. Effect of doping mode on the photocatalytic activities of Mo/TiO₂. *Journal of Photochemistry and Photobiology A: Chemistry*. 163: 517–522.
- Yu, C. L., Shu, Q., Zhang, C. X., Xie, Z. P. and Fan, Q. Z., 2012. A sonochemical route to fabricate the novel porous F, Ce-codoped TiO₂ photocatalyst with efficient photocatalytic performance. *Journal of Porous Materials*. 19(5): 903–911.
- Yu, J., Zhou, M., Cheng, B. and Zhao, X. 2006. Preparation, characterization and photocatalytic activity of *in situ* N, S-codoped TiO₂ powders. *Journal of Molecular Catalysis A: Chemical*. 246: 176–184.
- Yu, J. G., Liu, W. and Yu, H. G. 2008. A one-pot approach to hierarchically nanoporous titania hollow microspheres with high photocatalytic activity. *Crystal Growth and Design*. 8(3): 930–934.
- Yu, J. G., Wang, W. G., Cheng, B. and Su, B. L. 2009. Enhancement of photocatalytic activity of mesoporous TiO₂ powders by hydrothermal surface fluorination treatment. *Journal of Physical Chemistry C*. 113(16): 6743–6750.
- Yuan, R. S., Fu, X. Z., Wang, X. C., Liu, P., Wu, L. and Xu, Y. 2006. Template synthesis of hollow metal oxide fibers with hierarchical architecture. *Chemistry of Materials*. 18(19): 4700–4705.
- Yunarti, R. T., Lee, M., Hwang, Y. J., Choi, J.-W., Suh, D. J., Lee, J., Kim, I. W. and Ha, J.-M. 2014. Transition metal-doped TiO₂ nanowire catalysts for the oxidative coupling of methane. *Catalysis Communications*. 50: 54–58.
- Zaleska, A. 2008. Doped-TiO₂: A Review. *Recent Patents on Engineering*. 2: 157–164.
- Zaleska, A., Sobczak, J. W., Grabowska, E. and Hupka, J. 2007. Preparation and photocatalytic activity of boron-modified TiO₂ under UV and visible light. *Applied Catalysis B: Environmental*. 78: 92–100.

- Zainal, Z., Hui, L. H., Hussein, M. Z. and Ramli, I. 2005. Removal of dyes using immobilized titanium dioxide illuminated by fluorescent lamps. *Journal of Hazardous Materials*. 125: 113–120.
- Zhang, X. M. and Liu, Q. Q. 2008. Preparation and characterization of titania photocatalyst co-doped with boron, nickel, and cerium. *Materials Letters*. 62(17–18): 2589–2592.
- Zhang, X. W. and Lei, L. C. 2008. Preparation of photocatalytic Fe₂O₃-TiO₂ coatings in one step by metal organic chemical vapor deposition. *Applied Surface Science*. 254(8): 2406–2412.
- Zhang, Y. H. and Reller, A. 2001. Nanocrystalline iron-doped mesoporous titania and its phase transition. *Journal of Materials Chemistry*. 11: 2537–2541.
- Zhang, Z. and Maggard, P. A. 2007. Investigation of photocatalytically-active hydrated forms of amorphous titania, TiO₂•nH₂O. *Journal of Photochemistry and Photobiology A: Chemistry*. 186: 8–13.
- Zhao, Z. and Liu, Q. 2008. Mechanism of higher photocatalytic activity of anatase TiO₂ doped with nitrogen under visible-light irradiation from density functional theory calculation. *Journal of Physics D Applied Physics*. 41: 1–10.
- Zhou, X. T., Ji, H. B. and Huang, X. J. 2012. Photocatalytic degradation of methyl orange over metalloporphyrins supported on TiO₂ Degussa P25. *Molecules*. 17: 1149–1158.
- Zou, Y., Tan, S., Yuan, Z. and Yu, Z. 2005. A novel green light-emitting material containing both hole and electron transporting units. *Journal of Materials Science*. 40: 3561–3563.

Appendix A

The calibration graphs

The calibration graph of CV dye solution was constructed from five standard solutions: 2.5×10^{-6} M, 5.0×10^{-6} M, 7.5×10^{-6} M, 1.0×10^{-5} M, and 2.5×10^{-5} M. The obtained straight line with $R^2 = 0.999$ is shown in Figure A1

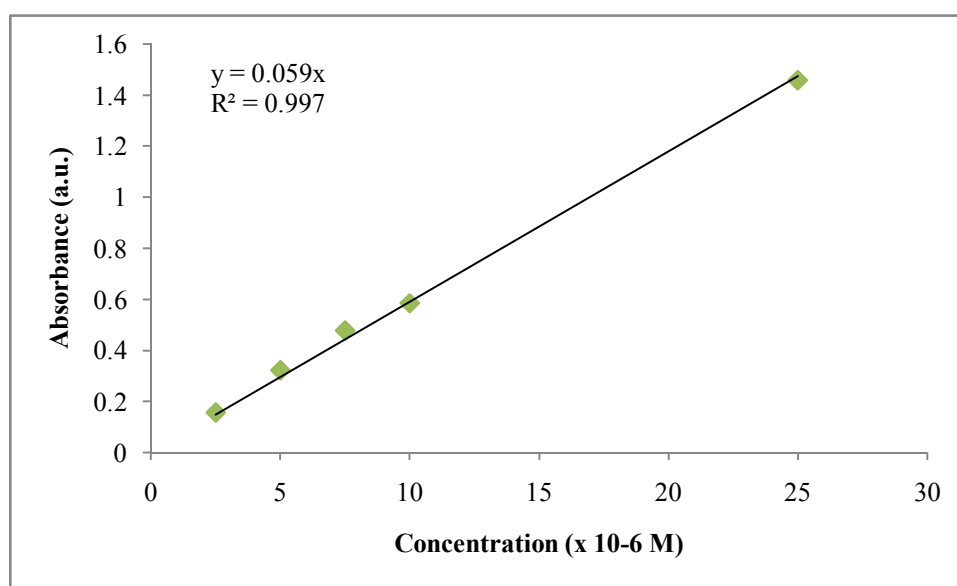


Figure A1 The standard calibration curve of CV dye solution in the range of 2.5×10^{-6} M to 2.5×10^{-5} M.

The calibration graph of MB dye solution was constructed from five standard solutions: 1.0×10^{-5} M, 2.5×10^{-5} M, 5.0×10^{-5} M, 7.5×10^{-5} M, and 1.0×10^{-4} M. The obtained straight line with $R^2 = 0.998$ is shown in Figure A2

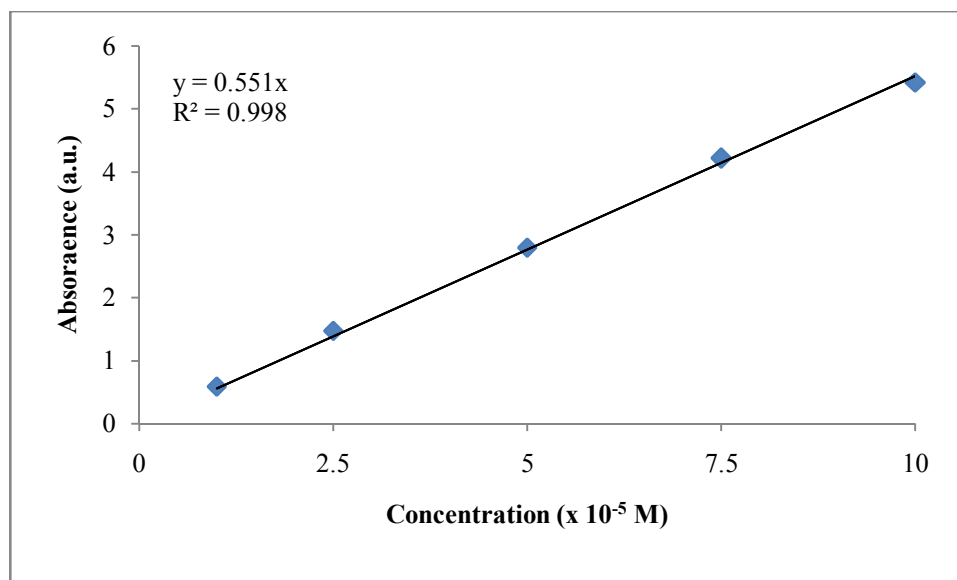


Figure A2 The standard calibration curve of MB dye solution in the range of 1.0×10^{-5} M to 1.0×10^{-4} M.

The calibration graph of OII dye solution was constructed from five standard solutions: 2.5×10^{-6} M, 5.0×10^{-6} M, 7.5×10^{-6} M, 1.0×10^{-5} M, and 2.5×10^{-5} M. The obtained straight line with $R^2 = 0.997$ is shown in Figure A3

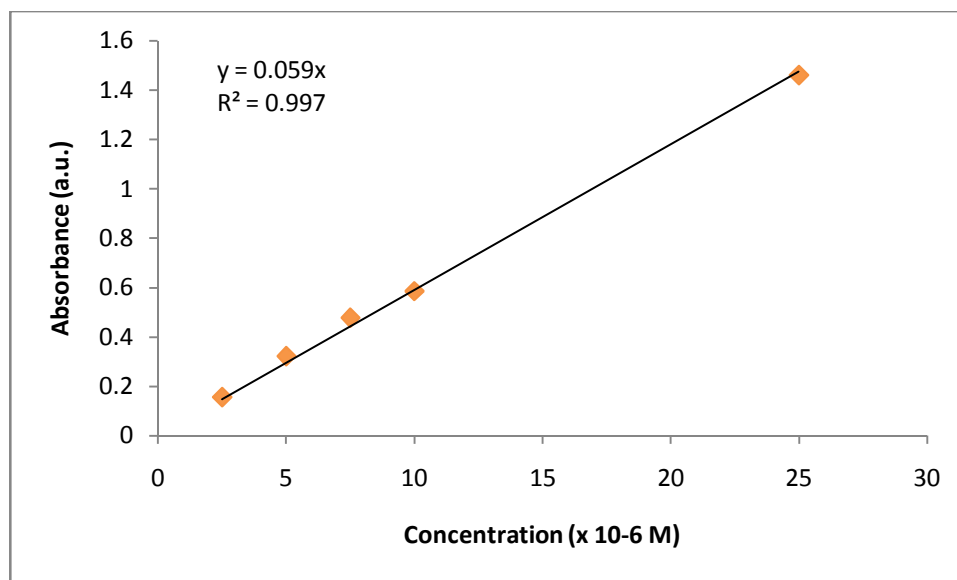


Figure A3 The standard calibration curve of OII dye solution in the range of 2.5×10^{-6} M to 2.5×10^{-5} M.

Appendix B

Cyclic voltammogram of curcumin

Cyclic voltammogram (CV) of curcumin was performed in DMSO, in the potential range at incremental scan rates (ν) from 100 mV/s to 500 mV/s. The CV of curcumin (5×10^{-3} M) obtained in DMSO (in the presence of 0.1 M tetrabutylammonium-hexafluorophosphate as supporting electrolyte at $\nu = 100$ mV/s) is shown in Figure B.

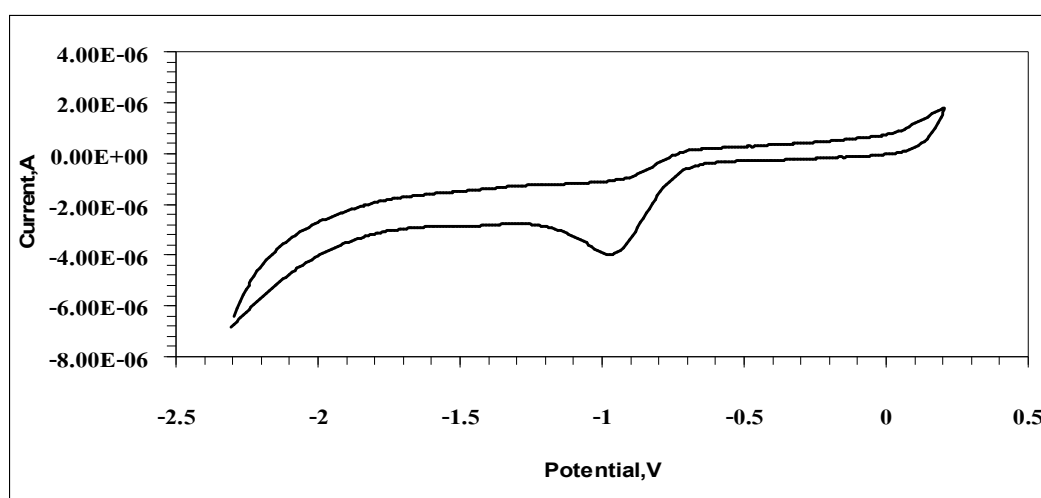


Figure B Cyclic voltammogram of curcumin (5×10^{-3} M) in DMSO.